

**The NW Amazonian Craton in Guainía and Vaupes departments, Colombia  
Transition between orogenic to anorogenic environments during the Paleo-  
Mesoproterozoic**

Bonilla, Amed; Cramer, Thomas; De Grave, Johan; Alessio, Brandon; Glorie, Stijn; Kroonenberg, Salomon

**DOI**

[10.1016/j.precamres.2021.106223](https://doi.org/10.1016/j.precamres.2021.106223)

**Publication date**

2021

**Document Version**

Final published version

**Published in**

Precambrian Research

**Citation (APA)**

Bonilla, A., Cramer, T., De Grave, J., Alessio, B., Glorie, S., & Kroonenberg, S. (2021). The NW Amazonian Craton in Guainía and Vaupes departments, Colombia: Transition between orogenic to anorogenic environments during the Paleo-Mesoproterozoic. *Precambrian Research*, 360, 1-37. Article 106223. <https://doi.org/10.1016/j.precamres.2021.106223>

**Important note**

To cite this publication, please use the final published version (if applicable).  
Please check the document version above.

**Copyright**

Other than for strictly personal use, it is not permitted to download, forward or distribute the text or part of it, without the consent of the author(s) and/or copyright holder(s), unless the work is under an open content license such as Creative Commons.

**Takedown policy**

Please contact us and provide details if you believe this document breaches copyrights.  
We will remove access to the work immediately and investigate your claim.



# The NW Amazonian Craton in Guainía and Vaupés departments, Colombia: Transition between orogenic to anorogenic environments during the Paleo-Mesoproterozoic

Amed Bonilla<sup>a,\*</sup>, Thomas Cramer<sup>a,b</sup>, Johan De Grave<sup>c</sup>, Brandon Alessio<sup>d</sup>, Stijn Glorie<sup>d</sup>, Salomon Kroonenberg<sup>e,f</sup>

<sup>a</sup> GEGEMA, Universidad Nacional de Colombia, Bogotá, Colombia

<sup>b</sup> Universidad Nacional de Colombia, Facultad de Ciencias, Departamento de Geociencias, Bogotá, Colombia

<sup>c</sup> Department of Geology, Ghent University, Krijgslaan 281.S8, WE13, 9000 Ghent, Belgium

<sup>d</sup> Department of Earth Sciences, School of Physical Sciences, University of Adelaide, Adelaide, Australia

<sup>e</sup> Delft University of Technology, Delft, Netherlands

<sup>f</sup> Anton de Kom University of Suriname, Paramaribo, Suriname

## ARTICLE INFO

### Keywords:

Guainía  
Vaupés  
U-Pb zircon  
Proterozoic  
Metamorphism  
Magmatism

## ABSTRACT

In order to improve our understanding of the NW-Amazonian Craton evolution, we present new petrographic, geochemical and geochronological analyses of 27 samples from the geotectonic Rio Negro-Juruena Province in eastern Colombia (Guainía and Vaupés departments). New LA-ICP-MS zircon U-Pb ages suggest that the oldest known rocks in Colombia are metamorphic rocks (migmatitic gneisses) with ages between ~ 1850 and ~ 1800 Ma, and gneisses and granitoids with ages between ~ 1800–1720 Ma which form part of the Mitú Complex, interpreted as the result of Statherian collisional and orogenic events (Querari Orogeny). Detrital zircons in low-grade *meta*-sedimentary sequences of the Tunuí Group (sandstones, conglomeratic sandstones and mudstones), that crop out over almost the entire basement, indicate older than ~ 1770 Ma source rocks. Intrusions of different suites of granitic rocks with syn- to post-collisional affinities suggest a termination of the collisional events between ~ 1600–1500 Ma which had affected the whole region, occasionally metasomatically overprinting parts of the Tunuí *meta*-sedimentary sequence. The recognizable metamorphic and magmatic-processes finish with ~ 1400–1340 Ma anorogenic granites without signs of tectonic deformation, resembling anorogenic granites in the Western Amazonian Craton in Brazil and the Parguaza Batholith in Venezuela. This study allows us to conclude that the basement records the collision of a continental arc (Rio Negro-Juruena Province) against the NW-Amazonian Craton (Ventuari-Tapajos Province) and its subsequent transition to anorogenic conditions in a continental rift setting long before the actual stable craton conditions.

## 1. Introduction

The Amazonian Craton (AMC) located in northern South America is one of the largest cratonic areas of the world, but its structure and evolution are still poorly understood. The Amazon-Solimões Basin splits it into a northern half, the Guiana Shield, and a southern half, the Central Brazilian Shield. The Guiana Shield extends from Brazil to Colombia, Venezuela, Guyana, Surinam and French Guyana (Fig. 1).

The AMC formed mainly during the Paleo-Mesoproterozoic and is bound to the east by the Neoproterozoic Araguaia Belt and to the west by the Phanerozoic Andean orogenic belt. Earlier subdivisions of the craton

in geochronological provinces (Cordani et al., 1979; Santos et al., 2000; Tassinari and Macambira, 1999; Teixeira et al., 1989) which suggested continental accretion to have taken place in general terms from east to west, have been discussed by recent models showing a general trend of younging southwards (Kroonenberg, 2019; Kroonenberg et al., 2016). One of the main orogenic events was the 2.26–1.95 Ga Trans-Amazonian Orogeny in the northern Guiana shield, that records ocean floor spreading, subduction and finally collision of older West-African and Amazonian Archean cores. Younger provinces accreted around 1.85–1.35 Ga at the western border of the Guiana Shield in the Rio Negro area in Colombia and Venezuela and the southeastern part of the

\* Corresponding author.

E-mail address: [abonillape@unal.edu.co](mailto:abonillape@unal.edu.co) (A. Bonilla).

<https://doi.org/10.1016/j.precamres.2021.106223>

Received 11 January 2021; Received in revised form 9 April 2021; Accepted 10 April 2021

Available online 10 May 2021

0301-9268/© 2021 Elsevier B.V. All rights reserved.

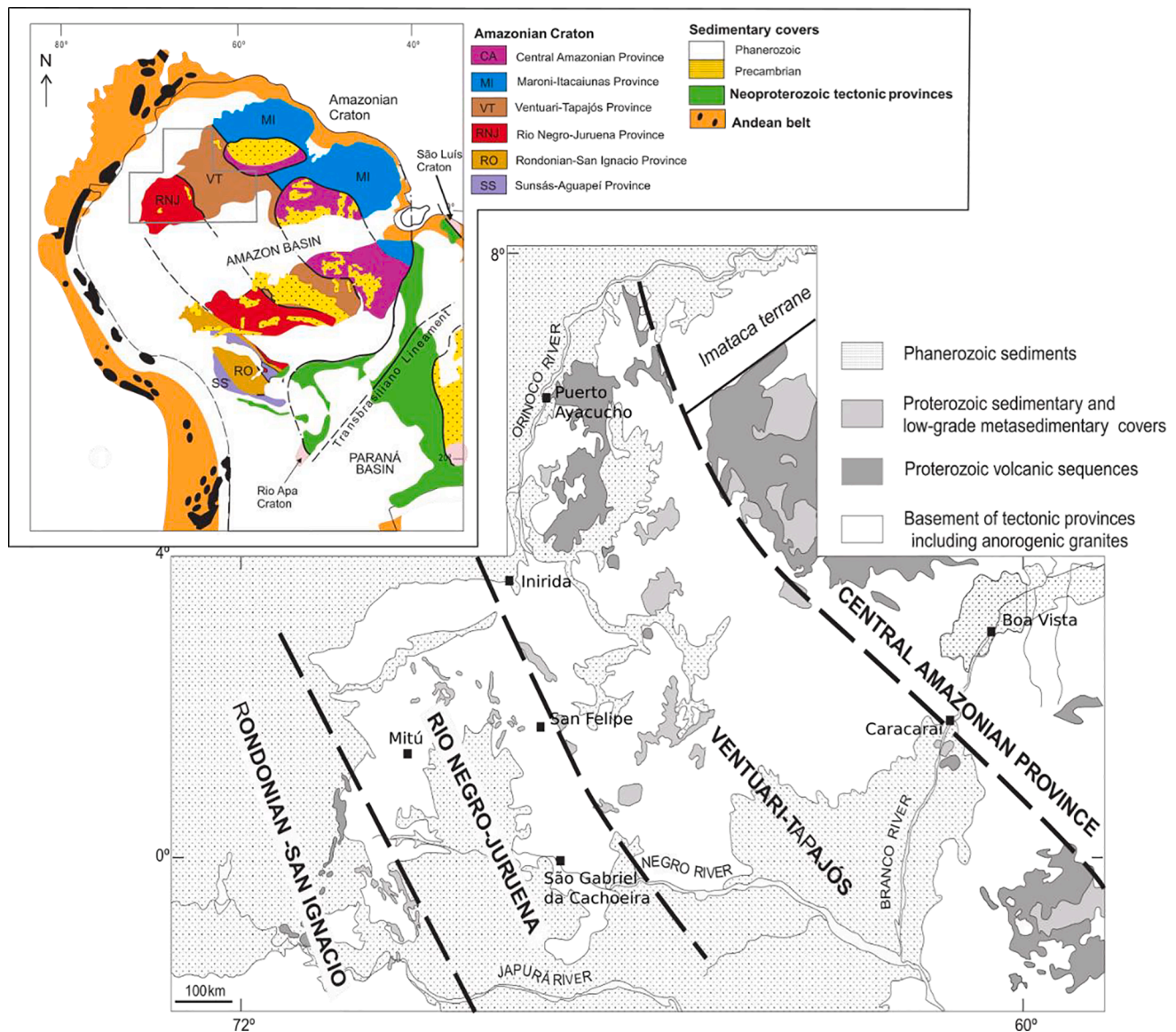


Fig. 1. Location of the study area (inset Fig. 3) within the NW Amazonian Craton after Cordani and Teixeira (2007).

Guiana Shield (Fig. 1).

Less than 10% of this Precambrian nucleus outcrops in the eastern Colombian departments Vichada, Guainía, Vaupés, Caquetá and Guaviare (Fig. 2). This is due to Cenozoic cover and tropical rain-forest, which hinders the recognition of boundaries between the geochronological provinces in the area. Earlier field observations, petrography, and geochemistry, in addition to Rb-Sr, K-Ar (mica, hornblende, whole-rock) and U-Pb (zircon conventional method) dating, provided an initial model for the geochronological development (Gaudette and Olszewski, 1985; Pinson et al., 1962; Priem et al., 1982). More recently, zircon U-Pb ages (Bonilla-Pérez et al., 2019; Cordani et al., 2016; Ibañez-Mejía, 2010) allowed to recognize the Rio Negro-Juruena Geochronological Province (1.8–1.55 Ga) in more detail as it is partially exposed in the Guainía and Vaupés departments of Colombia (Fig. 1, Fig. 2).

In the framework of this study, rocks outcropping mainly along riversides in Vaupés and Guainía departments were sampled (Fig. 2) and analyzed petrographically, geochemically and geochronologically. In particular, we provide 27 new LA-ICP-MS zircon U-Pb ages. These data are integrated with the results of geological reconnaissance during

several fieldtrips and existing work to further understand the evolution of the northwestern AMC, which is a key step in understanding the genesis and prospectivity of strategic mineral deposits in this region.

## 2. Geological setting and background

### 2.1. Regional geology

The Guainía and Vaupés departments in Colombia are part of the northwestern sector of the AMC, and more specifically of the Rio Negro-Juruena Province of the Guiana Shield according to the classification of Tassinari and Macambira (1999) or to the Rio Negro Province according to Santos et al. (2000).

The Rio Negro-Juruena Province (RNJP) as described by Tassinari and Macambira (1999) and Tassinari et al. (1996) is located on the western side of the AMC involving the basement of southwest Venezuela, southeast Colombia and northwest Brazil. It was formed between 1.8 and 1.7 to 1.65–1.55 Ga ago. The protolithic rocks of granitic and meta-sedimentary composition were partly metamorphosed

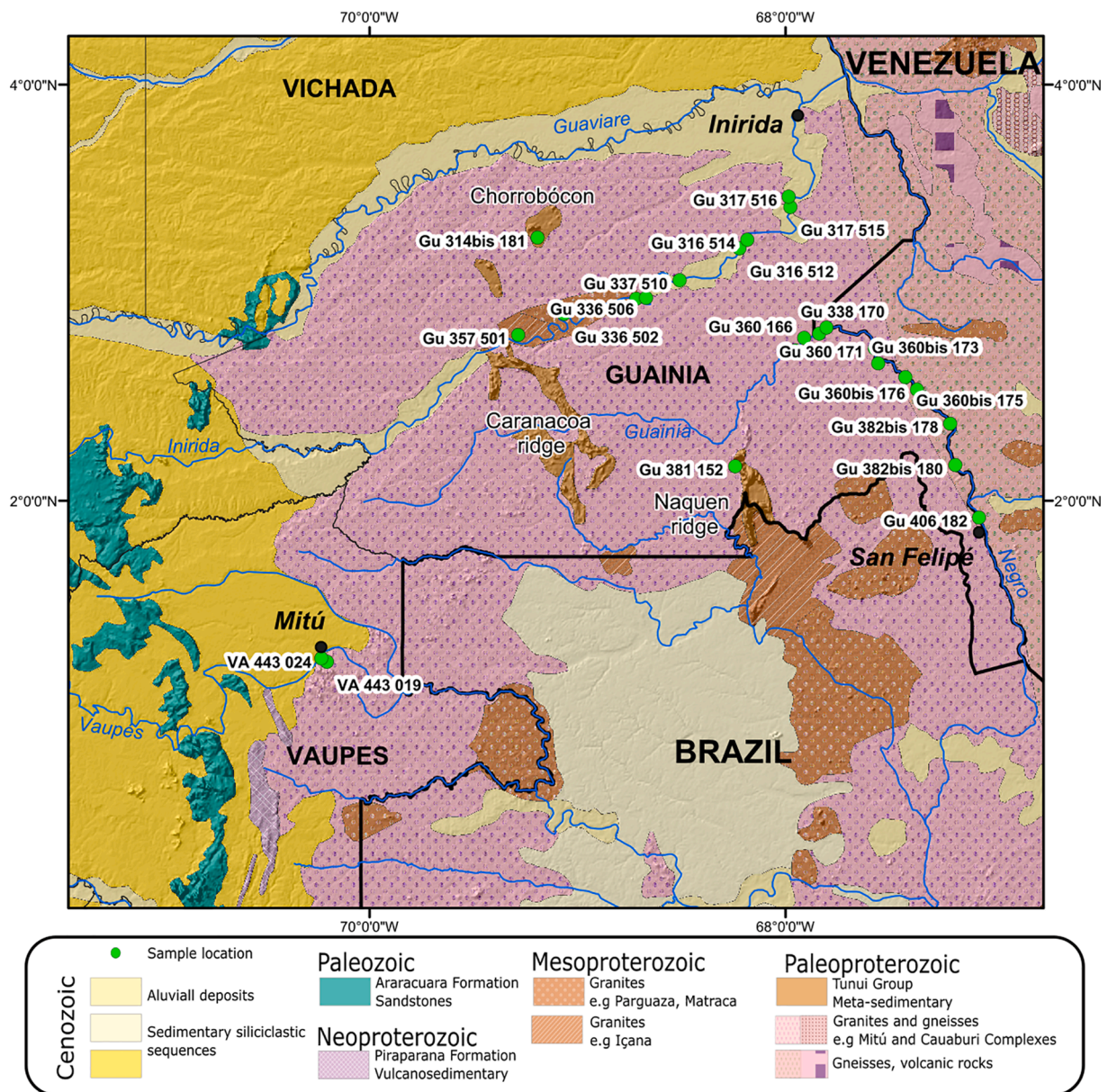


Fig. 2. Geological map with sampling locations used in this study along the Inirida River (GU 317- GU 357), the E-Rio Negro (or Guainía) River (from Naquén Ridge GU 381 near to San Felipe in the Colombian-Venezuelan border GU 406) as well as sampling points to the W near Mitú (VA 443) and Bócon to the N.

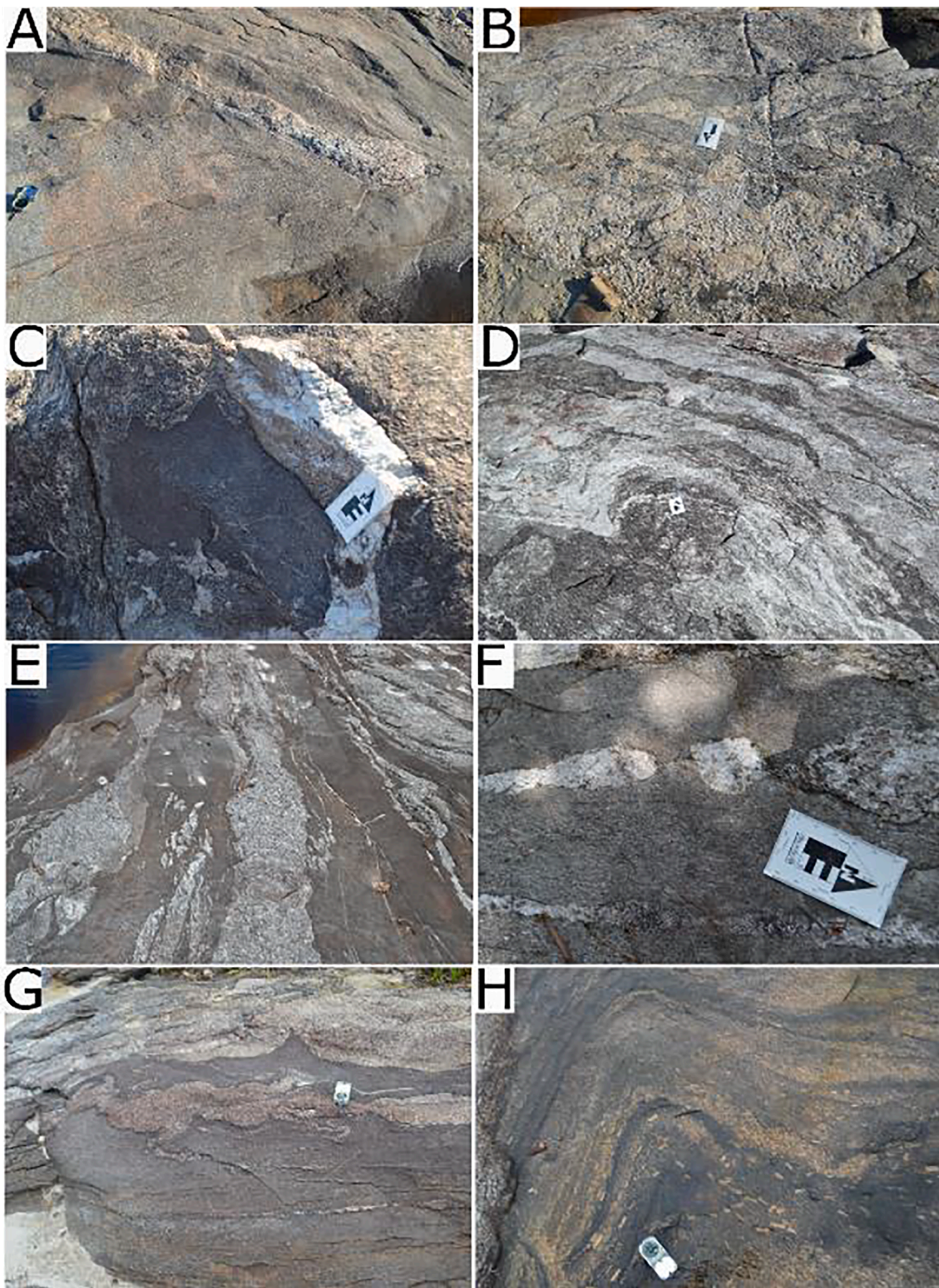


Fig. 3. A) “Inselberg” outcrop of the Mitú Complex granitoids (Mavicure hills on the Inirida River side); B) Escarpment morphology of the Naquén Mountain chain composed of Tunuí Group sandstones (Fig. 2).

**Table 1**

U-Pb ages reported for the study area and geologically similar surroundings after different authors (Bonilla-Pérez et al., 2019; Cordani et al., 2016; Gómez et al., 2015; Mendes et al., 2020; Veras et al., 2018) and authors cited therein.

Lithology	Locality/ coordinates	Sample code	Age (Ma)	Method	Reference
Colombia					
Gneiss			1480 ± 70	U-Pb zircon	Bogotá, 1981
Gneiss			1846 ± 45	U-Pb zircon	Bogotá, 1981
Matraca rapakivi granite	Matraca	MT-16	1343 ± 8	Zircon LA-ICP-MS	Bonilla-Pérez et al., 2016
	Guainía				
Orthogneiss	Naquen	J-127	1775 ± 7.7	SHRIMP Zircon	Cordani et al., 2016
	Guainía				
Orthogneiss	Cuaubén	PR-3141	1501.0 ± 9.5	SHRIMP Zircon	Cordani et al., 2016
	Guainía				
Orthogneiss	Araracuara	EP-2	1721.0 ± 9.6	SHRIMP Zircon	Cordani et al., 2016
	Caqueta				
Monzogranite	Mavicure	J-84	1507 ± 22	SHRIMP Zircon	Cordani et al., 2016
	Guainía				
Monzogranite	Naquen Guainía	J-159	1770 ± 40	SHRIMP Zircon	Cordani et al., 2016
Orthogneiss	Negro river	J-199	1796 ± 3.7	SHRIMP Zircon	Cordani et al., 2016
	Guainía				
Monzogranite	Caruru	HB-667	1778.0 ± 5.9	SHRIMP Zircon	Cordani et al., 2016
	Vaupés				
Orthogneiss	Tucunaré	AH-1213A	1736 ± 19	Zircon LA-ICP-MS	Cordani et al., 2016
	Vaupés				
Monzogranite	Mitu	AH-1231	1510 ± 26	Zircon LA-ICP-MS	Cordani et al., 2016
	Vaupés				
Monzogranite	Nabuquén	J-98	1752 ± 21	Zircon LA-ICP-MS	Cordani et al., 2016
	Guainía				
Orthogneiss	Cuduyari Vaupés	PR-3001	1769 ± 33	Zircon LA-ICP-MS	Cordani et al., 2016
Deformed syenogranite Araracuara	Araracuara	PR-3215	1756 ± 08	Zircon LA-ICP-MS	Ibañez-Mejía, 2010
	Caqueta				
Weakly sheared Syenogranite Araracuara	Araracuara	J-263	1732 ± 24	Zircon LA-ICP-MS	Ibañez-Mejía, 2010
	Caqueta				
Undeformed Granitoid Mitu	Mitu	AH-1216	1574 ± 10	Zircon LA-ICP-MS	Ibañez-Mejía, 2010
	Vaupés				
Undeformed granite Mitu	Mitu	PR-3092	1578 ± 27	Zircon LA-ICP-MS	Ibañez-Mejía, 2010
	Vaupés				
Taraira Granitoid	Taraira	AH-1419	1530 ± 21	Zircon LA-ICP-MS	Ibañez-Mejía, 2010
	Vaupés				
Syenogranite	Taraira	CJR-19	1593 ± 6	Zircon LA-ICP-MS	Ibañez-Mejía, 2010
	Vaupés				
Mitu Complex-granite	Mitu	PRA-4	1552 ± 34	U-Pb Zircon	Priem et al., 1982
	Vaupés				
Mitu Complex-granite	Cuaiari	Gu 403 125	1775–1783	Zircon LA-ICP-MS	Bonilla-Pérez et al., 2019
	Guainía				
Mitu Complex-granite	Cuaiari	Gu 404 134	1769–1800	Zircon LA-ICP-MS	Bonilla-Pérez et al., 2019
	Guainía				
Paragneiss	Cuaiari	Gu 403 123	1000–1800	Zircon LA-ICP-MS	Bonilla-Pérez et al., 2019
	Guainía				
Mitu Complex-granite	Cuaiari	Gu 403 135	1771 ± 4	Zircon LA-ICP-MS	Bonilla-Pérez et al., 2019
	Guainía				
Mitu Complex-granite	Cuaiari	Gu 404 130	1762 ± 4	Zircon LA-ICP-MS	Bonilla-Pérez et al., 2019
	Guainía				
Mitu Complex-granite	Cuaiari	Gu 404 133	1766 ± 4	Zircon LA-ICP-MS	Bonilla-Pérez et al., 2019
	Guainía				
Granite	Cuaiari	Gu 403 121	1550–1590	Zircon LA-ICP-MS	Bonilla-Pérez et al., 2019
	Guainía				
Granite	Cuaiari	Gu 403 124	1752 ± 5	Zircon LA-ICP-MS	Bonilla-Pérez et al., 2019
	Guainía				
Venezuela					
Macabana gneiss	Macabana	8699	1847 ± 65	TIMS Zircon	Gaudette and Olszewski, 1985
Minicea gneiss	Minicia	8697–8679	1859 ± 47	TIMS Zircon	Gaudette and Olszewski, 1985
Macabana gneiss	Macabana	8699	1823 ± 15	TIMS Zircon	Gaudette and Olszewski, 1985
Casiquiare tonalite	Casiquiare	6580–6085	1834 ± 17	SHRIMP Zircon	Tassinari et al., 1996
Brazil					
Iá-Mirim monzogranite	Sao Gabriel da Cachoeira	MS-63	1810 ± 9	SHRIMP Zircon	Santos et al., 2000
Cauaburi Complex	Caparro Mountain	MA21A	1813 ± 19	Zircon LA-ICP-MS	Veras et al., 2018
Taiuaçu–Cauera diatexite	Içana river	MA29	1798 ± 11	Zircon LA-ICP-MS	Veras et al., 2018
Taiuaçu–Cauera diatexite	Içana river	MA44	1788 ± 11	Zircon LA-ICP-MS	Veras et al., 2018
Taiuaçu–Cauera diatexite	Cuairi river	TM-R-082	1782 ± 5.6	Zircon LA-ICP-MS	Mendes et al., 2020
Igarapé Tocandira Granite	Cuairi river	TM-R-079B	1770 ± 8.4	Zircon LA-ICP-MS	Mendes et al., 2020
Cauaburi Complex	Içana river	TM-R-026	1759 ± 5.3	Zircon LA-ICP-MS	Mendes et al., 2020
Cauaburi Complex	Cuairi river	GH-R-006	1763 ± 7	Zircon LA-ICP-MS	Mendes et al., 2020
Cauaburi Complex	Caparro Mountain	GH-R-016	1754 ± 7	Zircon LA-ICP-MS	Mendes et al., 2020



**Fig. 4.** Megascopic migmatitic gneisses structures A) elongated enclaves oriented concordant to foliation in GU-360-171; B) convolute folds of leucosome in biotite-muscovite-sillimanite paragneiss in GU-360bis-172; C) agmatic structure in GU-360bis-172, fragments of granodiorite surrounded by paragneiss and leucosome; D) layered and folded structure in heterogeneous migmatitic gneiss in GU-360bis-175; E-F) Pegmatoidal leucosomes in gneisses showing pinch-and swell-structure in GU-360bis-177; G) fragmentation of leucosomes between a partial mobilized gneiss in GU-182bis-181; H) layered and folded structures in GU-316-513 showing some K-feldspar megacrysts (Raudal Cuale).

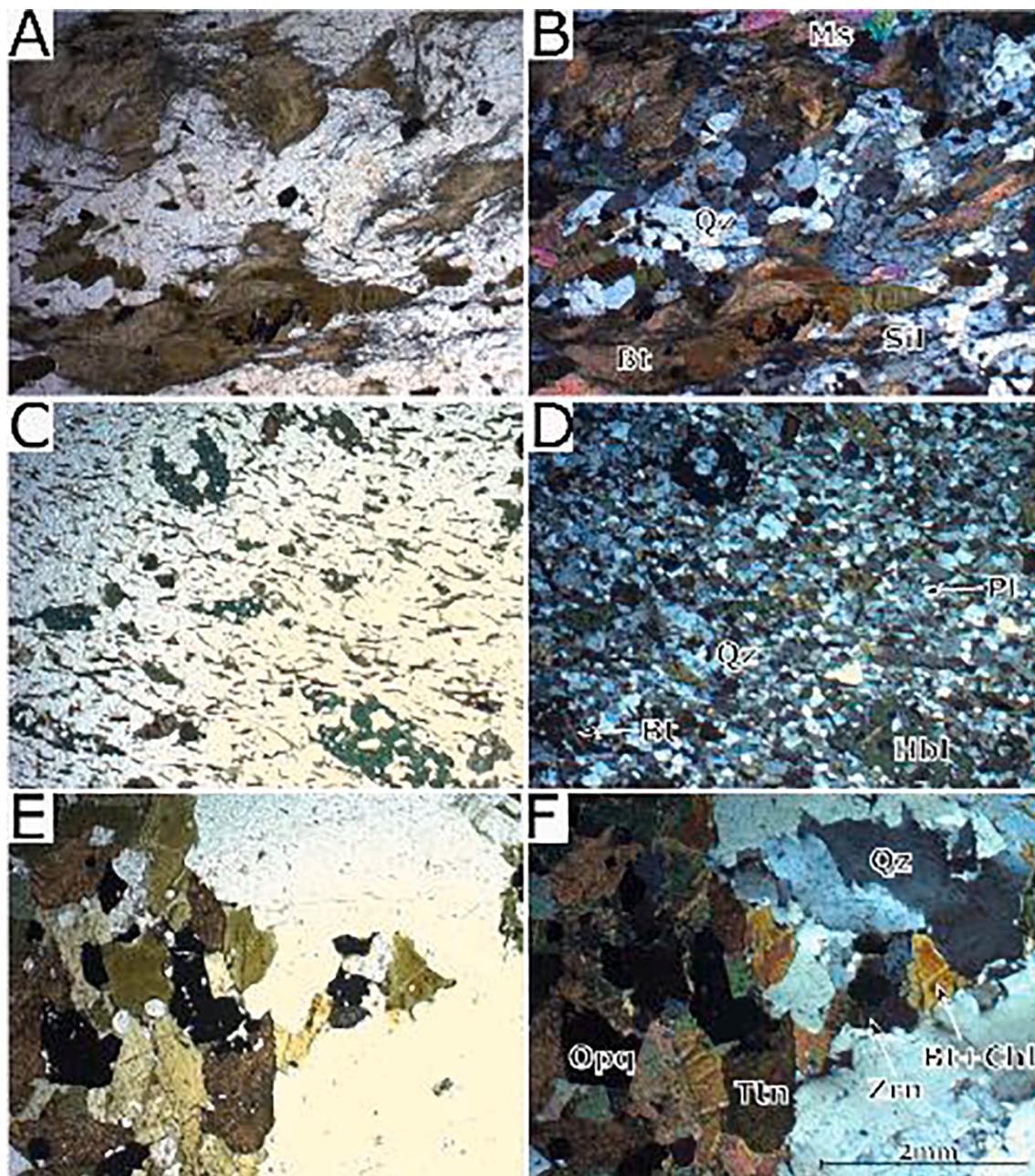


**Fig. 5.** Thin section microphotographs of migmatitic gneisses, left PPL, right XPL. A-B) large biotite bands with quartz crystals and lesser muscovite and sillimanite in sample GU-360bis-173; C-D) partly altered hornblende and biotite in a finer grained plagioclase and quartz matrix in sample GU-382bis-178 E-F) Coarser biotite (partly altered to chlorite) with quartz crystals and opaques, titanite and zircon in sample GU-382bis-180.

from amphibolite to granulite facies with anatectic gneisses to migmatites as characteristic lithologies. In Brazil the RNJP was named the Cauaburi (1.81–1.78 Ga) and Querari Complex (1.74–1.70 Ga) (CPRM, 2006; Santos, 2003), while in Colombia it is known as the Mitú Migmatitic Complex (Galvis-Vergara et al., 1979) or Mitú Complex (López et al., 2007) with ages between 1.8 Ga and 1.5 Ga (Bonilla-Pérez et al., 2019; Cordani et al., 2016; Ibanez-Mejía et al., 2011).

## 2.2. Mitú complex

The Mitú Migmatitic Complex as proposed by Galvis-Vergara et al. (1979) was described as a set of metamorphosed sedimentary and igneous rocks with migmatitic textures of leucogranitic (alaskite) to monzonite composition; previously it had been named “Basement group” (Gansser, 1954) and “Guayanes Complex” (Pinheiro et al., 1976). Bruneton et al. (1982) described this complex in Colombia in more detail in the eastern Guainía department, differentiating metamorphic rocks

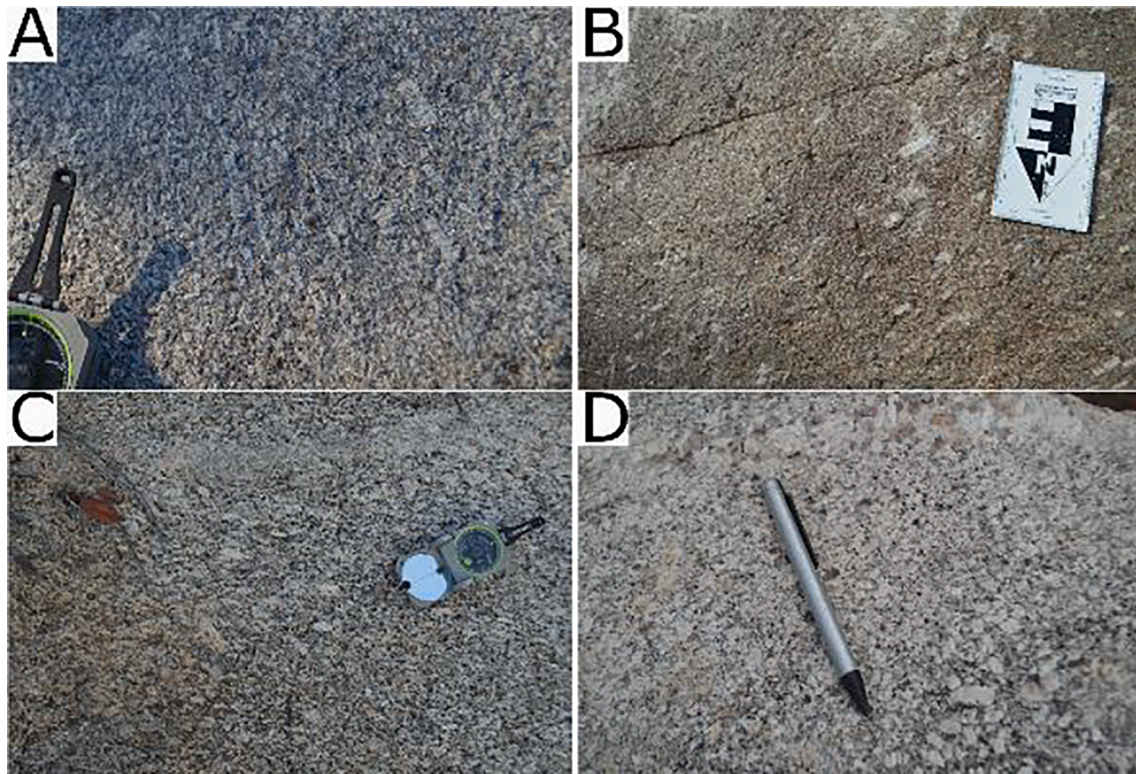


Fig. 6. Porphyritic granitoids of different grain size, color and matrix, where large K-feldspar crystals are either rather isolated (A and B), or may form part of a flow structure or accumulate to rapakivi-similar aggregates. A) GU-338-170 B) GU-360-162 C) GU-336-506 D) Tabular and ovoid K-feldspars in GU-406-182, similar to rapakivi texture but without plagioclase rings.

(e.g. biotite-gneiss with feldspar and granite-gneiss) and different types of granitoids with ages between 1.7 and 1.45 Ga (Priem et al., 1982). The latter often appear as inselbergs in the current landscape (Fig. 3A). Kroonenberg (2019) suggest that the Mitú Complex is only composed of metamorphic and migmatitic rocks with ages between 1.85 and 1.72 Ga.

López et al. (2007) proposed to use the term Mitú Complex instead of Mitú Migmatitic Complex (Galvis-Vergara et al., 1979), emphasizing that most rocks there are in fact not migmatites. However, Rodríguez-García et al. (2011a) continued using the term Mitú Migmatitic Complex when differentiating petrographically and geochemically three recognizable units of the basement near Mitú City: (1) Monzogranite (monzogranite) de Mitú, (2) Granofels de Pringamosa, and (3) Neis (gneiss) del Yi. Mendoza (2012) correlates the Colombian part of the basement with the 1630 to 1842 Ma old Venezuelan Casiquiare Domain, which is composed of gneisses, migmatites and tonalites. This author hereby assumes that the complex is totally allochthonous, initially belonging to the Supamo Granitic Complex which was affected by the Transamazonian Orogeny and the ~ 1.5 Ga Parguazan and ~ 1.2 Ga Nickerian events (Mendoza, 2012).

The Brazilian part of the Mitú-Complex basement has been subdivided into two zones: the paragneisses and migmatites were assigned to be part of the Taiuaçu-Cauera Complex (Mendes et al., 2020; Veras et al., 2018) whereas gneisses and metagranitoids as part of the Cauaburi and Querari complexes (CPRM, 2006) because each one represents different accretionary orogens (Almeida et al., 2011). The Cauaburi Complex has been subdivided into the Santa Izabel do Rio Negro, Cumati and São Jorge facies (Carneiro et al., 2017). The gneisses of the Santa Izabel do Rio Negro and Cumati facies are metaluminous and of calc-

alkaline affinity; in turn, the rocks of the São Jorge facies are peraluminous and of alkaline affinity. They vary from (amphibole) - biotite granodiorites over monzogranites (Cumati and Santa Izabel do Rio Negro facies), to spessartine-bearing biotite monzogranites (São Jorge facies). The age of the Cauaburi Orogeny has been constrained to be between 1.77 and 1.81 Ga (zircon U-Pb) (Almeida et al., 2013; Veras et al., 2018). In contrast, the Querari Complex is composed of calc-alkaline orthogneisses and metagranitoids with younger ages between 1.74 and 1.70 Ga. Both complexes were generated as result of juvenile magmatic arc accretion and their geochemical signature is compatible with granites generated in compressional settings, similar to the Mitú Complex gneisses and granites (Almeida et al., 2013; Bonilla-Pérez et al., 2019; Carneiro et al., 2017; Mendes et al., 2020; Veras et al., 2018).

Younger granites with ages ~ 1.5 Ga have been recognized as separate units in Brazil; S-type granites of the Içana and Igarape Reilau suites and I-type granites of the Uaupés (CPRM, 2006). In Colombia, similar granites with ages between 1.6 and 1.5 Ga (Bonilla-Pérez et al., 2019; Cordani et al., 2016; Ibanez-Mejía et al., 2011) intruded into the Mitú Complex and represent magmatism from its partial melting (Bonilla-Pérez et al., 2019) and some of them show A-type geochemical patterns (Rodríguez-García et al., 2011b; Rodríguez-García et al., 2011a).

K-Ar ages of 1.21–1.38 Ga and Rb-Sr ages of 1.15–1.34 Ga obtained from micas from granites and gneisses outcropping near the Inírida River (Cordani et al., 2016; Priem et al., 1982) are much younger than what are considered “normal” ages of the Mitú Complex. They are in fact very similar to K-Ar ages of 1.26–1.32 Ga and Rb-Sr of 1.15–1.4 Ga obtained near the Vaupés River, which were interpreted as expressions

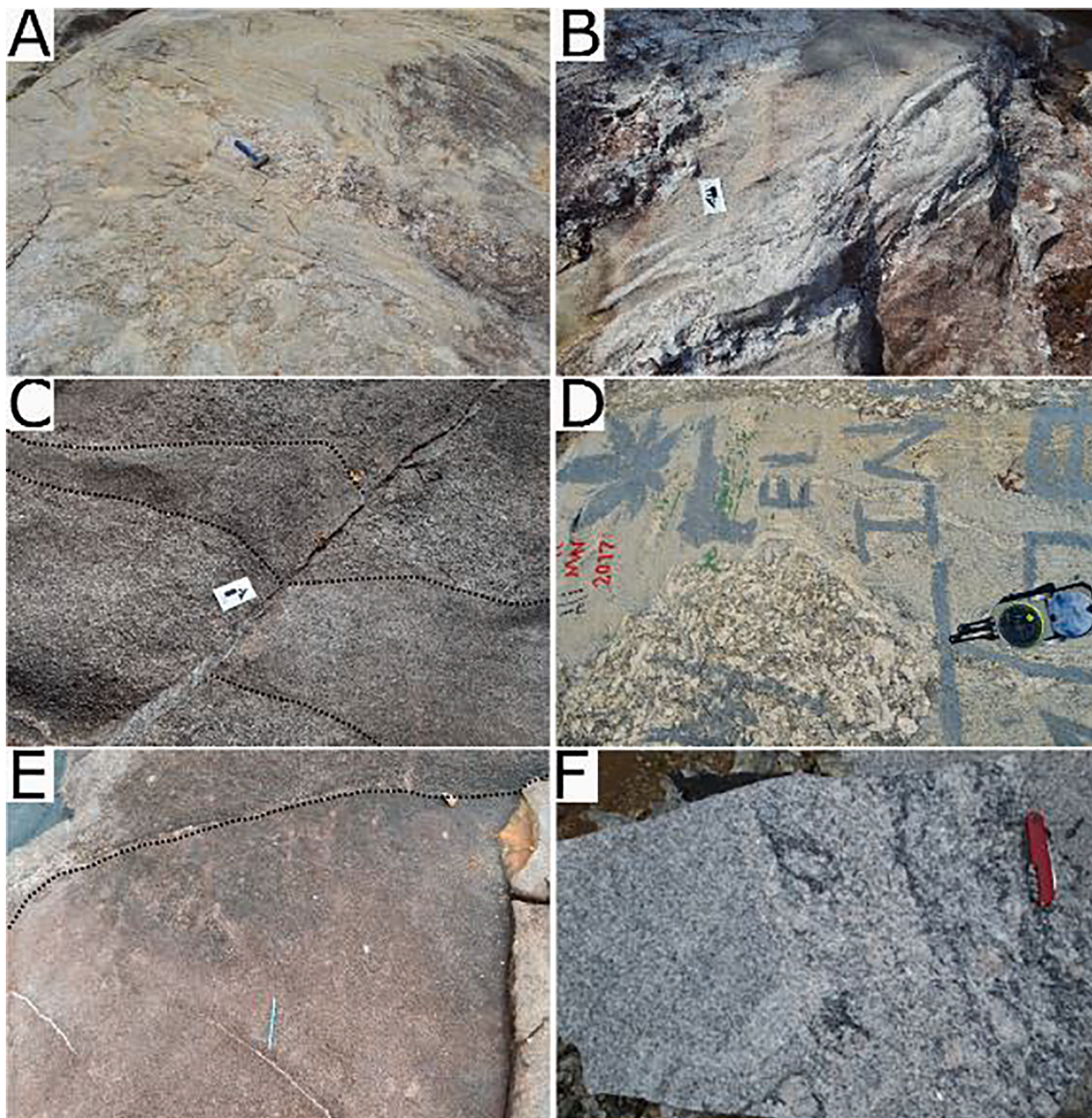


**Fig. 7.** Granitoids with homogenous texture showing sharp contacts against porphyritic textural group A) fine-grained granite with pegmatitic dikes showing shear deformation in GU-360-160 B) irregular pegmatitic dikes of quartz, K feldspar and biotite in GU-360-162 C) dextral fault filled with quartz in GU-360-167 D) transitional boarder between porphyritic to fine-grained granites GU-316-512 E) fine-grained granite at Mavicure hills GU-317-516 F) Two-micas granite near Mitú city (VA-443-024) showing a transitional zone to coarse-grained texture.

of thermal or metamorphic resetting events  $\sim 1.3$  Ga ago (Cordani et al., 2016; Priem et al., 1982), as found also in several other places of the Guiana shield.

### 2.3. Tunuí group

At several localities, deformed, low-grade *meta*-sedimentary sequences composed of protolithic sandstones, conglomeratic sandstones and mudstones overly the basement. They form elongated NW-trending mountain chains (e.g. Taraira, Caranacoa and Naquén mountain ranges – Fig. 3B, Fig. 2). Similar rocks were defined in Brazil as the Tunuí Group (Paiva, 1928), but in Colombia other names were used such as the Maimachi Formation (Renzone, 1989a) or La Pedrera Formation (Galvis-Vergara et al., 1979; Galvis-Vergara, 1993) with depositional ages between 1.55 and 1.81 Ga (Santos et al., 2003). Paiva (1928) described this unit of quartzites with sericite on the Içana River (Tunuí waterfall), and several authors, including ourselves, propose to interpret the Maimachi

and La Pedrera Formation in Colombia as part of the Tunuí Group (Bonilla-Pérez et al., 2019; Montalvao and Fernandes, 1975; Toussaint, 1993). The lithology of this unit varies slightly from locality to locality: (a) the northern Naquén mountain for example consists of quartz sandstones and claystones (Bruneton et al., 1982), (b) the central Naquén and Caranacoa mountains of sericite-quartz sandstone and *meta*-conglomerates (Galvis-Vergara, 1993), (c) in the Machado-Taraira mountains, phyllites, quartzites and conglomerates dominate (Carrillo, 1995), (d) in the Caparro mountain range quartzites, biotite-chlorite-muscovite quartzites and phyllite are present (Montalvao and Fernandes, 1975), and finally, (e) near the Yurupari waterfall in the southern Caranacoa mountains we found quartzites with tourmaline as result of contact metasomatism by a granite intrusion of  $\sim 1600$  Ma age (Bonilla-Pérez et al., 2019). Hence, we interpret the Caranacoa, Naquén and Taraira mountain chains as part of the *meta*-sedimentary Tunuí Group.

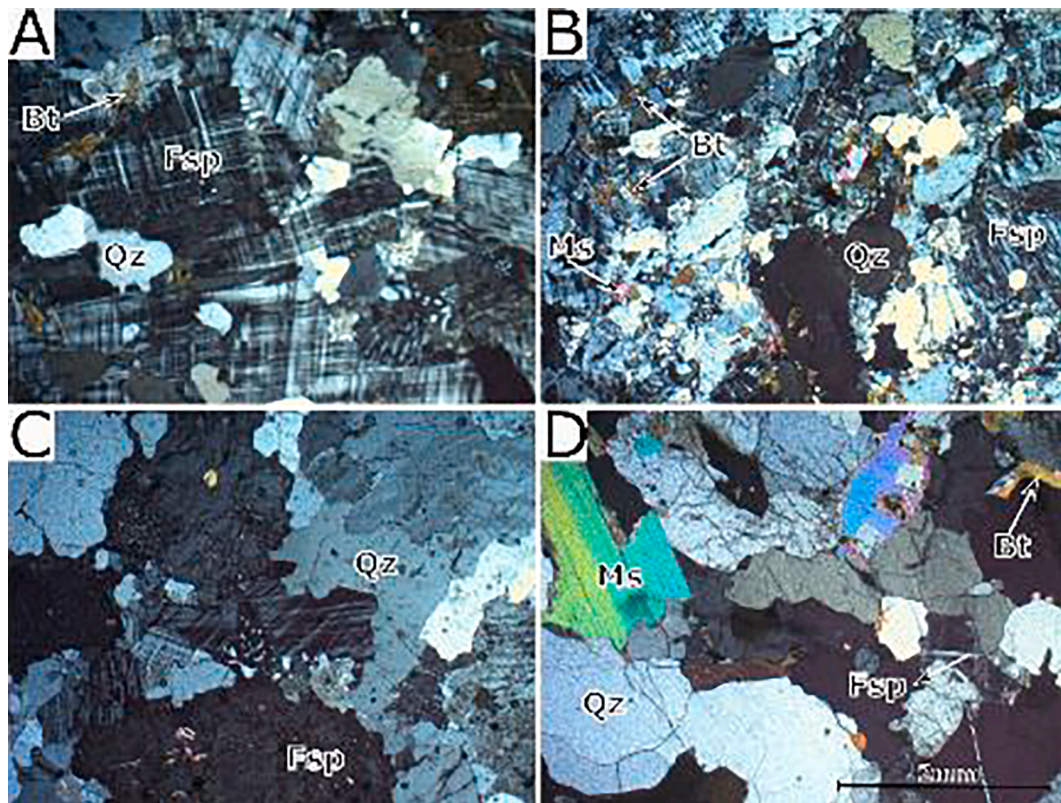


Fig. 8. Microtextures in the granitoids A) GU-336-506 B) GU-317-516 C) GU-360-164 D) GU-338-168.

#### 2.4. Rapakivi granites

All over the NW Amazonian Craton, large plutons such as the Parguaza, Surucucu and Mucajai granites reflect intense A-type magmatism (Fig. 2) with ages between 1.4 and 1.55 Ga (Bonilla-Pérez et al., 2013; Gaudette et al., 1978; Heinonen et al., 2012). Most of them are syeno- to monzogranites and alkali feldspar granites often exhibiting a characteristic rapakivi texture. Another anorogenic granite found in the Guainía department in Colombia is the considerably younger Matraca granite (Fig. 2) with LA-ICP-MS zircon U-Pb ages of 1.34 Ga (Bonilla-Pérez et al., 2016). Apart from the rapakivi texture that is made up of > 1 cm feldspar crystals showing no preferential orientation, and an ovoid to tabular habit, the Parguaza and Matraca granites also show homogeneous fine-grained and aplitic zones as well as antiperthitic, perthitic, myrmekitic and poikilitic textures. Gaudette et al. (1978) suggested that the Parguaza granites reflect a within-plate extension event affecting about 1500 to 1400 Ma ago a large part of the northwestern and

southern Guyana shield. Rifting was accompanied by high temperature gradients, slow migration of magma from subcrustal depths and deep faulting through the lithosphere. Rapakivi textures are thought to be the outcome of extremely slow cooling, with large age differences, within a single intrusion (Dempster et al., 1994).

#### 3. Materials and methods

For this study, rock samples were obtained during a detailed geological field-trip along the Inírida river between Zancudo and Inírida town in the northern part of the Guainía Department, and the Guainía-Río Negro river between San José and San Felipe town in the southeast part of the Guainía Department, and also in the surroundings of Mitú City in the Vaupés Department (Colombia, Fig. 2). Twenty-seven of these samples were analyzed petrographically, geochemically and dated by means of LA-ICP-MS zircon U-Pb geochronology. Sample preparation, petrographical and geochemical analyses were carried out in the

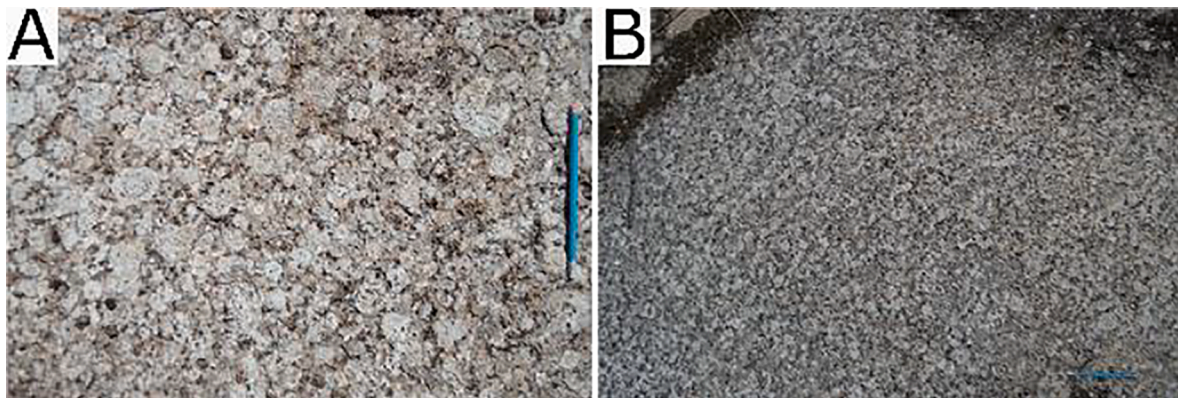


Fig. 9. (A) Homogeneous *Matraca rapakivi granite* with large pterilite feldspars. (B) Site GU-357-502. Pen for scale.



**Fig. 10.** Quartzites with interlayering mica-schists, showing sedimentary relict structures such as bedding. Sample site GU-314Bis-181 in N-Caranacoa Mountain (in Fig. 2).

Mineralogy & Petrology laboratory at Ghent University (Belgium) and UNAL Bogotá. U–Pb zircon data were measured at Adelaide Microscopy (Australia).

The zircon grain separates for U–Pb isotopic analyses were extracted from crushed rock samples using conventional magnetic and density separation techniques. Zircon separates were hand-picked and mounted in epoxy resin, which were then polished to expose the grains. Zircon images were obtained with an FEI Quanta 600 Scanning Electron Microscope and attached Gatan cathodoluminescence (CL) detector. CL imagery was used to identify compositional domains within grains prior to U–Pb analysis. Zircon grains were analyzed for U–Pb isotopes using an Agilent 7900 ICP-MS and ASI RESOLUTION M50 Laser Ablation System. Ablation of zircon was performed in a He-atmosphere with a frequency of 5 Hz. A spot size of 30  $\mu\text{m}$  was used for all analyses. A total acquisition time of 60 s was used, consisting of 30 s of background acquisition followed by 30 s of sample ablation. The reference material GJ-1 ( $^{206}\text{Pb}/^{238}\text{U} = 608.5 \pm 0.4 \text{ Ma}$  (Jackson et al., 2004)) was used as the primary reference for all zircon analyses. Plešovice ( $^{206}\text{Pb}/^{238}\text{U} = 337.13 \pm 0.37 \text{ Ma}$  (Sláma et al., 2008)) and 91,500 ( $^{206}\text{Pb}/^{238}\text{U} = 1065.4 \pm 0.6 \text{ Ma}$  (Wiedenbeck et al., 1995)) were used as secondary references. Plešovice yielded a 95% concordant average  $^{206}\text{Pb}/^{238}\text{U}$  age of  $338.5 \pm 1.4 \text{ Ma}$  ( $2\sigma$ ,  $n = 15$ ). 91,500 yielded a 95% concordant average  $^{206}\text{Pb}/^{238}\text{U}$  age of  $1057.5 \pm 3.4 \text{ Ma}$  and  $^{207}\text{Pb}/^{206}\text{Pb}$  age of  $1056 \pm 13$  ( $2\sigma$ ,  $n = 30$ ). U–Pb data were reduced using IOLITE (Paton et al., 2011) and plotted using Isoplot (Ludwig, 2012). For calculating the weighted averages, the less than 10% discordant (without inherited or Pb loss zircon ages)  $^{207}\text{Pb}/^{206}\text{Pb}$  ages were used and all individual spot dates discussed throughout this article are calculated using  $^{207}\text{Pb}/^{206}\text{Pb}$  values.

Major and minor elements on 25 samples were determined using inductively coupled plasma optical emission spectrometry (ICP-OES) at the Mineralogy & Petrology laboratory of Ghent University (Belgium), following protocol no. 14869-2:2002(E) of the International Organization for Standardization (2002) on a Varian 720-ES ICP-OES apparatus, whereas trace element geochemistry and Al, Ca, Fe, K, Mg, Mn were determined by means of ICP-MS in Actlabs Colombia using Code UT-4 Total Digestion ICP-MS. ICP-MS-Detection limit for Na, Mg, Al, K, Ca and Fe is reported as 0.1%, for B as 20 ppm, for V, Cr, Mn, Zr, Sn, Ba 1 ppm; for Li, Ni, Pb 0.5 ppm; for Zn, Rb, Cu, Sr 0.2 ppm; for Cd, Hf, Er, Be, Ho, Co, Se, Ga, As, Y, Nb, In, Sb, Te, La, Ce, Pr, Nd, Sm, Gd, Tb, Dy, Ge, Tm, Yb, Lu, Ta, W, Th, U, for Ag, Cs, Eu, Mo, Tl 0.05 ppm; for Bi 0.02 ppm; for Hg 0.01 ppm and for Re 0.001 ppm. The results are listed in Table 3.

Data treatment and interpretation was done using Excel spreadsheet and the GCDkit software (Janoušek et al., 2006).

A geochronological database (Table 1) of mainly zircon U–Pb ages relevant for this study obtained during the last 40 years from basement

**Table 2**

Comparison of ICP-OES and ICP-MS measurements, indicating a rather good agreement between both methods.

ELEMENT	ICP-OES wt.%	ICP-MS wt.%
Al	7.89	7.41
Ca	0.90	1.02
Fe	2.35	2.34
K	4.02	3.91
Mg	0.36	0.35
Mn	0.03	0.03
Na	1.57	1.80
Sum	17.11	16.83

rocks in E-Colombia, SW-Venezuela and NW-Brazil consists mainly of ages from the Colombian Radiometric Database (Gómez et al., 2015), but also newer ages by Cordani et al. (2016) from samples collected by Galvis-Vergara et al. (1979), Cordani et al. (2016) and by Bonilla-Pérez et al. (2019) are included.

#### 4. Field work observations and petrography

As the rivers continue to be the main communication arteries in the Colombian East, this sampling can only be undertaken efficiently during the dryer summer season, when the lower water levels permit a better rock exposure and sampling of material which during the long rain season normally is not accessible.

##### 4.1. Medium to high-grade metamorphic rocks

Metamorphic rocks represent less than 30% of all exposed basement rocks in the study area and consist mainly of gneisses outcropping occasionally along the main rivers (Vaupés, Inírida and Guainía-Río Negro rivers, Fig. 2). Locally well-developed megascopic migmatite structures result from high-grade metamorphism and anatexis with polyphase-deformation textures like augen (ophthalmic), agmatic, folded, stromatic, schlieren and pygmatic features (Fig. 4).

The samples GU-360-171 to GU-360bis-173 in the easternmost study area along the Guainía-Río Negro River (Fig. 2) correspond to migmatitic paragneisses with strongly banded and folded textures in a general N35E (GU-360-171 and GU-360bis-173) and N75W (GU-360bis-172) trend. The mesosomes consist of quartz, K-feldspar megacrysts, plagioclase, biotite, muscovite and accessory sillimanite, zircon, apatite and opaque minerals (Fig. 5A, B). Biotite-muscovite-sillimanite are arranged in dark layers which appear as bands in thin-section, plagioclase may exhibit myrmekite and antiperthite textures and is often replaced by sericite alteration, whereas biotite alters to chlorite. Main minerals in the leucosomes are quartz, K-feldspar and sparse biotite. Stretched elliptical mafic enclaves are of varied sizes and oriented according to foliation (Fig. 4A). Rare pegmatitic dikes are composed of quartz, alkali feldspar and may contain, as in GU-360bis-173, also tourmaline.

Migmatitic gneisses at sites GU-360bis-174 to GU-382bis-180 have a granodioritic mesosome with augen and well-developed folded texture where quartz, K-feldspar, plagioclase and biotite predominate. Hornblende was observed in sample GU-382bis-178 (Fig. 5C, D) and calcite in GU-360bis-175. Accessory minerals are apatite, opaques, titanite and zircon (Fig. 5E, F). Secondary chlorite, sericite and epidote are alteration products of biotite and plagioclase (Fig. 5C, D). Some elongated ribbon quartz has been observed as well as varied grain sizes and sutured grain boundaries of quartz crystals. Less common than K-feldspar are megacrysts of plagioclase which are often deformed and myrmekitic. The syenogranite to K-feldspar granite leucosome is composed of K-feldspar 56%, quartz 31% and plagioclase 11%, whereas muscovite, apatite, zircon and biotite may account for  $\sim 3\%$  as in GU-360bis-175. This can lead to stromatic pegmatitic dikes with convolute folds and pinch-and-swell structure or pygmatic texture (Fig. 4). Quartz exhibits undulatory extinction and sutured grain boundaries while the plagioclase is

Table 3

Geochemical analyses of rocks from the eastern Colombian basement, Rio Negro-Juruena Province; Main elements are in %, minor and trace elements are in ppm.

Sample#	GU -317-515	GU-360Bis-175	GU-360Bis-175-L	GU-360Bis-176	GU-360Bis-176-II	GU-357-501	GU-336-506	GU-336-505	GU-316-512	GU-316-514	GU-317-516	GU-338-170	GU-382Bis-178
Rock type	Monzogranite	Migmatite	Migmatite	Migmatite	Migmatite	Syenogranite	Quartz syenite	Quartz syenite	Monzogranite	Paragneiss	Monzogranite	Monzogranite	Migmatite
Al <sub>2</sub> O <sub>3</sub>	15.25	15.9	15.64	16.25	15.83	15.36	15.12	14.71	14.9	13.02	14.29	16.54	15.97
CaO	2.26	2.68	0.38	2.42	2.99	1.14	1.99	1.36	1.26	0.85	0.39	1.83	3.3
Fe <sub>2</sub> O <sub>3</sub>	4.58	6.02	0.51	5.98	6.46	2.03	4.39	2.98	3.36	1.24	2	2.91	6.84
K <sub>2</sub> O	3.67	3.25	6.84	4.52	3.48	4.73	4.35	4.73	4.84	3.6	5.72	3.73	3.74
MgO	0.83	1.06	0.13	1.09	1.44	0.34	0.68	0.41	0.6	0.13	0.34	0.81	1.4
MnO	0.05	0.07	0.01	0.06	0.07	0.05	0.07	0.04	0.04	0.02	0.02	0.05	0.08
Na <sub>2</sub> O	2.47	2.7	1.73	2.06	2.13	2.53	2.41	2.21	2.11	2.44	1.58	2.76	2.29
P <sub>2</sub> O <sub>5</sub>	0.07	0.1	0.01	0.11	0.09	0.03	0.14	0.06	0.13	0.01	0.06	0.14	0.11
SiO <sub>2</sub>	65.9	67.75	74.16	66.1	65.19	72.92	69.42	72.88	71.31	73.11	74.37	70.3	66.01
TiO <sub>2</sub>	0.52	0.65	0.06	0.71	0.64	0.19	0.59	0.34	0.46	0.1	0.29	0.32	0.74
LOI	0.19	0.36	0.52	0.75	0.83	0.3	0.52	0.32	0.76	0.52	0.89	0.76	0.3
B												30	
Li	71.9	96.3	16.8	84.4	78	62	51.1	31.8	36	37.9	30.3	104	179
Na	1.99	2.32	1.43	1.67	1.77	2.19	2.05	1.79	1.8	1.99	1.31	2.24	1.78
Mg	0.46	0.62	0.08	0.58	0.83	0.18	0.37	0.22	0.35	0.07	0.19	0.39	0.71
Al	7.63	8.31	8.01	7.88	7.65	7.85	7.25	7.01	7.41	6.47	7.43	7.01	7.22
K	3.8	3.77	4.32	3.2	3.66	4.59	4.4	4.32	3.91	2.83	4.66	2.57	3.51
Ca	1.78	2.27	0.33	1.87	2.37	0.95	1.6	1.06	1.02	0.67	0.32	1.39	2.42
Cd													0.1
V	23	33	5	41	36	15	26	32	36	6	21	37	31
Cr	78	139	23	116	205	12	62	31	69	75	33	27	106
Mn	433	577	107	452	605	382	540	382	385	150	186	425	631
Fe	3.05	4.17	0.48	3.87	4.18	1.44	2.92	2.06	2.34	0.94	1.51	1.93	4.24
Hf	3.6	4.4	0.6	2.4	3.1	5.5	1.3	2.8	0.5	4.8	0.2	3.5	3.3
Ni	8.4	10.4	1.4	11	15.3	1.2	4.3	1.9	4.6	1.3	1.5	7.4	12.1
Er	3.9	4.1	2.2	5	4.1	3.2	5	2.8	4.4	1.2	2.5	1	5
Be	4.7	3.3	1.7	2.9	5.3	4.9	5.3	4.4	2.8	2	1.3	5.1	9.8
Ho	1.4	1.5	0.7	1.9	1.5	1.2	2	0.9	1.6	0.5	1.1	0.4	1.9
Hg	20			10	10	20		10	30		20	20	20
Ag		0.06	0.11	0.05	0.29	0.08	0.08	0.11	0.21	0.13	0.08	0.19	0.09
Cs	11.6	13.5	11.8	29.8	13	9.09	5.62	4.8	2.89	5.19	3.03	15.4	100
Co	9.2	11.9	1.2	11	13.8	2.4	5.6	4.3	5.2	1	2.9	6.1	14.6
Eu	1.5	1.7	0.6	1.9	1.6	0.9	1.6	1.7	1.2	0.4	1.6	0.7	2.3
Bi	0.14	0.16	0.09	0.78	0.51	0.04	0.18	0.12	0.02	0.08	0.02	0.36	1.37
Se										0.1		0.1	
Zn	55.9	71	13	65.8	71.3	45.9	77.5	53.2	59.7	19.7	34.6	50.2	70.1
Ga	14.3	13.6	13.7	13.9	14.2	15.8	17	13.1	15.7	14.4	10.3	15.6	15.1
Rb	244	252	242	220	206	320	281	271	304	221	257	142	239
Y	36.8	40.3	16.9	47.6	37.9	31	46	24.4	40.9	12.4	26.5	11	46.3
Zr	140	168	19	126	118	192	106	227	76	142	37	137	128
Nb	0.2	0.2	8	0.3	0.6	23.3	1.6	6.8	16	7.4	4.7	12.9	0.3
Mo	0.32	0.79	12.6	0.54	1.91	1.3	0.89	3.22	6.44	7.48	4.41	0.81	0.5
Sn			2			4	1	1	5	6	4		
Ba	836	774	479	826	707	410	507	781	540	231	816	552	631
La	46.6	53.6	8.5	93.9	56.2	81.7	62.8	173	81.4	37.8	97.3	28.9	118
Ce	102	117	15.7	192	123	165	163	275	187	87.6	205	71.8	218
Pr	11	13.3	2.3	21.2	13.7	17.9	19	24.9	22.4	9.3	24.3	7.1	27.5
Nd	40.6	49.9	8.8	78.2	52.3	62	80.2	75.8	86.3	33.8	89.9	28	103
Sm	7.4	8.4	2.5	12.6	9.2	10	16.3	11.3	14.2	6.4	14.6	4	16.1
Gd	6.5	7.4	2.1	11	8.2	7.2	12.5	7.5	10.3	4.7	10.4	3.5	12.8
Tb	0.9	1	0.4	1.4	1	0.9	1.5	0.7	1.3	0.6	1.2	0.4	1.4
Dy	6.1	7	3.1	9	7.1	6	9.8	4.7	8.5	3	6.5	2.1	8.9
Cu	10.4	10.9	2.3	38.6	5.2	5.7	18.1	6.7	9.9	1.3	2.9	8.5	14.8
Tm	0.6	0.6	0.4	0.7	0.6	0.5	0.7	0.5	0.7	0.2	0.3	0.1	0.8

(continued on next page)

Table 3 (continued)

Sample#	GU -317-515	GU-360Bis-175	GU-360Bis-175-L	GU-360Bis-176	GU-360Bis-176-II	GU-357-501	GU-336-506	GU-336-505	GU-316-512	GU-316-514	GU-317-516	GU-338-170	GU-382Bis-178
Rock type	Monzogranite	Migmatite	Migmatite	Migmatite	Migmatite	Syenogranite	Quartz syenite	Quartz syenite	Monzogranite	Paragneiss	Monzogranite	Monzogranite	Migmatite
Yb	3.9	4.1	2.4	4.6	3.8	3.3	4.7	3.2	3.9	1.3	2	0.9	4.7
Lu	0.5	0.6	0.3	0.6	0.5	0.4	0.6	0.5	0.5	0.2	0.3	0.1	0.6
Ta			0.3			2.1	0.2	0.4	0.8	0.1	0.2	1.1	
Sr	104	113	109	113	133	96.6	103	154	120	213	131	139	101
W	0.1	0.1	2	0.1	0.2	0.6	0.3	1.2	2.6	4.7	1.2	1	0.3
Re	0.001			0.001	0.001			0.001					
Tl	1.4	1.45	1.72	1.46	1.08	1.92	1.75	1.63	2.13	1.51	1.86	1	1.49
Pb	36.3	34.8	67.4	35.7	25.1	45.8	52.5	49.4	62.6	64.7	62.3	26.4	29
Th	34.4	54.4	12.4	51.3	22.3	58.5	82.9	133	59.3	43.7	78	11.9	27.9
U	8.1	6.7	15.1	4.5	3.2	14.2	14	16.1	28.7	13.6	5.5	3.1	7.3
Sample#	GU-182Bis-180	GU-406-182	GU-366-502	GU-337-510	GU-338-168	GU-360-161	GU-360-166	GU-360-171	GU-360-171-II	GU-360-171-III	GU-360Bis-173	GU-360Bis-173-II	
Rock type	Migmatite	Monzogranite	Rapakivi granite	Monzogranite	Monzogranite	Syenogranite	Syenogranite	MigmSill	MigmSill	MigmSill	MigmSill	MigmSill	
Al <sub>2</sub> O <sub>3</sub>	15.31	15.16	18.48	14.62	15.49	15.24	15.54	17	16.96	16.34	16.83	14.02	
CaO	0.89	2.65	3.13	1.02	1.07	0.6	0.97	2.81	1.34	1.72	0.91	0.77	
Fe <sub>2</sub> O <sub>3</sub>	1.53	5.76	2.95	2.65	2.59	0.89	1.76	4.24	5.01	4.8	6.54	5.61	
K <sub>2</sub> O	5.39	3.99	3.59	4.74	4.48	5.71	4.85	3.27	3.32	3.38	3.12	2.86	
MgO	0.16	0.96	0.28	0.42	0.44	0.13	0.31	1.54	1.13	1.08	1.68	1.27	
MnO	0.02	0.08	0.05	0.05	0.05	0.01	0.04	0.05	0.06	0.06	0.07	0.05	
Na <sub>2</sub> O	2.24	2.5	0	2.17	2.35	2.14	2.44	2.63	2.15	2.9	2.13	1.9	
P <sub>2</sub> O <sub>5</sub>	0.03	0.25	0.07	0.06	0.13	0.04	0.13	0.08	0.08	0.1	0.05	0.05	
SiO <sub>2</sub>	73.84	66.61	67.25	73.59	71.65	74.21	73.73	65.04	66.5	67.89	67.71	71.42	
TiO <sub>2</sub>	0.13	0.81	0.35	0.24	0.32	0.06	0.18	0.47	0.51	0.49	0.58	0.53	
LOI	0.42	0.45	0.42	0.8	0.79	0.94	0.58	0.57	1.96	0.54	0.83	0.76	
B						30		30		20		20	
Li	23	51.1	43.9	34	67	20.1	56.4	101	56.8	61.1	79.5	60.5	
Na	1.94	1.95	3	1.85	1.97	1.84	1.95	2.08	1.83	2.32	1.86	1.55	
Mg	0.09	0.5	0.12	0.24	0.25	0.07	0.17	0.7	0.62	0.56	1.15	0.67	
Al	7.8	7	8.14	7.33	7.51	7.98	7.41	5.72	8	7.5	8.68	6.9	
K	4.93	3.74	3.81	4.24	4.38	3.77	4.3	1.6	3.26	2.15	3.53	2.01	
Ca	0.76	2	2.51	0.82	0.84	0.47	0.73	1.99	1.11	1.36	0.78	0.61	
Cd													
V	8	46	2	14	23	7	11	61	28	47	37	50	
Cr	26	44	22	61	11	23	29	74	81	79	65	104	
Mn	220	650	413	423	381	110	379	461	475	445	530	443	
Fe	1.17	3.67	2	1.89	1.83	0.7	1.24	2.78	3.4	3.12	4.52	3.69	
Hf	1.5	2.6	5	2.4	0.5	0.8	1.3	3.6	3.5	3.7	3.4	4.4	
Ni	1.3	4.9	0.6	2.8	1.5	0.6	1.7	17.9	13.3	12	35	29.6	
Er	2.2	11.4	4.6	1.2	2.3	1.8	1.6	1	1.2	1	0.9	0.8	
Be	2.4	4.5	8.3	1.4	3.7	1	3	2.9	4.7	2.6	1.7	2.3	
Ho	0.9	4.1	1.6	0.4	1	0.5	0.8	0.4	0.5	0.5	0.4	0.4	
Hg	40	20	30			20	20	20	30	30	10		
Ag	0.14	0.06	0.06	0.14	0.27	0.1	0.22	0.18	0.05	0.1	0.15		
Cs	4.23	8.36	2.62	4.12	5.82	3.73	20.4	7.94	10.3	9.89	19.3	15.5	
Co	1.5	8.6	2.4	2.8	3.3	1	1.9	11.3	9.9	8.6	15.3	12.4	
Eu	1	3.2	2.1	1.1	1.2	0.7	0.9	0.6	1.2	0.9	1.7	1.7	
Bi	0.12	0.16	0.15	0.12	0.03	0.05	0.06	0.22	0.03	0.07	0.58	0.17	
Se						0.1		0.1					
Zn	31.3	80.8	85.8	46.9	66.7	19.9	58.1	56.3	71.3	80.2	79.3	60.5	
Ga	14.7	12.1	21.6	13.5	19.6	13.9	17.3	15.1	15.2	19.4	12.3	10.4	
Rb	265	207	203	215	338	238	334	68.7	228	214	150	102	
Y	21.2	101	45.1	11.7	26.3	16.3	23.5	9.1	12.2	12.7	10.8	9.7	
Zr	68	130	175	62	162	29	77	143	135	143	130	177	
Nb	8.7	0.3	1.8	7.7	22.3	5.8	17.4	9.9	0.2	4.4	0.2	1.6	
Mo	3.85	2.63	0.42	6.6	0.84	1.56	2.59	2.08	0.25	2.72	0.11	0.72	

(continued on next page)

Table 3 (continued)

Sample#	GU-182Bis-180	GU-406-182	GU-366-502	GU-337-510	GU-338-168	GU-360-161	GU-360-166	GU-360-171	GU-360-171-II	GU-360-171-III	GU-360Bis-173	GU-360Bis-173-II
Rock type	Migmatite	Monzogranite	Rapakivi granite	Monzogranite	Monzogranite	Syenogranite	Syenogranite	MigmSill	MigmSill	MigmSill	MigmSill	MigmSill
Sn	1		2	1	3	2	3	3	6	6		
Ba	390	1150	809	495	356	392	290	704	690	316	979	978
La	57.4	65.4	28.1	84.9	120	7.8	116	16	38.9	44.8	53.6	53.2
Ce	126	189	68.3	184	268	15.9	251	47.5	89.7	102	117	116
Pr	13.9	26.1	7.9	20.4	33.1	1.6	30.5	4.6	9.8	11.4	13.1	12.8
Nd	49.1	107	34.6	73.7	122	6	107	18.3	38	42.1	49.4	48.2
Sm	9.1	23.5	7.5	10.4	23.9	1	24.5	3.3	6.3	7.4	9	8.4
Gd	6.5	17.5	7.3	6.2	13.2	1.3	14	2.7	5	5.6	6.1	6.1
Tb	0.8	2.5	1	0.5	1.3	0.2	1.5	0.3	0.6	0.6	0.6	0.6
Dy	4.7	18.2	7.5	2.6	6.5	2.1	6.4	2.1	3	3.2	3.3	2.8
Cu	3.2	27.3	2.2	2	9.6	1.3	3.6	21.6	8.6	8.1	87.5	27
Tm	0.3	1.8	0.7	0.2	0.3	0.3	0.2	0.2	0.2	0.2	0.1	0.1
Yb	2	11.1	4.7	1.2	1.8	2.3	1.2	1	0.9	0.9	0.7	0.5
Lu	0.3	1.4	0.6	0.2	0.2	0.3	0.2	0.1	0.1	0.1	0.1	0.1
Ta	0.3			0.2	1.3	0.3	1.1	0.9	0.1	0.2		
Sr	91.8	236	187	136	83	111	79	238	88.8	72.3	181	162
W	2.8	0.2	0.1	4.2	1.3	1.4	2.7	1.6	0.1	0.5	0.1	0.6
Re		0.006	0.001							0.247		
Tl	1.76	1.19	1.15	1.27	2.12	1.66	2.13	0.76	1.42	1.51	0.67	0.54
Pb	66.1	36.7	32.8	47.3	45.8	57.2	46.2	24.6	26.5	26.3	26.5	27.1
Th	63.5	39.6	6	75.6	101	4.2	102	5.1	14.9	20.2	19.8	18.9
U	11.7	7	2.7	12.7	9.2	7.3	5.1	1	3.6	5	3.7	3.4

altered to sericite.

An orthogneiss at Raudal Payara (site GU-336-508), composed of quartz, K-feldspar, plagioclase and biotite, exhibits S85W trending foliation/banding cut by some  $\leq 3$  cm-thick N5-15 W trending quartz veins. At locality GU-336-509, the metamorphic texture of the gneiss with a N80W trending banding is developed more strongly, as large eye-shaped K-feldspars form an “augen gneiss” texture, whereas finer-grained zones contain both less K-feldspar megacrysts and quartz.

At the Cuale and Zamuro rapids (GU-316-513 to GU-316-514), layered and folded augen paragneisses (Fig. 4H) show a monzogranitic composition and medium-grained texture of the light layers composed of quartz 40%, plagioclase 26% and K-feldspar 33%. Megacrysts surrounded by a finer grained quartz groundmass give the impression of a strong mylonitic texture with a general S85W trend, similar to the river waterfall orientation and some S60W trending pegmatitic dikes.

#### 4.2. Granitoids

Igneous rocks represent around 70% of the observed basement outcrops in the study area, and almost 95% of them are felsic. They can be subdivided into three megascopic textural groups: (a) porphyritic, (b) homogeneous and (c) rapakivi granitoids.

- (a) Porphyritic granitoids exposed along the Inírida and Guainía-Rio Negro rivers may behave very resistant to deep weathering, perhaps due to thin crust formation, and thus often form isolated “Inselberg” hills (Huggett, 2007) in the landscape (GU-317-516 to GU-317-517, Fig. 2). Their characteristic large euhedral to subhedral K-feldspars embedded in a finer matrix exhibit a tabular to ovoid habit and sometimes a preferred orientation (Fig. 6). Their syenogranite to monzogranite composition is in the range of 15–34% quartz, 24–52% K-feldspar, 26–28% plagioclase, and 6–11% biotite with varying accessory minerals content such as muscovite, apatite and zircon in sample GU-338-170 and titanite, pyrite, apatite and zircon in GU-406-182. Plagioclase may have developed myrmekite and reaction textures mostly along K-feldspars boundaries (Fig. 8A). Fluids prompted alteration of the biotite to chlorite and plagioclase to sericite. Monzogranite outcrops at Raudal Morroco (GU-336-506, Fig. 6) exhibit up to 3-cm-large K-feldspar phenocrysts and several biotite lenses containing smaller K-feldspar and quartz crystals, its general trend of S55-40 W is the same as the Inírida River direction in this section. Late magmatic processes express themselves in up to 2-cm-thick, S60W and S40E trending quartz vein clusters, but also up-to-5-cm thick, S40E and S20-30 W trending pegmatitic dikes. At sample sites GU-337-510 and GU-334-511, large K-feldspar with ovoid shapes  $\sim 1$  cm and magmatic foliation in N75W direction were observed. At Chorrobocón (GU-316-512) granitic rocks exhibit  $\sim 3$ -cm-large K-feldspar megacrysts and a S50-77 W trending poly-deformation, whereas quartz and K-feldspar pegmatitic dikes follow an E-W to N60W trend. Banding of fine grained lighter and biotite-rich darker layers is complemented by a fine-grained zone (Fig. 7D) potentially representing part of an intrusive suite or partial melting that probably also is source of considerable gold, REE- and tantalum mineralization which is base of artisanal mining activities by indigenous communities.
- (b) Among the homogeneous textural group, both coarse-grained and fine-grained granitoids of similar composition are distinguishable and can be found in “sharp” contact with the porphyritic textural group (Fig. 7) (Bonilla-Pérez et al., 2019). At sites GU-357-501 and GU-317-516 (Fig. 2), homogeneous two-mica syenogranites are composed of K-feldspar 47%, quartz 23%, plagioclase 22%, biotite 7% and muscovite 6% (Fig. 8B). However, the Mavicure inselberg granites (Fig. 2) show textural and compositional variations from porphyritic K-feldspar granite to fine-grained two-

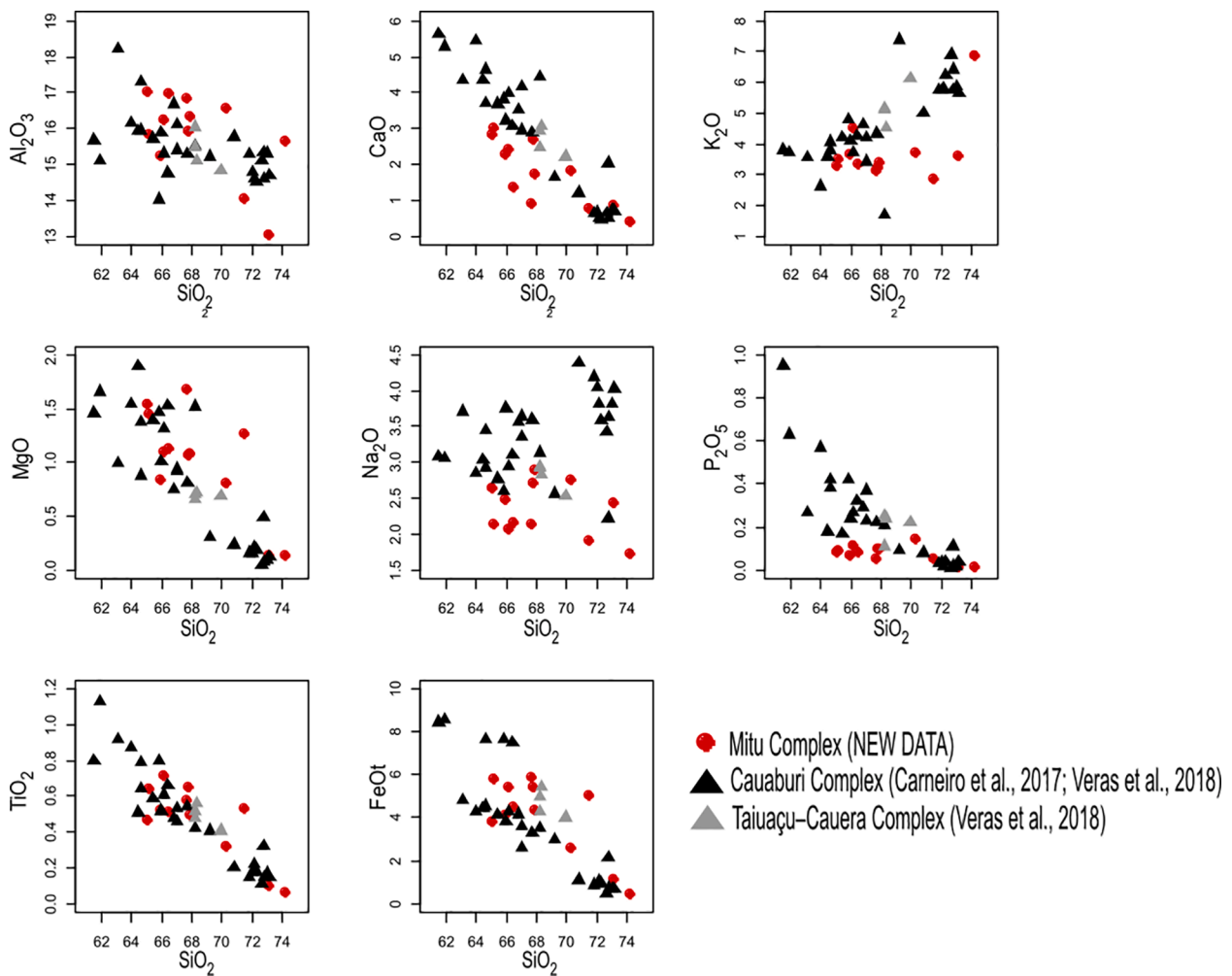


Fig. 11. Harker variation diagrams applied to metamorphic rock analyses in this study (red globes) and literature data (black and grey triangles) from the Cauaburi and Taiuaçu-Cauera Complex (Carneiro et al., 2017; Veras et al., 2018).

mica granite (Fig. 7E). In the Guainfa-Rio Negro River (GU-360-162 to GU-338-168), several two-mica granites show coarse-grained as well as fine-grained textures (Fig. 8C, D).

At site GU-316-512, the porphyry granite is intruded by a fine-grained monzogranite composed of quartz 32%, plagioclase 28%, K-feldspar 27% and biotite 9%, accessory minerals are muscovite, zircon and apatite. A two-mica monzogranite near Mitú City (VA-443-24, Fig. 2) varies from fine to medium-grained texture (Fig. 7F) and is composed of 26% quartz, 27% plagioclase, 24% K-feldspar, 12% biotite, 2% muscovite and minor opaque, zircon and apatite grains. Among macro textures, schlieren are abundant as well as microscopic myrmekite and perthite. The medium-grained monzogranite of sample VA-443-19 lacks muscovite but is enriched in K-feldspar and titanite.

(c) The only rapakivi granites found in the study area are located between Matraca and Danta Communities (Fig. 2), where they represent a single, large pluton along 40 km on the Inirida riverside (GU-357-502 to GU-336-504). They are described as the Matraca Rapakivi Granite (Bonilla-Pérez et al., 2016) with piterlite rapakivi texture (Fig. 9) and monzonite to granodiorite composition (quartz 25–27%, K-feldspar 22–31%, plagioclase 43–50%, biotite 3–7%). Perthite, antiperthite and myrmekite textures are well-developed. As far as possible to observe in the field, this body is homogeneous with sparse late magmatic expressions such as S20W trending pegmatitic dikes.

#### 4.3. Low-grade meta-sedimentary sequences

Meta-sedimentary outcrop samples were obtained from the west side of the Naquén Serranía (GU-381-153, Fig. 2) and the Bocon creek in the N-Caranacoa Serranía (GU-314Bis-181, Fig. 2), which are both well-known for their gold deposits (Goldfarb et al., 2001; Renzoni, 1989b). At both sites, the meta-sedimentary sequences show signs of low-grade metamorphism, and a varying structure and mineralogy. GU-381-153 corresponds to a N75W/55SW trending phyllitic meta-mudstone composed of micas and quartz, whereas at GU-314Bis-181, quartzite layers predominate and subordinately mica-schist with N48W/62NE trending relict sedimentary structures occur (Fig. 10).

#### 4.4. Whole rock geochemistry

All ICP-OES measurements sum, including LOI (lost of ignition, median 0.57%), nearly 100% with exception of samples GU-317-515, GU-360-171 and GU-316-514 which sum 95–96% (Table 3). Comparing results of Al, Ca, Fe, K, Mg and Mn, which were measured both by ICP-OES and ICP-MS, oxide to element transformed OES values without normalization to 100% sum for example in the case of sample GU-316-512 17113 ppm, whereas their MS-sum deliver 168300 ppm of a total of 170633 ppm. The comparison shown in Table 2 indicates a rather good agreement between both methods, but especially in the case

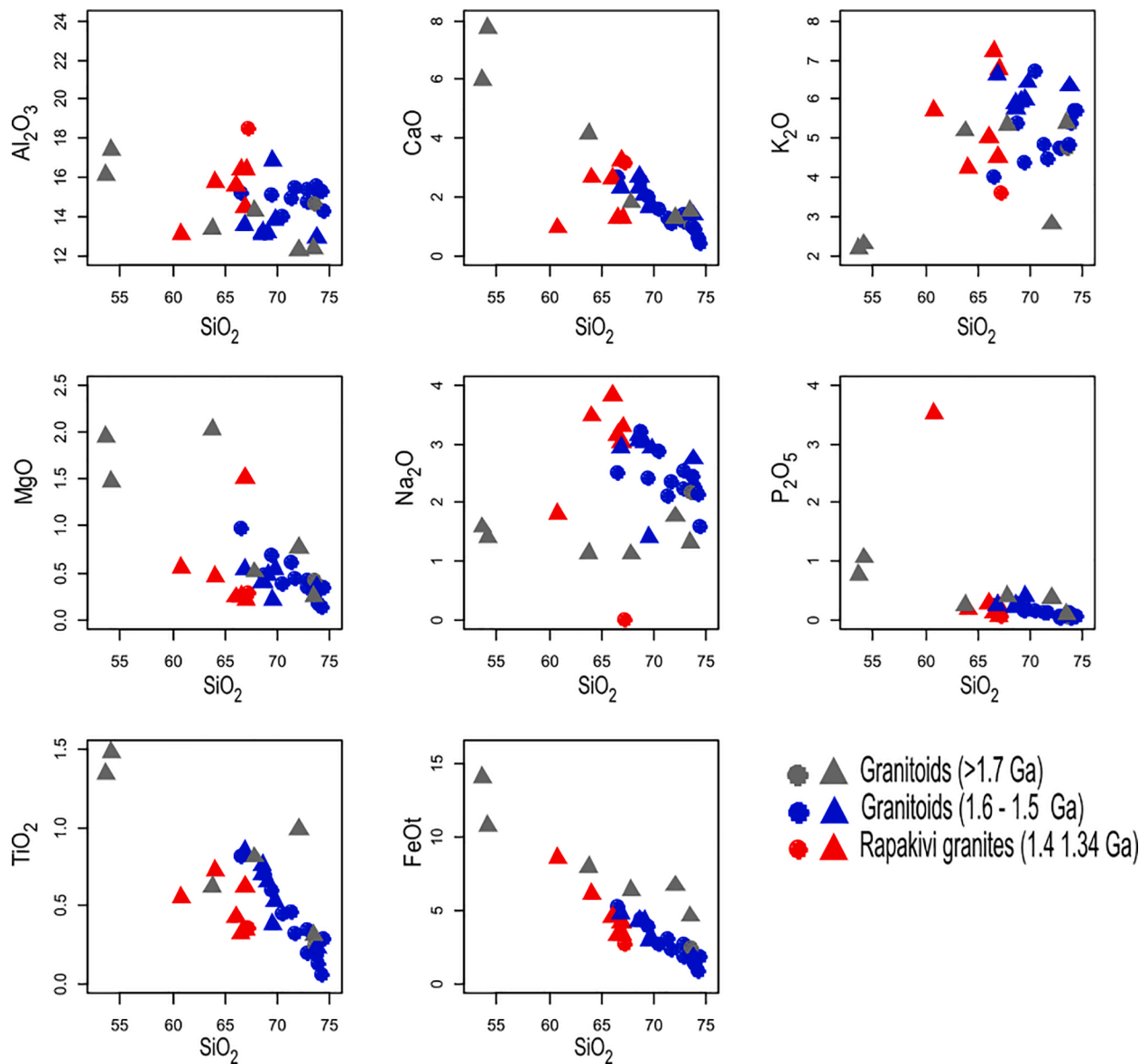


Fig. 12. Harker variation diagrams for major elements (filled circles for new data) together with former data (triangles) of Paleo- to Mesoproterozoic E-Colombian granitoids (Bonilla-Pérez et al., 2016, 2019).

of defining geochemical or petrotextonic borders or realms, the scatter suggests caution if the results are near one of those limits.

Geochemistry results of the migmatitic rocks, gneisses and granites (Table 3) indicate high concentrations of silica ( $\text{SiO}_2$  66.01–74.37%) and alkali elements ( $\text{Na}_2\text{O}$  1.58–2.76%,  $\text{K}_2\text{O}$  3.59–5.72%),  $\text{Al}_2\text{O}_3$  varies from 13.02% to 16.54%. Only the Al- and Ca-rich rapakivi granite (GU-366-502) with 18.48%  $\text{Al}_2\text{O}_3$  and very low  $\text{Na}_2\text{O}$  falls outside the general range. The total iron contents range from 0.89 to 5.76%  $\text{Fe}_2\text{O}_3(\text{t})$ , CaO from 0.39 to 3.13% whereas the other element contents are below 1%: MgO 0.13–0.96%,  $\text{TiO}_2$  0.06–0.81%, MnO 0.01–0.08%.

Among the high-grade metamorphic rocks, migmatitic paragneisses with sillimanite (in the mesosomes) are enriched in  $\text{Al}_2\text{O}_3$  and MgO (Table 3). The mesosomes of all migmatitic paragneisses have higher values of  $\text{TiO}_2$  and  $\text{Fe}_2\text{O}_3(\text{t})$  and lower values of  $\text{K}_2\text{O}$  than the igneous rocks, a difference to their granitic leucosomes which points to their residual or restite character. Mitú-Complex geochemistry exhibit a good correlation with the one of Cauaburi Complex from Brazil. Most of the major elements show a negative correlation between  $\text{SiO}_2$  and CaO,

MgO,  $\text{TiO}_2$ ,  $\text{P}_2\text{O}_5$  and  $\text{FeO}_t$  (weak for  $\text{Al}_2\text{O}_3$ ) and a positive one with  $\text{K}_2\text{O}$  (Fig. 11).

Major element compositions in the granitoids show a negative correlation between  $\text{SiO}_2$  and  $\text{Al}_2\text{O}_3$ , CaO, MgO,  $\text{TiO}_2$  and  $\text{FeO}_t$  whereas  $\text{P}_2\text{O}_5$  shows a low negative correlation trend with  $\text{SiO}_2$  and a positive one with  $\text{K}_2\text{O}$  (Fig. 12).

Among the trace elements, in general, plutonites, orthogneisses and migmatitic rocks without sillimanite are enriched in Rb and Y, whereas higher contents of Ni and Cr in metamorphic rocks are indicative of a more juvenile mafic origin. The depletion of Cr, Ni, Ba and Sr in the granitoids of the sample area as well as their enrichment in Rb, La and Ce (which could also indicate economic mineral fertility (Pohl, 2011)) may help to distinguish them from similar-looking metamorphic rocks (Table 3).

The new results as well as former studies from magmatic rocks of the Mitú Complex with ages between 1800 and 1700 Ma and younger granitoids between 1600 and 1500 Ma (Bonilla-Pérez et al., 2019; Cramer et al., 2011) and the Matraca rapakivi granite (Bonilla-Pérez

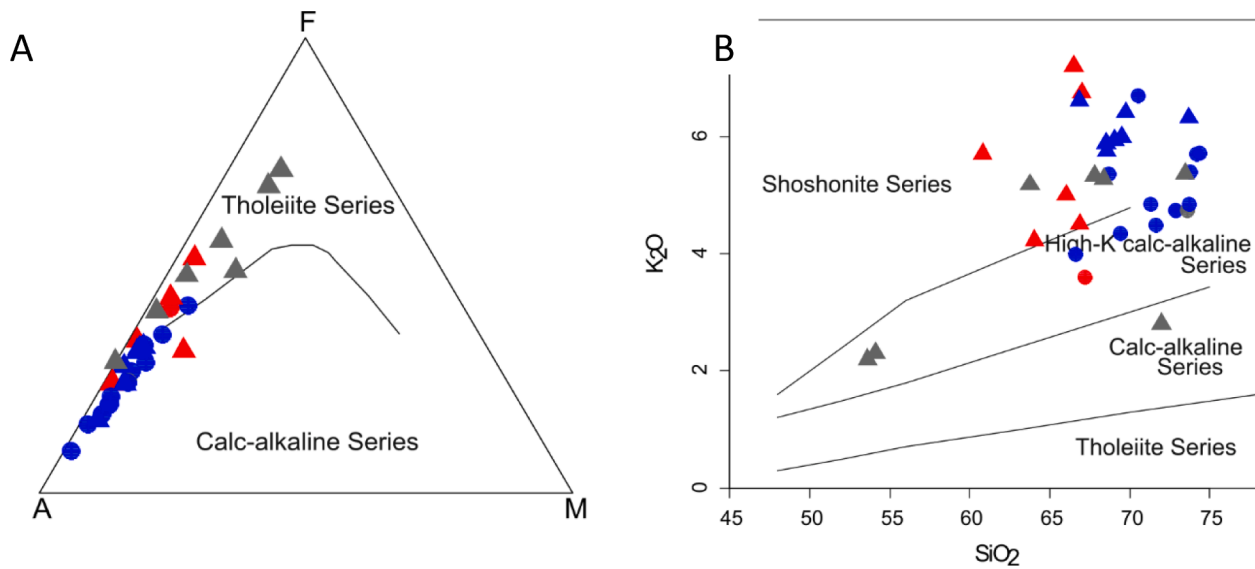


Fig. 13. A) AFM diagram (A = Na<sub>2</sub>O + K<sub>2</sub>O, F = FeOt, M = MgO) (Irvine and Baragar, 1971) B) K<sub>2</sub>O vs SiO<sub>2</sub> diagram of the studied samples after Peccerillo and Taylor (1976). Symbols same as in Fig. 12.

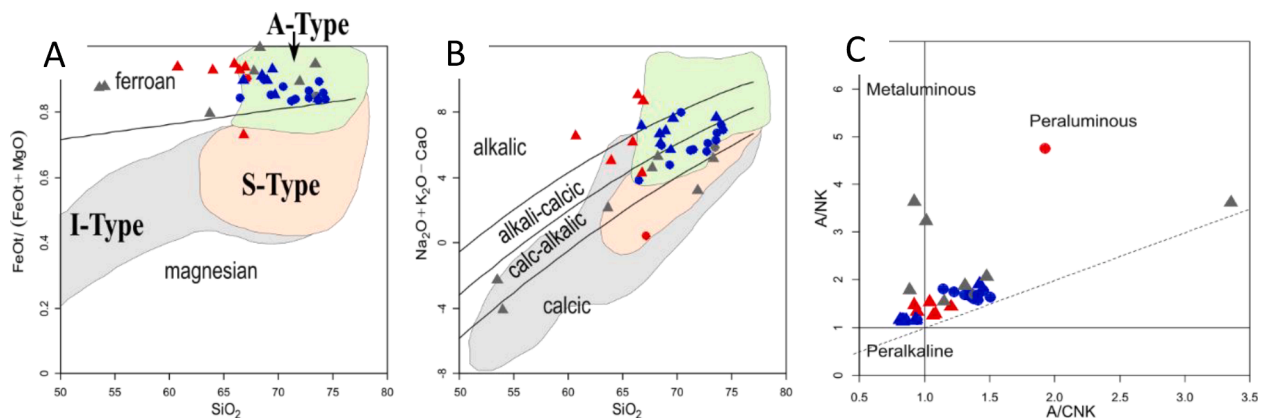


Fig. 14. Geochemical discrimination diagrams of studied rocks (shaded fields, literature data, triangles, current study and own data published before). A) Fe<sub>tot</sub>/(Fe<sub>tot</sub> + MgO) vs SiO<sub>2</sub> diagram (Frost et al., 2001), B) Na<sub>2</sub>O + K<sub>2</sub>O - CaO vs. SiO<sub>2</sub> diagram (Frost et al., 2001), C) A/NK vs. A/CNK (Shand, 1943). Symbols same as in Fig. 12.

et al., 2016), indicate a pronounced High-K to shoshonitic trend (Irvine and Baragar, 1971; Peccerillo and Taylor, 1976) (Fig. 13), fall into the ferroan field and follow the calc-alkaline trend after Frost et al. (2001), with a strong peraluminous character after Shand (1943) (Fig. 14).

In the diagrams of Whalen et al. (1987), most of the studied rocks are placed in the upper field of S & I-type granites but touching the transitional zone to A-type granites, equal for K & Na or Fe/Mg vs Ga/Al discrimination (Fig. 15A and B), whereas the Fe<sub>tot</sub>/(Fe<sub>tot</sub> + MgO) vs SiO<sub>2</sub> correlation (Frost et al., 2001) emphasizes an A-type affinity. However, the I- and S-type granite affinity shown in Fig. 15 is in accordance with data from other authors of Mitú Complex magmatic rocks. The rapakivi granite samples tend to be more alkaline and with ferroan A-type characteristic (Fig. 14).

From a geodynamic point of view, these rocks fall into the field of Volcanic Arc to Within Plate Granites (Fig. 15C, D) (Pearce et al., 1984). Syn-collisional to post orogenic conditions for the basement rocks are also indicated in the R<sub>1</sub>-R<sub>2</sub>-diagram (Batchelor and Bowden, 1985), where some granites and the rapakivi granite exhibit a late orogenic to anorogenic trend (Fig. 16). Using the source diagram by Laurent et al.

(2014), the I- and S-type granites point to a meta-sedimentary source, while the rapakivi granites suggest a high-K mafic source rock.

The CI-chondrite-normalized (McDonough and Sun, 1995) REE contents of nearly all samples exhibit clear upper continental crustal patterns (Rudnick and Fountain, 1995) with LREE-enrichment and both depletion and horizontal patterns of HREE relative to CI following a pronounced negative Eu-anomaly. The paragneiss GU-316-514 exhibits the most pronounced negative Eu-anomaly and is more strongly depleted in HREE (Fig. 17).

The sillimanitic migmatites GU-360-171 to GU-360Bis-173-II have rather high LREE, weak to no negative Eu-anomaly and steep depletion of HREE. The feldspathic pegmatitic leucosome of the migmatite sample GU-360Bis-175-L has very low REE-contents and lacks also the negative Eu-anomaly of the other migmatites but is enriched in Si and K, and depleted in typically mafic-environments compatible elements (Fe, Mg, Mn, Ca, Ba, Cr, V, Ni, Co, Zn, Cu, Bi). Th, Zr, Hf, Li are slightly decreased, U, W, Pb increased in comparison to the corresponding mesosome GU-360Bis-175.

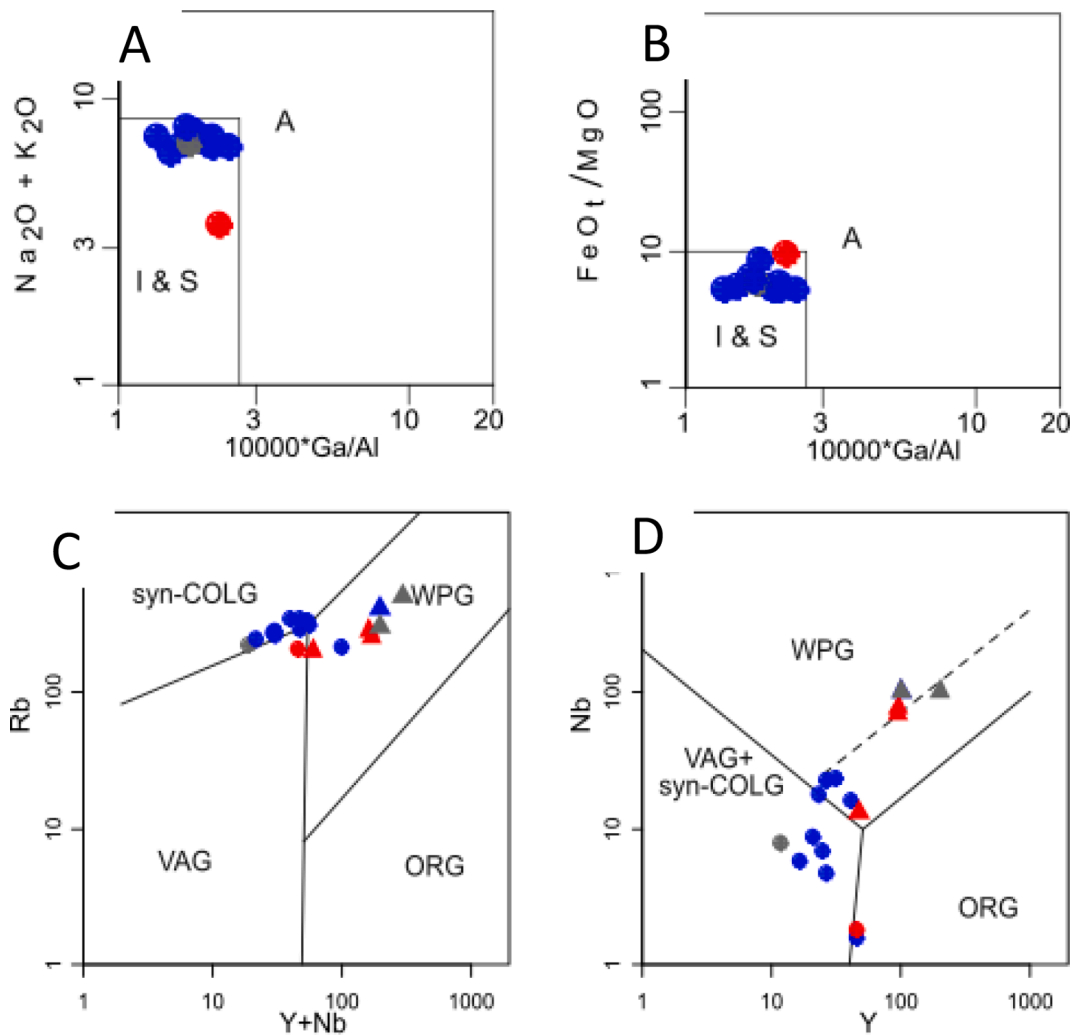


**Fig. 15.** Discrimination diagrams of analyzed Eastern Colombian basement rocks: A-B) A, I and S type granites after Whalen et al., (1987); C-D) Geotectonic environment diagrams using Rb, Nb and Y after Pearce et al. (1984). Syn-COLG: syn-Collisional Granites, WPG: Within Plate Granites, VAG: Volcanic Arc Granites, ORG: ORG Ocean Ridge Granites. Symbols same as in Fig. 12.

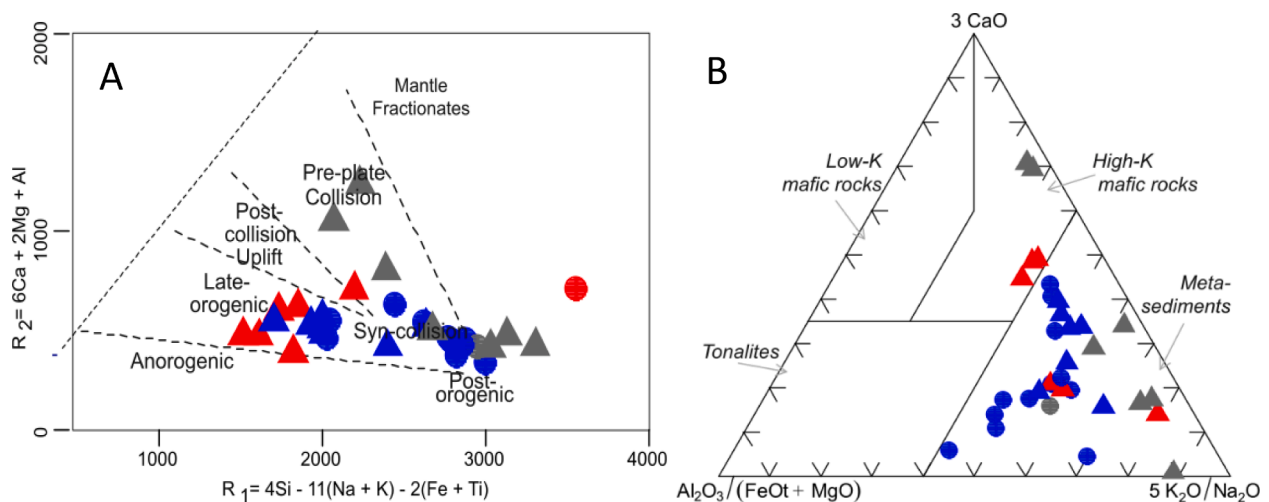


**Fig. 16.** A) Geotectonic discrimination of the studied basement samples using the  $R_2 = 6Ca + 2Mg + Al$  vs  $R_1 = 4Si - 11(Na + K) - 2(Fe + Ti)$  diagram after Batchelor and Bowden (Batchelor and Bowden, 1985); B) Source diagram after Laurent et al. (2014).

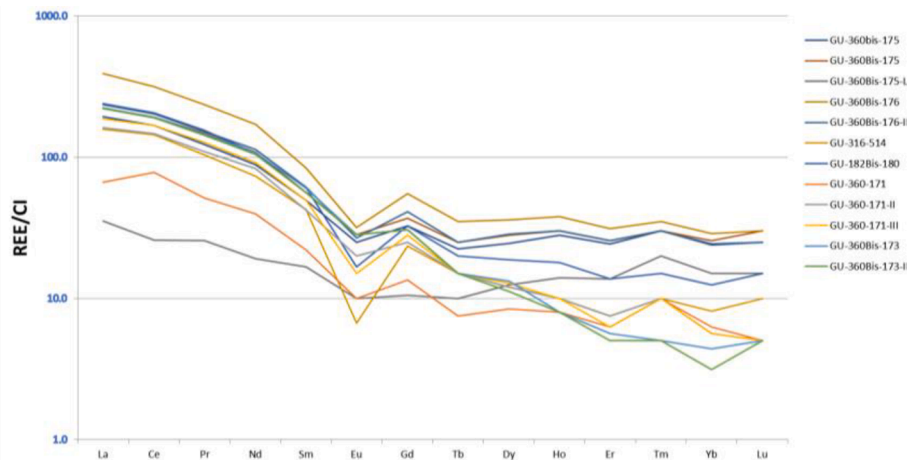


Fig. 17. CI-chondrite-normalized REE contents of all metamorphic samples (McDonough and Sun, 1995).

## 5. Geochronology

All the calculated ages are summarized in the Table 4.

### 5.1. Medium to high-grade metamorphic rocks

Zircons from a sillimanitic migmatitic paragneiss at site GU-360-171 (Fig. 18A, Fig. 2, Fig. 4, Fig. 5) in the (1) leucosome are euhedral and of prismatic habit, whereas in the (2) mesosome, tabular and sub-rounded zircons were found. Both populations show clear core-rim structures (Fig. 18A); two core-data of population (1) yield concordant inherited ages of 1941 and 2194 Ma, thirty-two grains suggest an upper intercept at  $1852 \pm 28$  Ma (MSWD 10.4), whereas the weighted average age of twelve grain cores yield an age of  $1836 \pm 17$  Ma (MSWD 1.5) and the weighted average age of five grain rims yield an age of  $1803 \pm 42$  Ma (MSWD 2.5). Mesosome (2) ages are similar: an inherited zircon core is 2015 Ma old, whereas twenty-seven grains show an upper intercept at  $1818 \pm 15$  Ma (MSWD 3.7) and sixteen grain cores show a weighted average age of  $1807 \pm 11$  Ma (MSWD 0.95).

Zircons from a sillimanitic migmatitic paragneiss at site GU-360bis-173 (Fig. 2, Fig. 5) are euhedral with prismatic and tabular to sub-rounded shapes. All the grains show concentric growth patterns and core-rim structures (

Fig. 18B). Several concordant core data with ages  $> 2100$  Ma may correspond to inherited zircons. One population with eight grains show a weighted average age of  $1982 \pm 28$  Ma (MSWD 2.4) which means that the sediments must have formed before this metamorphic peak age, other sixteen grains show a weighted average age of  $1853 \pm 13$  Ma (MSWD 1.2) while five grain rims suggest an age of  $1832 \pm 19$  Ma (MSWD 1.15).

Zircons from the pegmatitic leucosome of a migmatitic rock sample at site GU-360bis-175 (Fig. 2, Fig. 5) exhibit prismatic and tabular habit, without sub-rounded borders and all data were discordant due to common Pb (GU-360bis-175-L); zircons from the two mesosome samples yield several discordant data with upper intercept ages of  $1815 \pm 14$  Ma and  $1826 \pm 13$  Ma, respectively. In the first mesosome sample eighteen grain cores show a weighted average age of  $1805 \pm 10$  Ma (MSWD 0.86) and five rim data points show  $1763 \pm 18$  Ma (MSWD 1.14). In the second mesosome sample twelve core data points show an  $1804 \pm 12$  Ma weighted average age (MSWD 0.89), but ten rim data suggests a weighted average age of  $1840 \pm 17$  Ma (MSWD 1.3). It does not give sense that rim ages are nearly 40 my older than core ages, and considering that the younger ages are also in better agreement with the other

ages from the site GU-360bis-175, most probably effects due to polishing procedure of grain mountings or Pb- or U-migration – quite common in migmatites – caused this behavior.

From two migmatitic rock samples at GU-360bis-176 (Fig. 2, Fig. 4, Fig. 5), a first contains euhedral tabular zircons with sub-rounded shapes, concentric growth zones and well defined core-rim structures, its upper intercept age is  $1796 \pm 16$  Ma (MSWD 3.0), whereas a population of nineteen grains yield a weighted average age of  $1782 \pm 10$  Ma (MSWD 0.73). The zircons of the second specimen are more prismatic than tabular but also with sub-rounded shapes, seventeen grains yield a weighted average age of  $1789 \pm 14$  Ma (MSWD 1.5). Spots were not located on the grain rims.

At the site GU-382bis-178 (Fig. 2, Fig. 5), the migmatitic rock presents subhedral zircons with tabular habit and sub-rounded edges. Concentric growth patterns and some rim-core structures are visible. The oldest age obtained (1950 Ma) corresponds to a core interpreted as an inherited zircon, while twenty grains show a weighted average age of  $1818 \pm 15$  Ma (MSWD 1.8). Here, the grain rims were not measured.

At the last migmatitic rock site on the Guainía-Negro River (GU-382bis-180, Fig. 2, Fig. 5), the sample has euhedral zircons with prismatic to tabular habit, most of them show concentric growth features, and among the discordant ages, two grain populations can be separated: the first population attributed to the protolith have an upper intercept age of  $1817 \pm 32$  Ma (MSWD 8.5), four grain cores with weighted average age of  $1813 \pm 42$  Ma (MSWD 1.4). The second population is attributed to the migmatization peak with an upper intercept age of  $1541 \pm 58$  Ma (MSWD 42), seven grain cores with a weighted average age of  $1534 \pm 16$  Ma (MSWD 0.94) and three grain rims with a weighted average age of  $1459 \pm 67$  Ma (MSWD 1.6).

In the Inirida River valley, the paragneiss at station GU-316-514 (Fig. 2) contains euhedral zircons with prismatic habit and concentric growth patterns, some of them showing clear core-rim structures. All the data are discordant and it is impossible to get any reasonable age. The upper intercept age of  $1840 \pm 76$  Ma (MSWD 34) is not age-equivalent. The strong deformation visible at the sample related to the Raudal Cuale shear zone may have caused isotopic disturbances of Pb and U.

### 5.2. Granitoids

#### 5.2.1. Late Orosirian to Early Statherian (1800–1700 Ma)

The oldest granitic rocks found in this study is a monzogranite at site GU-338-170 (Fig. 2, Fig. 6) where zircons are euhedral with tabular and prismatic to sub-rounded shapes. Concentric growth patterns in tabular

**Table 4**  
Overview of the zircon U/Pb data obtained in this study.

SAMPLE	ROCK TYPE	U-Pb ZIRCON				ZIRCON HABIT	ISOPLOT FIGURES
		AGE	METHOD	n	MSWD		
GU-360-171-1	Migmatitic paragneiss with sillimanite leucosome	1852 ± 28 Ma	Upper Intercept - limited statistical meaning	32	10.4	Prismatic	Fig. 22A
		1836 ± 17 Ma	Weighted Average	12	1.5		
		1803 ± 42 Ma	Weighted Average rims	5	2.5		
GU-360-171-2	Migmatitic paragneiss with sillimanite mesosome	1818 ± 15 Ma	Upper Intercept	27	3.7	Tabular and sub-rounded	Fig. 22B
		1807 ± 11 Ma	Weighted Average	16	0.95		
GU-360bis-173	Migmatitic paragneiss with sillimanite	1982 ± 28 Ma	Weighted Average	8	2.4	Prismatic and tabular to sub-rounded	Fig. 22C
		1853 ± 13 Ma	Weighted Average	16	1.2		
		1832 ± 19 Ma	Weighted Average rims	5	1.15		
GU-360bis-175-1	Migmatitic rock Mesosome	1815 ± 14 Ma	Upper Intercept	33	4.8	Prismatic and tabular	Fig. 22D
		1805 ± 10 Ma	Weighted Average	18	0.86		
		1763 ± 18 Ma	Weighted Average rims	5	1.14		
GU-360bis-175-2	Migmatitic rock Mesosome	1826 ± 13 Ma	Upper Intercept	36	3.7	Prismatic and tabular	Fig. 22E
		1804 ± 12 Ma	Weighted Average	12	0.71		
		1840 ± 17 Ma	Weighted Average rims	10	1.3		
GU-360bis-176-1	Migmatitic rock	1796 ± 16 Ma	Upper Intercept	22	3	Tabular and sub-rounded	Fig. 22F
		1782 ± 10 Ma	Weighted Average	19	0.73		
GU-360bis-176-2	Migmatitic rock	1789 ± 14 Ma	Weighted Average	17	1.5	Prismatic to sub-rounded	Fig. 22G
GU-382bis-178	Migmatitic rock	1818 ± 15 Ma	Weighted Average	20	1.8	Tabular and sub-rounded edges	Fig. 22H
GU-382bis-180	Migmatitic rock	1817 ± 32 Ma	Upper Intercept - has no statistical meaning	12	8.5	Prismatic to tabular	Fig. 22I
		1813 ± 42 Ma	Weighted Average	4	1.4		
		1541 ± 58 Ma	Upper Intercept	42	19		
		1534 ± 16 Ma	Weighted Average	7	0.94		
		1459 ± 67 Ma	Upper Intercept	3	1.6		
GU-316-514	Paragneiss	1840 ± 76 Ma	Upper Intercept - is not an equivalent age	21	34	Prismatic	Fig. 22J
GU-357-501	Syenogranite	1554 ± 19 Ma	Upper Intercept-no statistical meaning	28	9.2	Prismatic and tabular	Fig. 22K
GU-336-502	Monzogranite	1389 ± 13 Ma	Weighted Average	21	1.1	Prismatic	Fig. 22L
GU-336-505	Quartz-syenite	1574 ± 25 Ma	Upper Intercept - has no statistical meaning	25	10.4	Prismatic	Fig. 22M
		1527 ± 17 Ma	Weighted Average	7	0.86		
		1548 ± 24 Ma	Weighted Average rims	3	0.18		
GU-336-506	Quartz-syenite	1641 ± 30 Ma	Upper Intercept - has no statistical meaning	22	11.9	Sub-rounded prismatic and tabular	Fig. 22N
		1601 ± 42 Ma	Weighted Average	5	2.4		
GU-337-510	Monzogranite	1798 ± 64 Ma	Upper Intercept - is not an equivalent age	20	28	Prismatic	Fig. 22O
GU-316-512	Monzogranite	1534 ± 31 Ma	Upper Intercept	26	23	Tabular and some prismatic	Fig. 22P
		1499 ± 30 Ma	Weighted Average	9	2.9		
GU-317-516	Monzogranite	1543 ± 22 Ma	Upper Intercept	25	10.2	Prismatic	Fig. 22Q
		1503 ± 16 Ma	Weighted Average	11	1.2		

(continued on next page)

Table 4 (continued)

SAMPLE	ROCK TYPE	U-Pb ZIRCON		n	MSWD	ZIRCON HABIT	ISOPLOT FIGURES
		AGE	METHOD				
GU-360-164	Monzogranite	1553 ± 42 Ma	Upper Intercept	19	29	Tabular	Fig. 22R
		1525 ± 27 Ma	Weighted Average	7	1.6		
GU-360-166	Syenogranite	1606 ± 46 Ma	Upper Intercept - has no statistical meaning	21	11.8	Tabular	Fig. 22S
GU-338-168	Monzogranite	1542 ± 25 Ma	Upper Intercept	22	6.5	Prismatic	Fig. 22T
		1530 ± 26 Ma	Weighted Average rims	3	0.71		
GU-338-170	Monzogranite	1839 ± 23 Ma	Upper Intercept	24	5.7	Tabular and prismatic to sub-rounded	Fig. 22U
		1825 ± 22 Ma	Weighted Average	8	1.5		
GU-406-182	Monzogranite	1527 ± 23 Ma	Weighted Average	11	1.6	Prismatic	Fig. 22V
		1507 ± 26 Ma	Weighted Average rims	8	1.8		
VA-443-024	Monzogranite	1542 ± 7 Ma	Concordant age	13	1.48	Prismatic and tabular	Fig. 22W
VA-443-019	Monzogranite	1518 ± 8 Ma	Concordant age	9	2.3	Prismatic and tabular	Fig. 22X

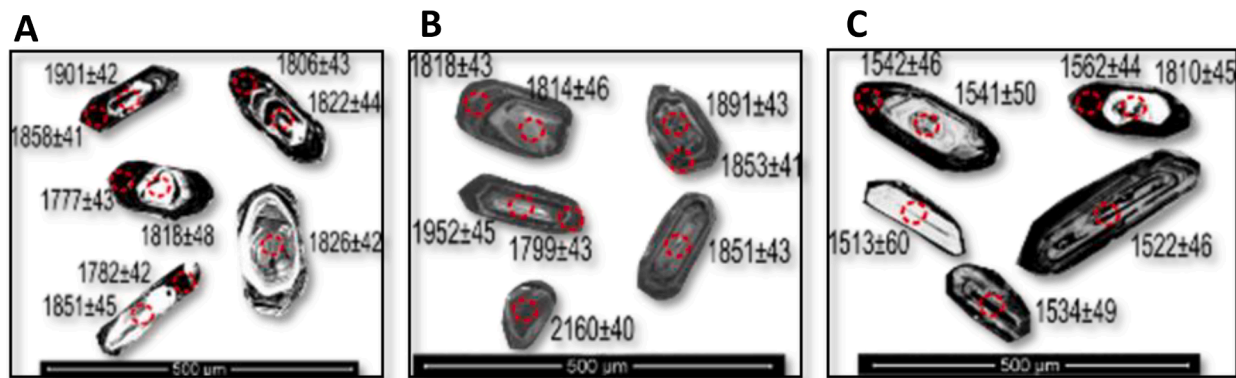


Fig. 18. CL-images showing the LA-ICP-MS spot and  $^{207}\text{Pb}/^{206}\text{Pb}$  ages. Observe the typical metamorphic zonations in A and B. A) GU-360-171 B) GU-360Bis-173 C) GU-338-168 monzogranite.

zircon with clear core-rim structure yield in cores the oldest concordant data of 2040, 2080 and 2420 Ma that are interpreted as inherited zircons. Most of the data are discordant and suggest an upper intercept age of  $1839 \pm 23$  Ma (MSWD 5.7). Data of eight grain cores yield a weighted average age of  $1825 \pm 22$  Ma (MSWD 1.5).

Zircons from a monzogranite at GU-337-510 (Fig. 2) have prismatic habit and concentric growth patterns; due to discordant data with high MSWD of the upper intercept age of  $1798 \pm 64$  Ma (MSWD 28) no reasonable ages can be obtained, possibly as result of strong Pb-loss.

### 5.2.2. Late Statherian to Calymnian (1650–1400 Ma)

Zircons from a syenogranite outcrop (GU-357-501) along the Inirida River (Fig. 2) exhibit prismatic and tabular crystals with concentric growth zonations. Most Pb/U-data are discordant with an upper intercept age of  $1554 \pm 19$  Ma (MSWD 9.2); although this age has limited statistical meaning as expressed by the large MSWD, it indicates a strong Pb-loss caused by a post-crystallization event on this granite.

Quartz-syenite sample GU-336-505 (Fig. 2) has euhedral zircons with a predominant prismatic habit and sample GU-336-506 (also a

quartz-syenite, Fig. 2, Fig. 6, Fig. 8) has sub-rounded prismatic and tabular zircons. Both show strong core-rim structures and concentric growth zonation. In sample GU-336-505 an upper intercept age of  $1574 \pm 25$  Ma (MSWD 10.4) is obtained which has limited statistical meaning, while seven grain cores yield a weighted average age of  $1527 \pm 17$  Ma (MSWD 0.86), with an oldest core age of 2413 Ma. In sample GU-336-506 most of the grains are discordant with an upper intercept age of  $1641 \pm 30$  Ma (MSWD 11.9) which has limited statistical meaning, while five grain cores yield a weighted average age of  $1601 \pm 42$  Ma (MSWD 2.4).

The monzogranite zircons from station GU-316-512 (Fig. 2, Fig. 7) have tabular habit and some prismatic grains. They show concentric growth patterns and a poorly developed core-rim structure. Several core ages older than 1600 Ma may belong to inherited zircons and an upper intercept age of  $1534 \pm 31$  Ma (MSWD 23) with limited statistical value can be calculated quite common by partial melting, whereas nine grain cores yield a weighted average age of  $1499 \pm 30$  Ma (MSWD 2.9).

The monzogranite zircons from Mavicure hills (GU-317-516, Fig. 2, Fig. 6, Fig. 7) have a prismatic habit with less-developed concentric

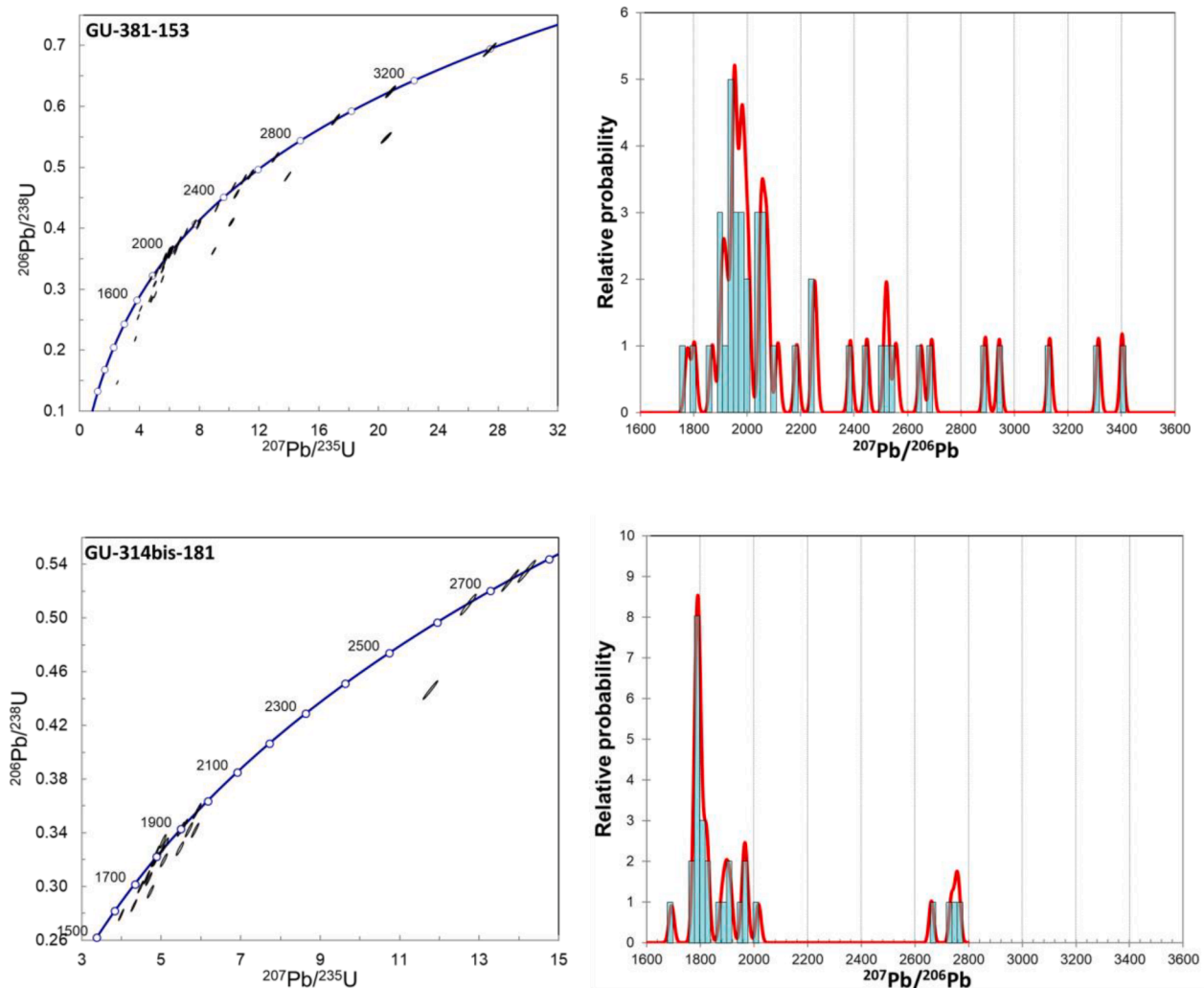


**Fig. 19.** Concordia diagrams and relative probability age histograms using ISOPLOT (Ludwig, 2012) for *meta*-sedimentary rocks from the Tunuí Group in Colombia (GU-381-153 and GU-314bis-181).

growth patterns and an upper intercept age of  $1543 \pm 22$  Ma (MSWD 10.2) with limited statistical significance, whereas eleven grain cores deliver a weighted average age of  $1503 \pm 16$  Ma (MSWD 1.2).

Sample GU-360-164 (Fig. 2, Fig. 8) from a monzogranite at the Guainía River (also called Río Negro) contains tabular zircons showing a concentric growth pattern; most data are discordant but an upper intercept age of  $1553 \pm 42$  Ma (MSWD 29) with little statistical significance is calculated. Four inherited ages yield 1758, 1766, 1941 and 1977 Ma, while seven grain cores suggest a weighted average age of  $1525 \pm 27$  Ma (MSWD 1.6). Also, younger concordant zircons were found with ages between 1280 and 1350 Ma. Data from the syenogranite site GU-360-166 are mostly discordant and yield an upper intercept age of  $1606 \pm 46$  Ma (MSWD 11.8) whereas inherited zircons yield ages between 1590 and 1800 Ma.

Most data of prismatic zircons (Fig. 18C) from monzogranitic site GU-338-168 (Fig. 2) are discordant, with an upper intercept age of  $1542 \pm 25$  Ma (MSWD 6.5) whereas three rim spots deliver a weighted average age of  $1530 \pm 26$  Ma (MSWD 0.71).

Zircons from monzogranitic site GU-406-182 (Fig. 2) have a prismatic habit, some of them with concentric growth zonation. Eleven grains yield a weighted average age of  $1527 \pm 23$  Ma (MSWD 1.6) while eight rim analyses return a weighted average age of  $1507 \pm 26$  Ma (MSWD 1.8). Older ages of 1740 and 1800 Ma in two cores correspond to

inherited zircons.

Among the zircons from the two monzogranite samples taken near to the city of Mitú (Fig. 2), nine zircon grains with prismatic to tabular habit from site VA-443-19 show a concordant age of  $1518 \pm 8$  Ma (MSWD 2.3) whereas thirteen grains from site VA-443-24 yield a concordant age of  $1542 \pm 6.5$  Ma (MSWD 1.48).

Early Ectasian (1400–1300 Ma)

The zircons of the Matraca rapakivi monzogranite at GU-366-502 (Fig. 2, Fig. 9) are euhedral with prismatic habit and well-developed concentric growth pattern. Most of the data are concordant in the range of 1350–1450 Ma; twenty-one grains return a weighted average age of  $1389 \pm 13$  Ma (MSWD 0.60).

### 5.3. Metasedimentary sequences

Among the *meta*-sedimentary samples assigned to the Tunuí Group in Colombia, the phyllite at site GU-381-153 and the quartzite at site GU-314bis-181 (Fig. 2) contain detrital zircons with subrounded shapes, some of them with well-developed core-rim structures. The zircons of sample GU-381-153 are more rounded whereas several GU-314bis-181 zircons preserved their prismatic habit. Most zircons in these samples yield ages between 1800 and 2000 Ma (Fig. 19) interpreted as crystallization ages, with a major peak at 1800 Ma, and smaller populations

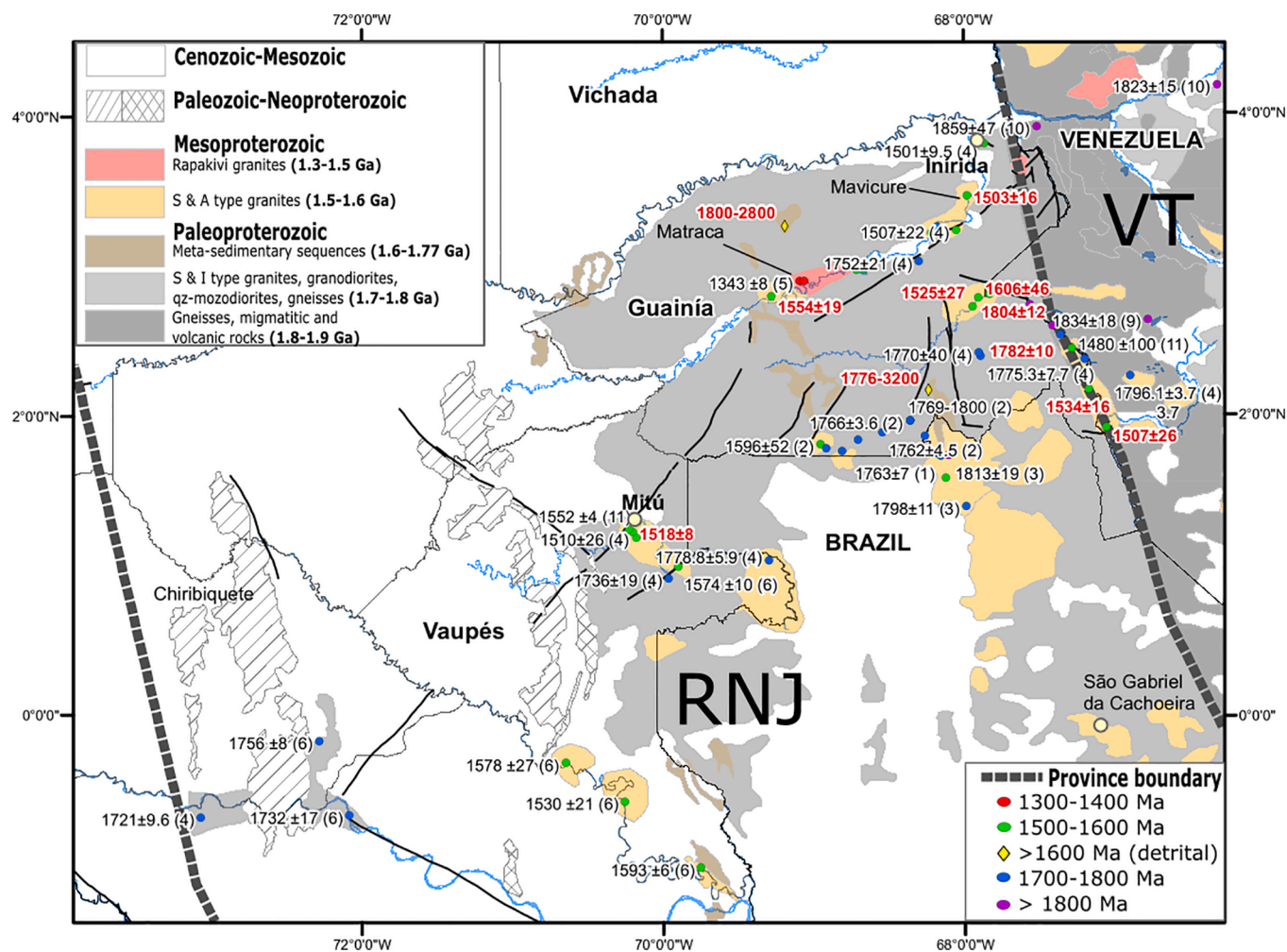


**Fig. 20.** Rio Negro-Juruena Province in the NW Amazonian Craton (Bonilla-Pérez et al., 2016; Cordani and Teixeira, 2007; Gómez et al., 2019; INGEOMINAS, 2010). Available U/Pb zircon ages for the study area: (red letter) this study, (1) Mendes et al., 2020; (2) Bonilla-Pérez et al., 2019; (3) Veras et al., 2018; (4) Cordani et al., 2016; (5) Bonilla-Pérez et al., 2016; (6) Ibanez-Mejía, 2010; (7) Santos et al., 2000; (8) Almeida et al., 1997; (9) Tassinari et al., 1996; (10) Gaudette and Olszewski, 1985; (11) Priem et al., 1982.

between 2600 and 2800 Ma for the quartzite sample GU-314bis-181, whereas in the phyllitic sample GU381-153 the main ages are not only slightly older but also resample up to 3400 Ma old zircons. Both samples suggest that the depositional age was not older than ~ 1770 Ma ago, with the youngest grains in the samples yielding > 90% concordant data of  $1778 \pm 19$  Ma and  $1694 \pm 21$  Ma.

## 6. Discussion

The earlier subdivisions of the Colombian basement are based mainly on textural and mineralogical features which resulted in informal units: e.g. Atabapo gneiss, “Remanso type” porphyroblastic granites, migmatitic granites (Bruneton et al., 1982; Galvis-Vergara et al., 1979). López et al. (2007) suggested to rename this unit as Mitú Complex because migmatitic rocks only occur in small portions of the area. In our study, migmatitic rocks are restricted to the eastern border of Colombia while orthogneisses and granitoids are the common lithologies, thus supporting the revision advocated by López et al. (2007). Local metamorphic and migmatitic rocks have been described in Guainía and Vaupés (Bonilla-Pérez et al., 2019; Cordani et al., 2016; Kroonenberg, 2019). However, most of them have not been dated or show ages around 1.0 Ga which is still matter of debate.

Eastern Colombia granitoids can be distinguished from each other

geochemically and geochronologically in three types of plutonic rocks. Units with common textural, mineralogical, geochemical, and/or geochronological patterns such as the Mitú Monzogranite, Pringamosa’s Granofels, Neis del Yi (Rodríguez-García et al., 2011a), Tiquie and Içana Intrusive suites (Bonilla-Pérez et al., 2019) and Matraca rapakivi granite (Bonilla-Pérez et al., 2016) are distinct from the Mitú Complex s.s. (Bonilla-Pérez et al., 2016; Rodríguez-García et al., 2011b).

Our study indicates that migmatitic gneisses near Puerto Colombia at the Guainía-Rio Negro River (Bruneton et al., 1982; Galvis-Vergara et al., 1979; SB, 1980) are the oldest reported rocks in Colombia with LA-ICP-MS zircon U-Pb ages between 1800 and 1850 Ma. They exhibit well-developed high-grade metamorphic features, including migmatitic textures. Their biotite-muscovite-sillimanite or hornblende paragenesis suggests amphibolite-facies metamorphism of a sedimentary protolith, significantly different to paragneisses reported in other areas (Bonilla-Pérez et al., 2019; Cordani et al., 2016; Galvis-Vergara et al., 1979; Kroonenberg et al., 2016; Mendes et al., 2020; Veras, 2012). Rocks older than 1800 Ma have also been reported from the Atabapo River and in western Venezuela (Gaudette and Olszewski, 1985; Tassinari et al., 1996). The different petrologic, geochemical and age characteristics of this Orosirian part of the basement allow to separate it from the Mitú Complex. The position of the suture of the Rio Negro Belt (Rio Negro-Juruena Province) with the adjacent older nucleus of the Guiana

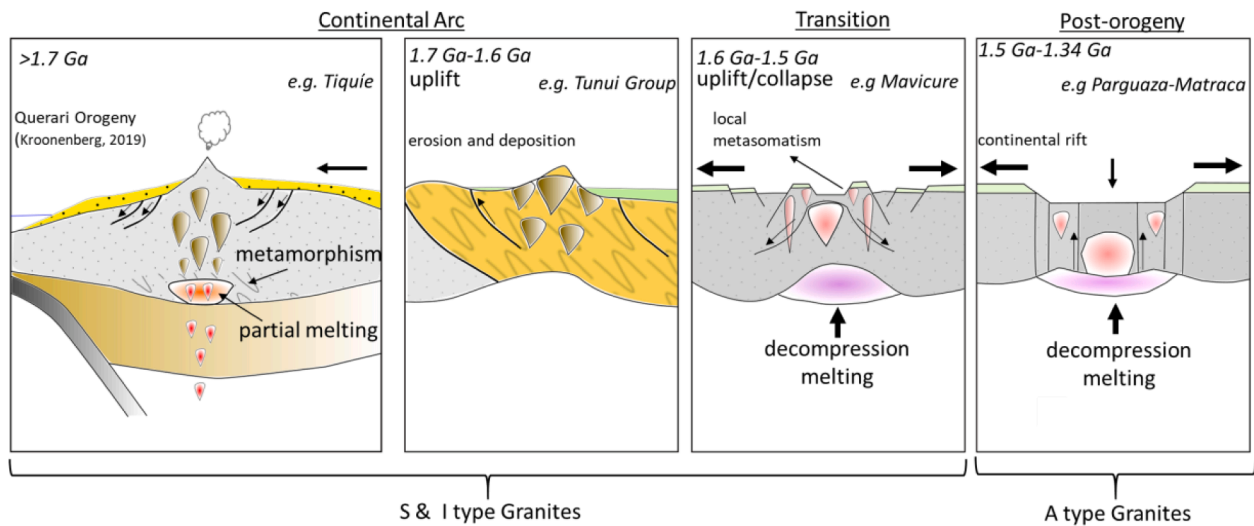


Fig. 21. Tectonic model of the Eastern Colombian basement based in granitoid rocks after (Hsu, 1982).

Shield (Ventuari-Tapajós Province) is still difficult to determine as modern geochronological data from the whole of the Venezuelan part of the shield are absent. However, our observations and results allow us to propose that the eastern limit of the Rio Negro-Juruena Province follows the +/- N10W trending lineaments along the Guainía-Rio Negro, Atabapo and Orinoco rivers (Fig. 2, Fig. 20), as was proposed by Cordani and Teixeira (2007) and Tassinari and Macambira (1999). Likewise, the RNJ-suture with younger belts to the west is still unknown because of the thin Cenozoic cover, at least the western basement outcrops in Araracuara (Chiribiquete ridge) suggest a RNJ boundary (Fig. 20).

Whilst the Mitú Complex was originally defined as a basement block with ages between 1500 and 1800 Ma (López et al., 2007; Priem et al., 1982), here we suggest to limit the Mitú Complex to the Statherian basement composed of metamorphic and igneous rocks with ages between 1800 and 1720 Ma. It outcrops in most of eastern Colombia (Vaupés, Guainía, and Amazonas departments - Fig. 20) and is composed of orthogneisses and granitoids with difficult-to-define transitions in the field. Typical Mitú orthogneisses are composed of quartz, K-feldspar, plagioclase and biotite. Among the granitoids, I- and S-type granites, granodiorites, and quartz-monzodiorites occur as described in previous studies (Bonilla-Pérez et al., 2019; INGEOMINAS, 2010; López et al., 2007; Rodríguez-García et al., 2011b). Strong foliated, folded and sometimes mylonitic textures are enhanced by ferromagnesian minerals controlled by high deformation processes which are sometimes associated with regional faults (e.g. delineating the river's rapids called "raudales"). Local studies may lead to subdivisions of new units like the one proposed for the Tiquié Intrusive Suite (Bonilla-Pérez et al., 2019).

Both the 1850 to 1800 Ma migmatitic gneisses, and the gneisses and I- and S-type granites (the Mitú Complex *sensu stricto*) with ages between 1800 and 1720 Ma show geochemical evidence of pre-plate to orogenic processes (Fig. 16), which first affected an early-Orosirian (>1850 Ma) continental crust with continental arcs and associated sedimentary deposition. A subsequent subduction and accretion resulted in the formation of a highly deformed continental crust (Fig. 21) and a continental arc between 1850 and 1720 Ma, actually interpreted as the Rio Negro-Juruena accretion to the Amazonian Craton. Some of these rocks progressed into the migmatite formation window experiencing local anatexis during an orogenic peak between 1800 and 1850 Ma. Such a magmatic arc was already postulated by Cordani et al. (2016) who proposed an 1800 to 1740 Ma Atabapo belt in Colombia as well as the continental arcs corresponding to the Cauaburi and Querari Orogens described in Brazil (Almeida et al., 2011; Mendes et al., 2020; Veras

et al., 2018). However, our new data indicate that in Colombia this orogeny represents an own continental arc for which we suggest to adopt the name Querari Orogeny (after a Colombian and Brazilian river of the same name) as defined by Kroonenberg (2019). This orogeny occurred between 1860 and 1720 Ma as an important succession of events which extended to similar expressions in the Brazilian basement. The available U/Pb zircon ages suggest that the accretion started eastwards of the Rio Negro River in Venezuela and became younger towards the southwest in Colombia (Fig. 20), but no evidence of arc migrations has been observed as Mendes et al. (2020) suggest for Brazil.

Over this Statherian basement, sedimentary sequences were deposited, which now form the Tunuí Group or Tunuí Formation outcropping both in Colombia and Brazil. Its age is still a matter of debate; the most recent compilation of Kroonenberg (2019) suggests ages between 1580 and 1350 Ma, based on data by Ibañez-Mejía (2010) who reported a basement crystallization age of  $1588 \pm 21$  Ma in Taraira and by Santos et al. (2003) who reported an Ar/Ar muscovite age of  $1334 \pm 2$  Ma in Brazil. Bonilla-Pérez et al. (2019) suggest a maximum deposition age of 1600 based on LA-ICP-MS zircon U-Pb ages from a granite which is clearly intrusive in the meta-sedimentary unit. Our new data further provides evidence for a deposition age > 1600 Ma, as detrital zircons from the Naquén and Caranacoa areas suggest an earliest depositional age of 1770 Ma and a thermal event produced by a granitic intrusion into this sequence at ~ 1600 Ma (Bonilla-Pérez et al., 2019). The Tunuí Group was described as continental deposition, specifically exhibiting alluvial facies (Galvis-Vergara, 1993; Renzoni, 1989a). This is in agreement with strong erosion and a deposition cycle during the compressional tectonic setting which was caused by uplift during the last orogeny stages, and transgressed into post-orogenic environments between 1700 and 1600 Ma (Fig. 21).

This Querari Orogeny can be followed in the whole western Colombian basement, which was intruded by several granites between 1600 and 1500 Ma (Bonilla-Pérez et al., 2019; Cordani et al., 2016; Kroonenberg et al., 2016). Some authors interpret them as A-type granites based on some geochemical characteristics. However, most of these rocks clearly exhibit S-type granite characteristics and we interpret them as resulting from crustal decompressional melting (Fig. 21). Rarely, also amphibole occurs (Rodríguez-García et al., 2011b). Moreover, all of the investigated S-type granites have geochemical syn- to post orogenic features very distinct from the older 1.8–1.72 Ma granitoids which point to an orogenic collapse setting (Fig. 16, Fig. 21) and not as magmatic arc proposed by Cordani et al. (2016) in Colombia or by

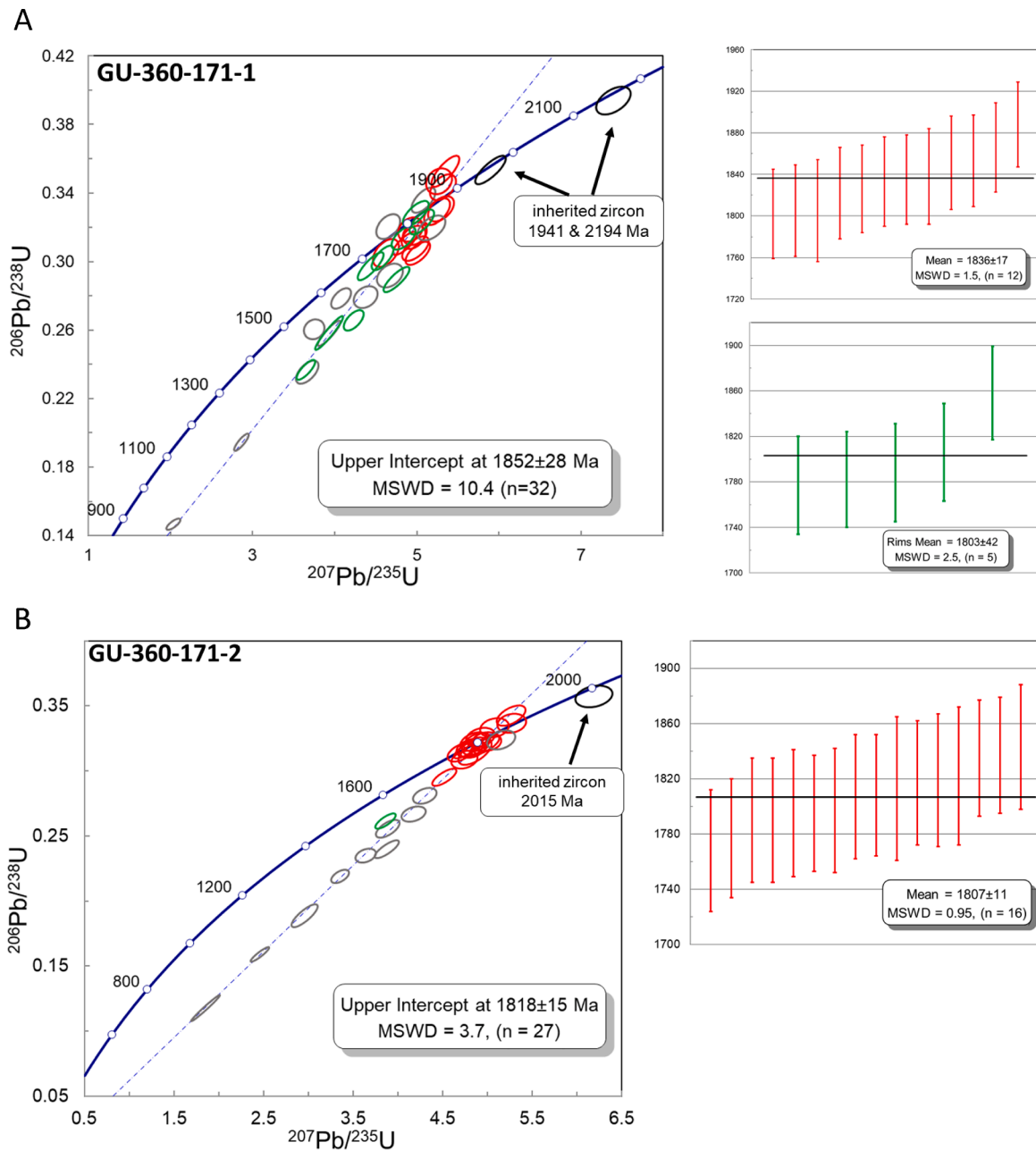
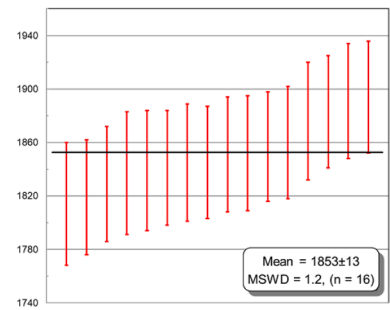
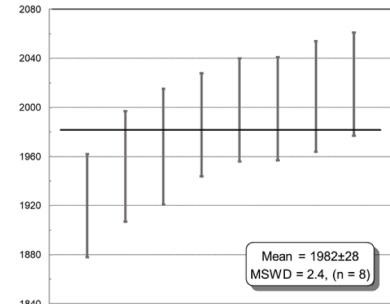
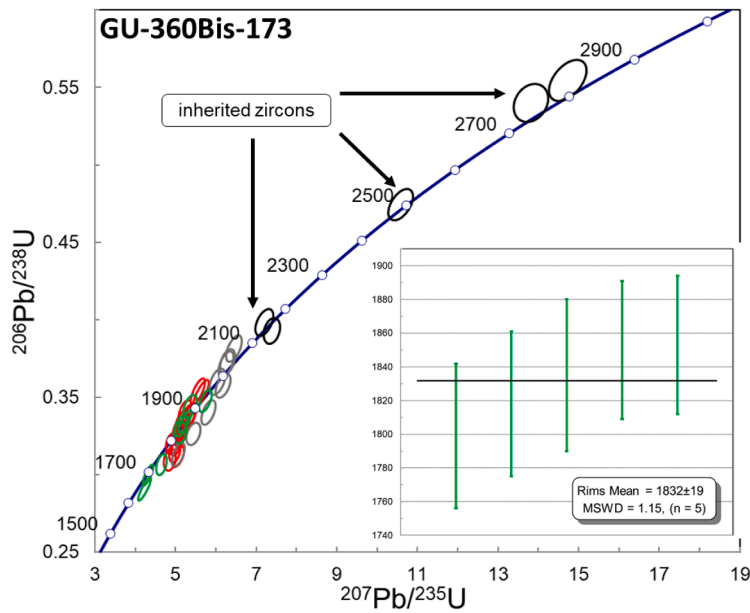


Fig. 22. Concordia diagrams and Weighted Average age for metamorphic and igneous rocks from the Eastern Colombia, Basement after ISOPLOT (Ludwig, 2012).

C



D

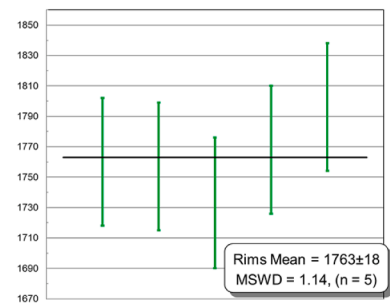
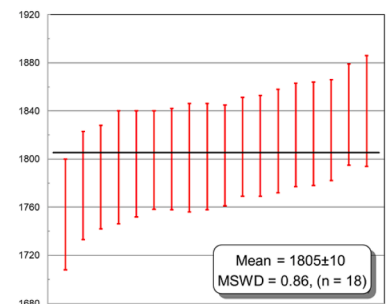
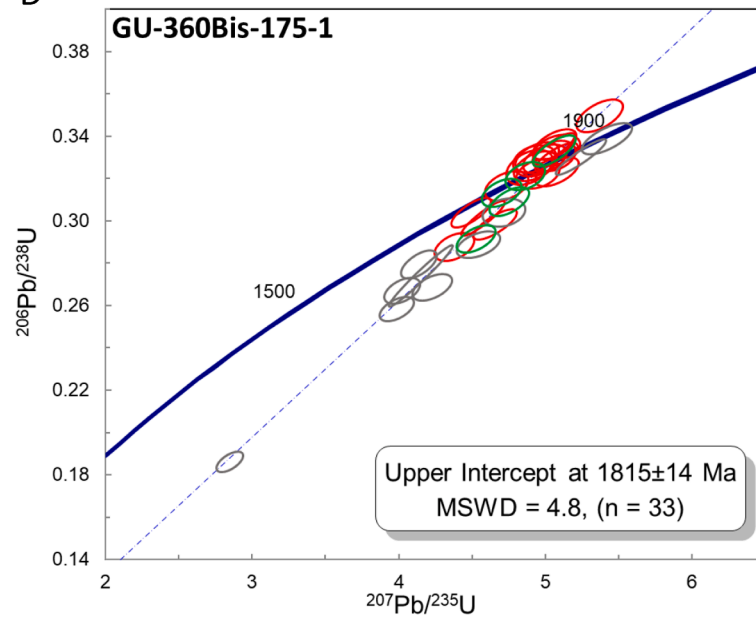


Fig. 22. (continued).

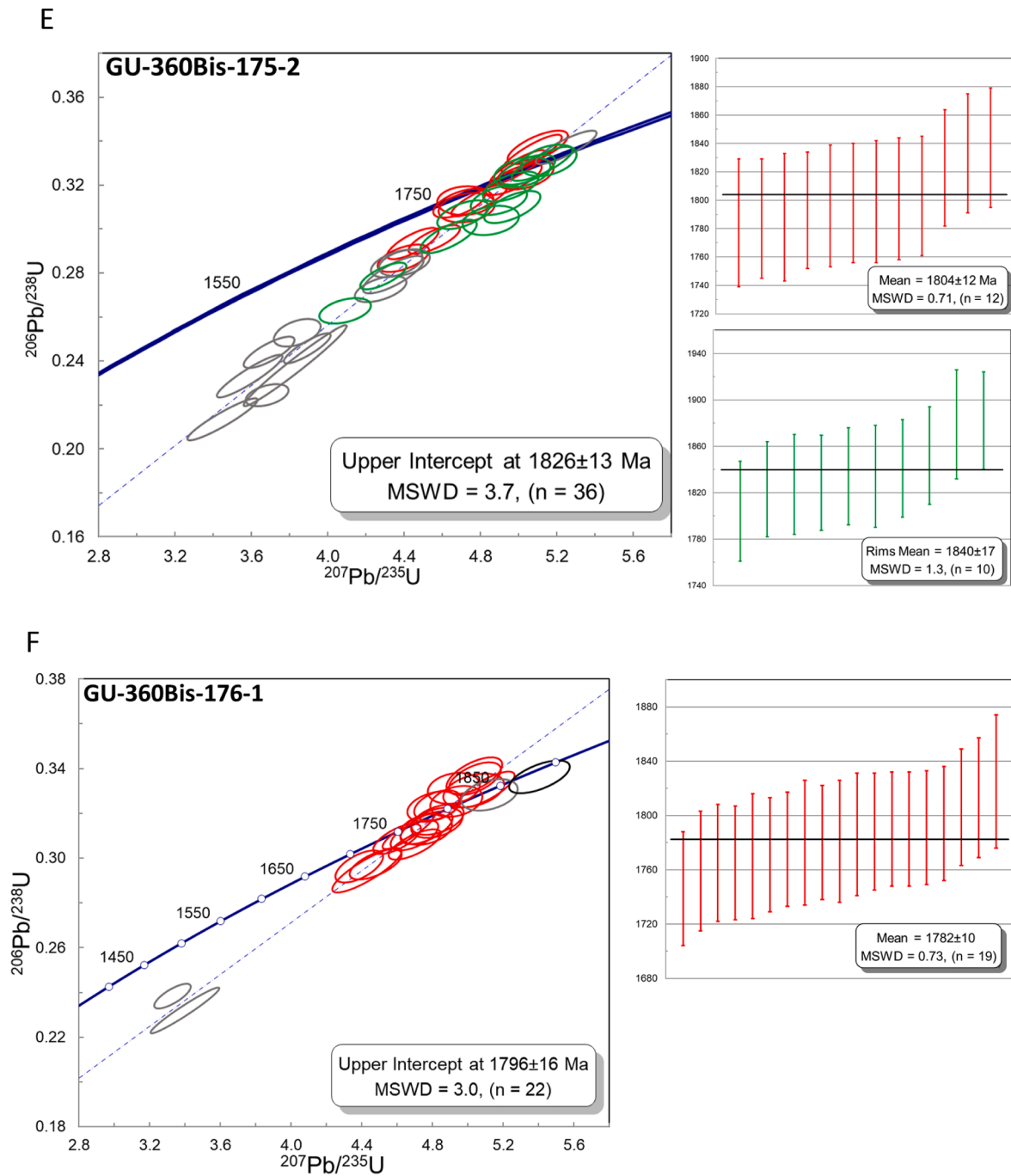


Fig. 22. (continued).

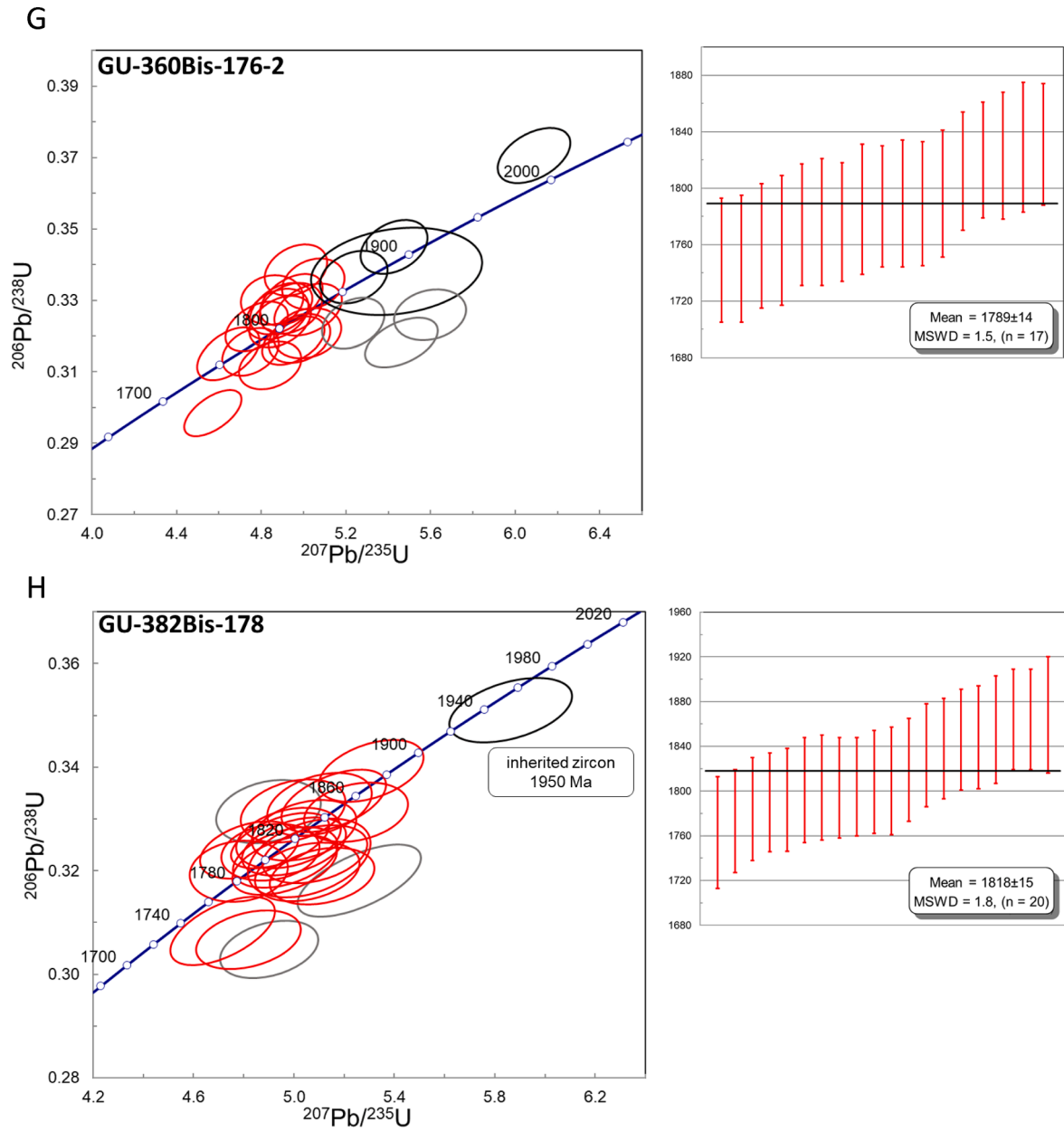


Fig. 22. (continued).

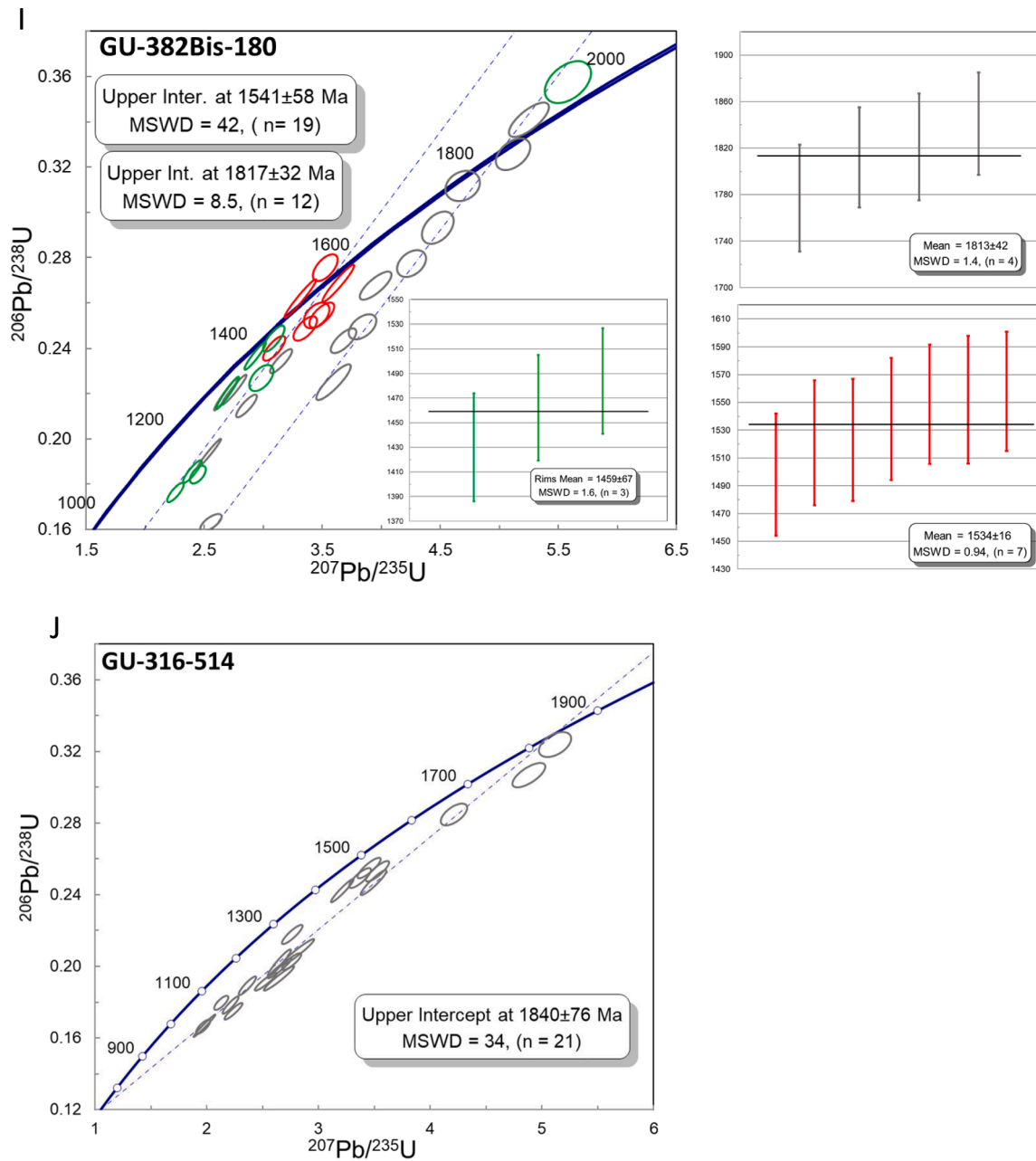
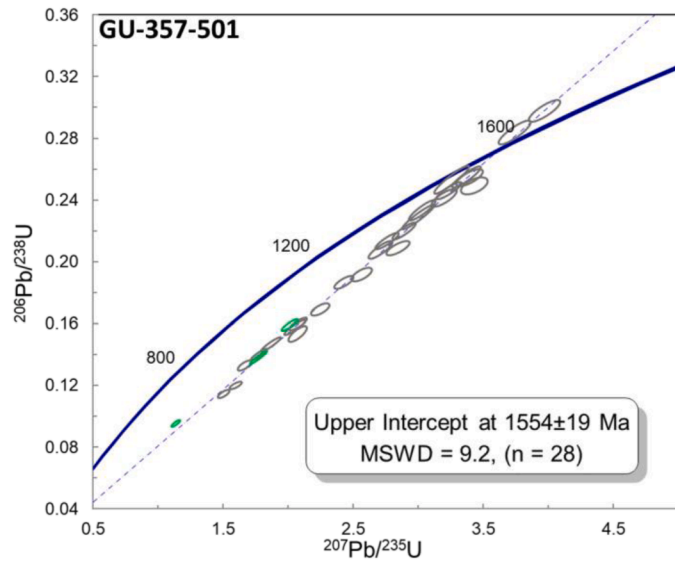


Fig. 22. (continued).

K



L

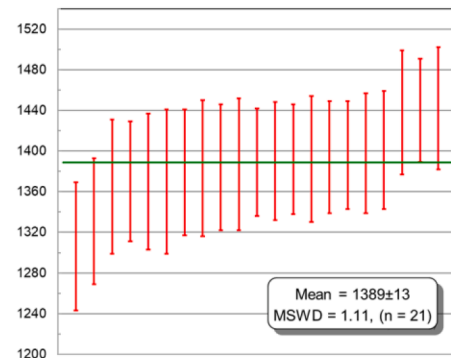
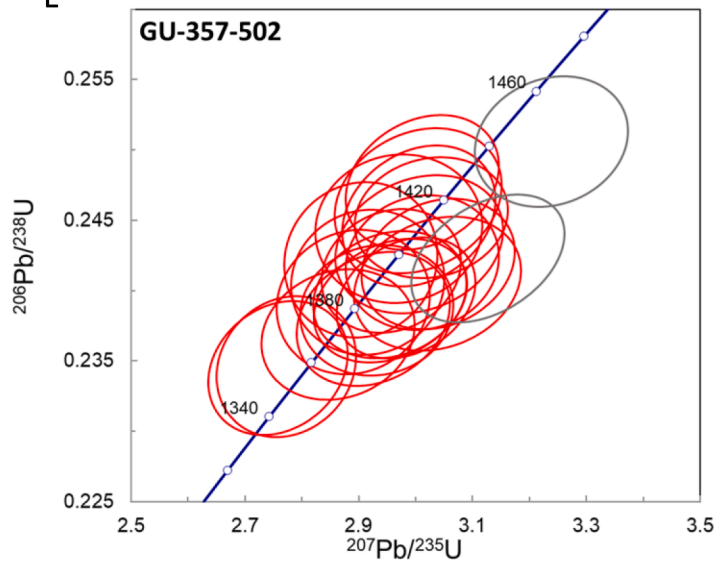
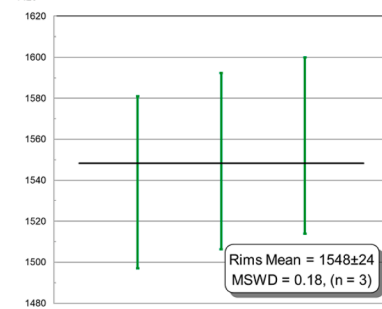
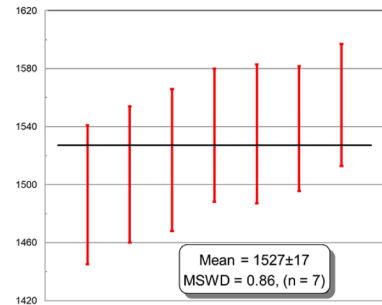
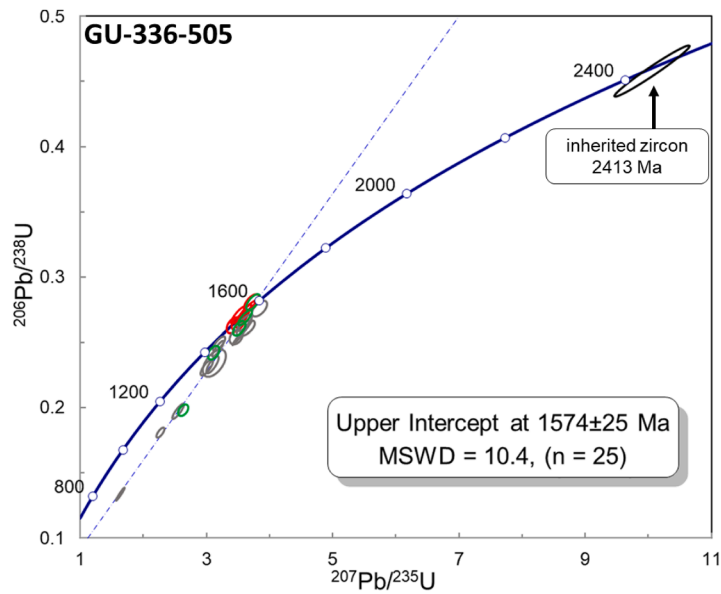


Fig. 22. (continued).

M



N

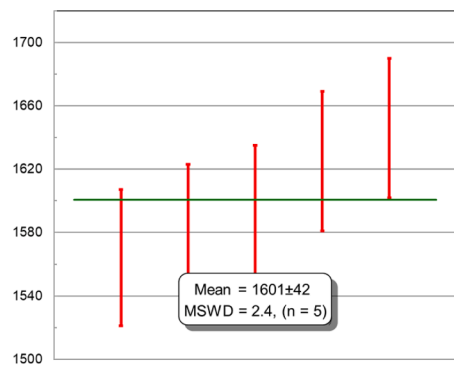
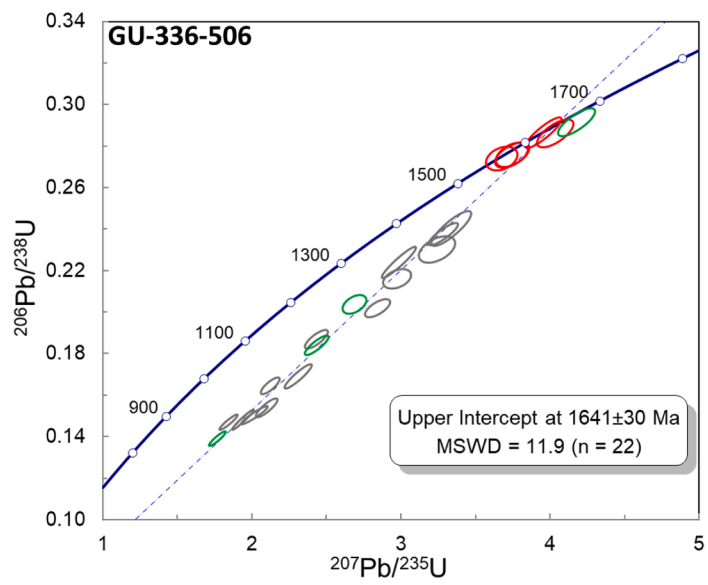


Fig. 22. (continued).

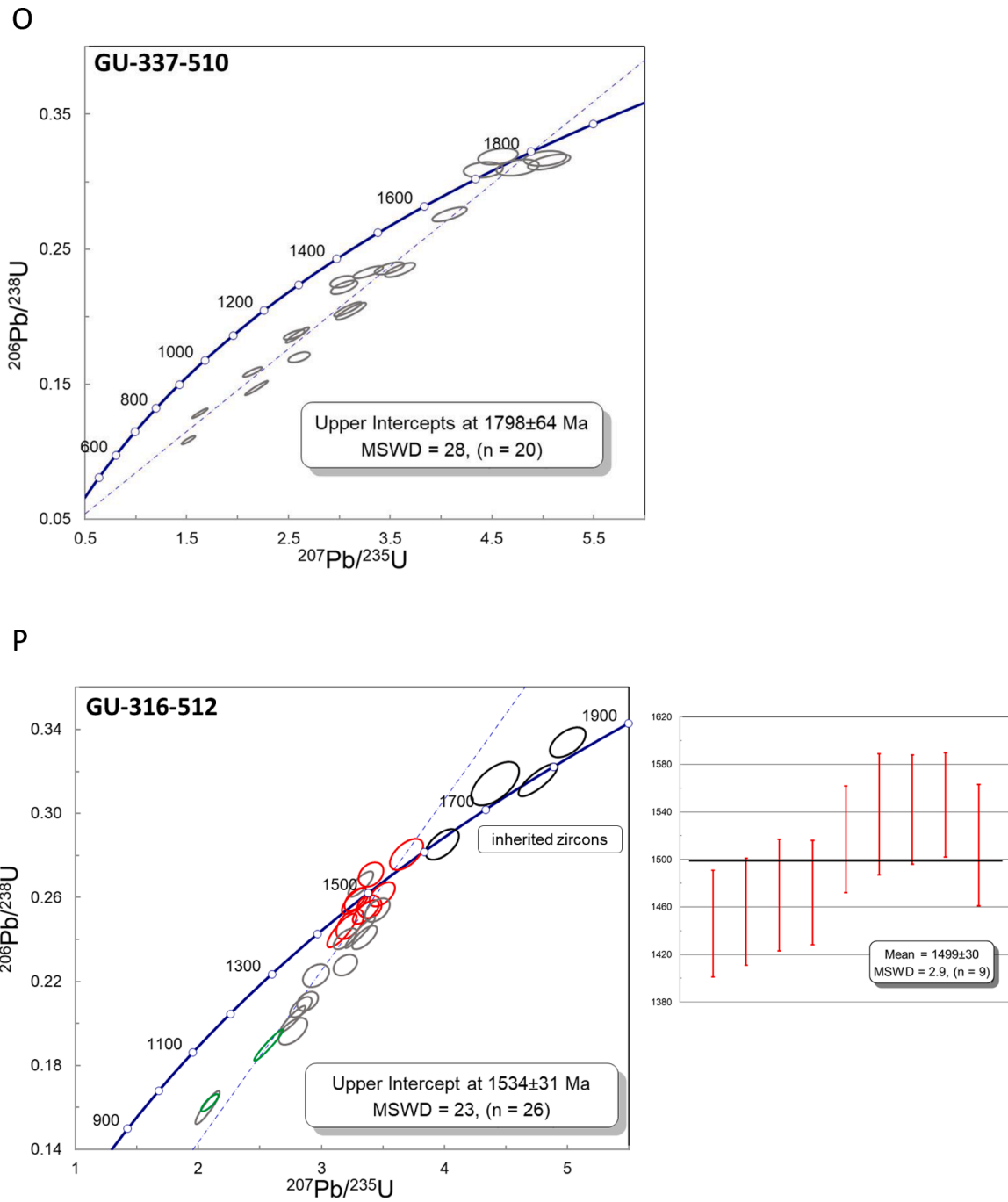


Fig. 22. (continued).

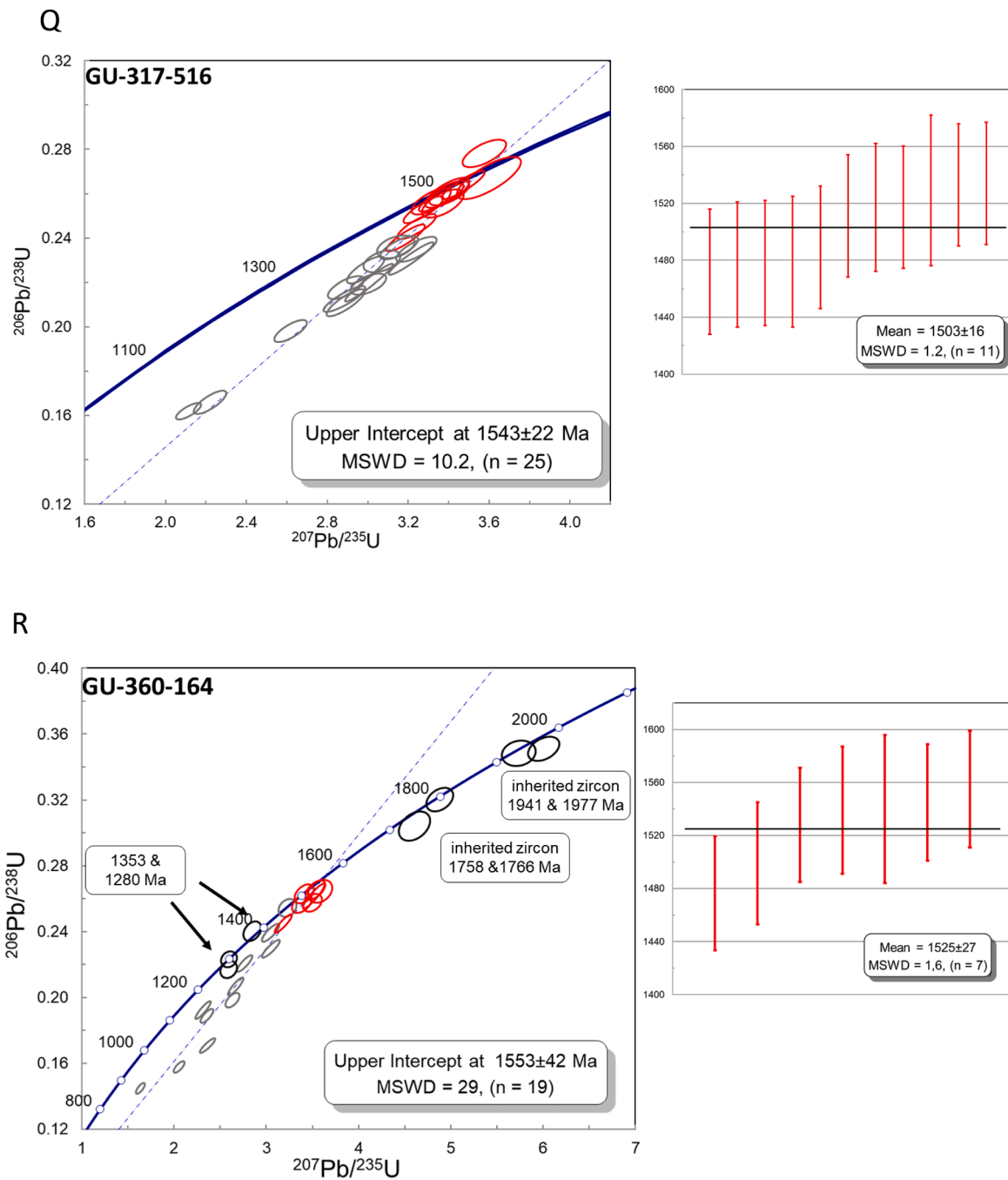
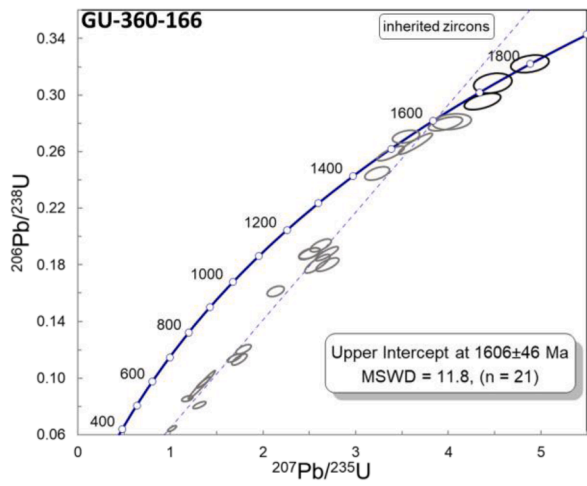


Fig. 22. (continued).

S



T

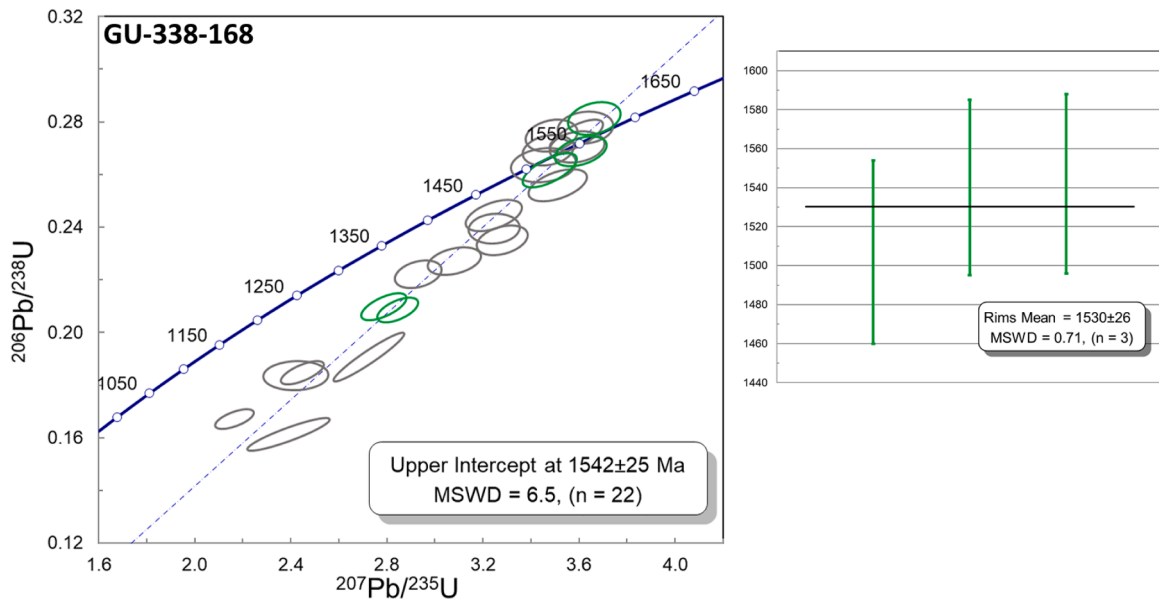


Fig. 22. (continued).

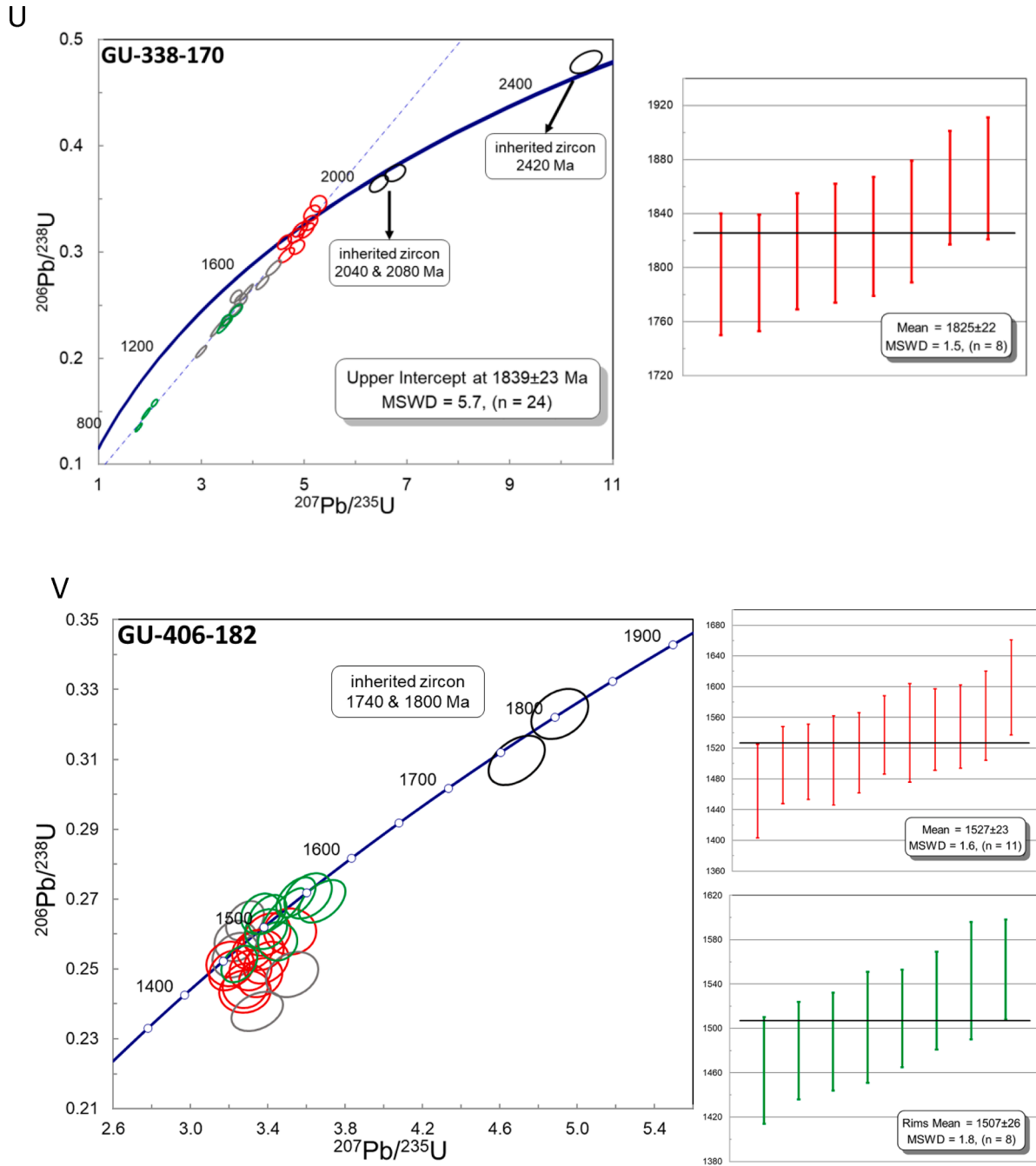


Fig. 22. (continued).

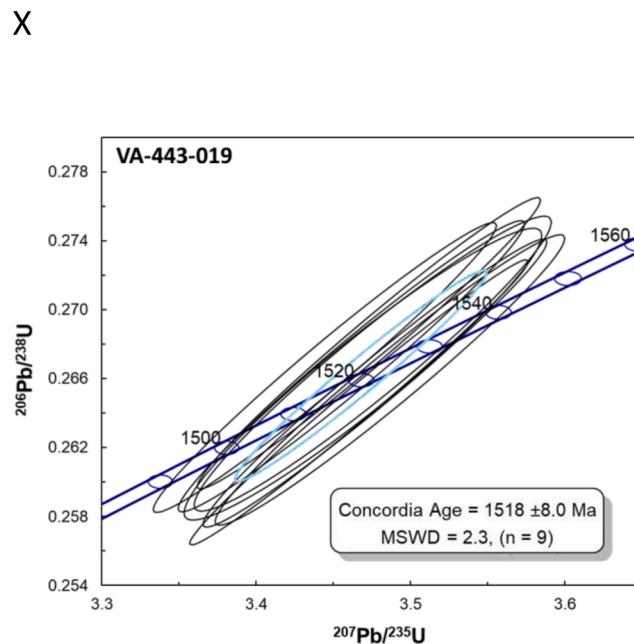
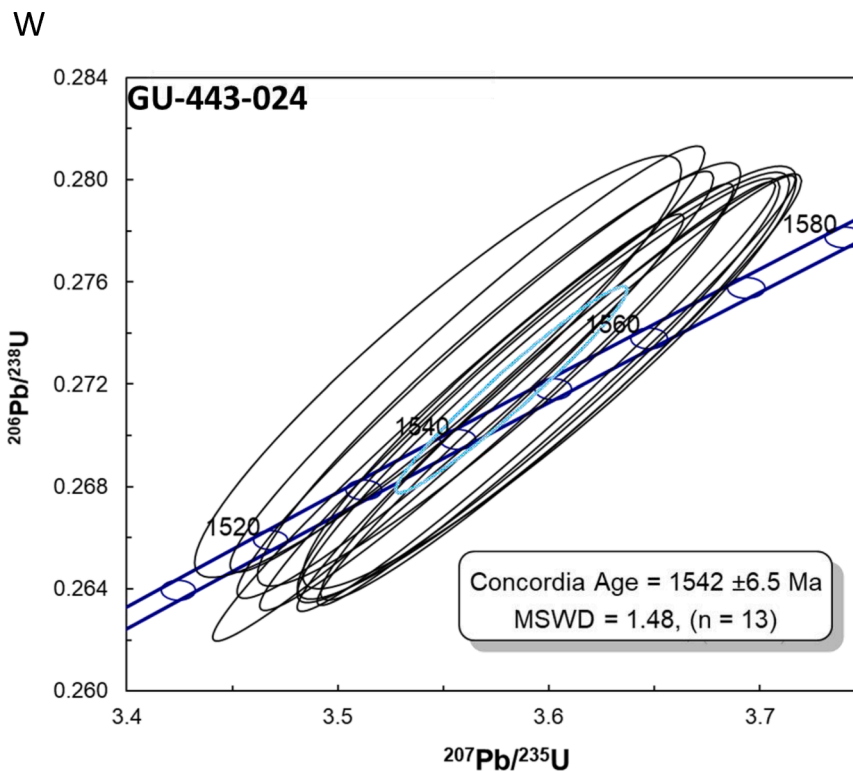


Fig. 22. (continued).

Veras et al. (2018) in Brazil. Most of the emblematic inselbergs from the Guainía and Vaupés department (e.g Mavicure Hills) are composed of these S-type granites (Fig. 3A and Fig. 2). Notably, some of these granites may have economic potential due to pegmatitic and postmagmatic Ta, Nb, Sn and REE mineralizations. This also holds true for the Tunuí Group where metasomatism-induced remobilization of gold occurred (Fig. 21).

Finally, the post-orogenic collapse setting continued into a transition to extensional tectonic forces and associated continental rifting, fostering anorogenic magmatism. A-type granites as the huge Parguaza Granite Batholith and the much smaller Matraca rapakivi granite (Bonilla-Pérez et al., 2013, 2016), with crystallization ages between 1400 and 1340 Ma in Colombia, are the result of episodic

decompressional melting and slow post-magmatic cooling (Fig. 21). This magmatism started earlier, to the east, in Venezuela, where the Parguaza Granite yields zircon-U/Pb ages of ~ 1500 to 1550 Ma, whereas the Colombian Parguaza granite portion seems to represent the central axis of the rift with later crystallization age and the Matraca intrusion corresponds to a western distal zone.

## 7. Conclusions

Based on a critical review of existing data and our new field observations, petrography, geochemical and geochronological data, we here propose a thoroughly modified geological and tectonic history of the

eastern Colombian basement, with direct implications with regard to a revised configuration for the Northwestern segments of the Amazonian Craton.

1. After extensive field campaigns in Eastern Colombia, with subsequent geochronological analyses, no evidence was found for pre-Orosirian rock units in this area, neither by us nor by other researchers. Although typical for large parts of the West Amazonian domain, these rocks seem not to be present in the investigated sections of the Eastern Colombian basement, not even as inliers. The oldest rocks found so far date from the end of the Orosirian period (1.85–1.8 Ga).
2. As part of the Rio Negro-Juruena Province, 1800–1720 Ma Statherian basement rocks built up the Mitú Complex s.s. which include granitoids and gneisses difficult to distinguish in the field. However, local studies may reveal further subdivisions like the Tiquié Intrusive Suite which would reflect *syn*-collisional magmatism during the Querari Orogeny (Kroonenberg, 2019).
3. Meta-sedimentary sequences of the Tunuí Group cover almost the entire basement of the Rio Negro-Juruena Province and its protolith include sandstones, conglomeratic sandstones and mudstones. They were feeded by the weathering of > 1770 Ma basement rocks. Older populations of detrital zircons in the Tunuí Group even testify that the oldest parts of the Amazonian Craton provided some sediment supply (e.g. Central Amazonia > 2.3 Ga). We propose that the Tunuí Group was deposited during more stable tectonic conditions after cessation of the Querari Orogeny and its metamorphism age is still matter of debate.
4. Intrusion of different suites of post-orogenic granitic rocks, dated between 1600 and 1500 Ma, reached to affect thermally and metasomatically the sedimentary sequences of the Tunuí Group as for example observed in Yurupari (Bonilla-Pérez et al., 2019). Those granites have been described in Brazil as result of the Içana Orogeny (Veras et al., 2018).
5. Anorogenic magmatism represented by rapakivi granites with zircon U-Pb ages of 1400–1340 Ma formed during the later stages of orogenic collapse and are associated with decompressional crustal melting during continental rifting.

#### Declaration of Competing Interest

The authors declare that they have no known competing financial interests or personal relationships that could have appeared to influence the work reported in this paper.

#### Acknowledgements

This research was supported by the Sistema General de Regalías (Convenio 031-2013). First author acknowledge a PhD grant from the Colombian science institution - COLCIENCIAS. We thank to indigenous communities for giving access to the study area. Zeze Amaya is greatly acknowledged for field work assistance; Veerle Vandenhende is thanked for assistance during geochemical analyses at Ghent University. Sarah Gilbert is thanked for assistance with geochronological analyses conducted at Adelaide Microscopy. Umberto Cordani and an anonymous reviewer are acknowledged for their helpful comments and hints.

#### Appendix A. Supplementary data

Supplementary data to this article can be found online at <https://doi.org/10.1016/j.precamres.2021.106223>.

#### References

- Almeida, M.E., Macabira, M.J.B., Santos, J.O.S., do Nascimento, R.S.C., Paquette, C., 2013. Evolução Crustal Do Noroeste Do Cráton Amazônico (Amazonas, Brasil) Baseada Em Dados de Campo, Geoquímicos e Geocronológicos. In: SBG/Núcleo Norte. 13º Simpósio de Geologia da Amazônia, Belem, pp. 1–4.
- Almeida, M.E., Macabira, M.J.B., Santos, J.O.S., Nascimento, R.S.C., Paquette, J.L., Vasconcelos, P., Luzardo, R., 2011. A new geodynamic model for the Northwestern Amazon Craton (Amazonas, Brazil) based on field geology, geochemistry and geochronology data. In: 14th Latin American Geological Congress, Medellín, Colombia.
- Almeida, M.E., Macabira, M.J., Scheller, T.B., 1997. Içana Intrusive Suite: age<sup>207Pb/206Pb</sup> (zircon evaporation) of muscovite-bearing granite, Amazonas State, Brazil. South-American Symposium on Isotope Geology, Campos do Jordão, Brazil 31–33.
- Batchelor, R.A., Bowden, P., 1985. Petrogenetic interpretation of granitoid rock series using multicationic parameters. *Chem. Geol.* 48 (1–4), 43–55. [https://doi.org/10.1016/0009-2541\(85\)90034-8](https://doi.org/10.1016/0009-2541(85)90034-8).
- Bogotá, J., 1981. Síntesis de La Geología Regional de Las Zonas Limítrofes Colombia-Brasil-Venezuela. Informe No. 40013, IAN-COGEA. Inédito.
- Bonilla-Pérez, A., Frantz, J.C., Charão-Marques, J., Cramer, T., Franco-Victoria, J.A., Mulocher, E., Amaya-Perea, Z., 2013. Petrografía, Geoquímica y Geocronología del Granito de Parguaza en Colombia. *Boletín de Geología* 35 (2), 83–104. <https://doi.org/10.18273/revbol>.
- Bonilla-Pérez, A., Frantz, J.C., Charão-Marques, J., Cramer, T., Franco-Victoria, J.A., Amaya-Perea, Z., 2016. Magmatismo Rapakivi En La Cuenca Media Del Río Inírida, Departamento de Guainía, Colombia. *Boletín de Geología* 38(1), 17–32. doi: <http://dx.doi.org/10.18273/revbol.v38n1-2016001>.
- Bonilla-Pérez, A., Cramer, T., Poujol, M., Cano, H., Franco-Victoria, J.A., Amaya-Perea, Z., 2019. Petrografía, Geoquímica y Geocronología U / Pb En Circones de Rocas Ígneas y Metamórficas a Lo Largo Del Río Cuiarí En El Sur Del Departamento de Guainía, Colombia. *Boletín de Geología* 41 (1), 55–84. <https://doi.org/10.18273/revbol.v41n1-2019003>.
- Bruneton, P., Pallard, B., Duselier, D., Varney, E., Bogotá, J., Rodríguez, C., Martín, E., 1982. Contribución a La Geología Del Oriente de Las Comisariías Del Vichada y Del Guainía (Colombia). *Geología Norandina* 3–13.
- Carneiro, M.C.R., Nascimento, R.S.C., Almeida, M.E., Salazar, C.A., da Trindade, I.R., de Oliveira-Rodrigues, V., Passos, M.S., 2017. The Cauaburi Magmatic Arc: Litho-Stratigraphic Review and Evolution of the Imeri Domain, Rio Negro Province, Amazonian Craton. *J. S. Am. Earth Sci.* 77, 310–326. <https://doi.org/10.1016/j.jsames.2017.06.001>.
- Carrillo, V.M., 1995. Sobre La Edad de La Secuencia Metasedimentaria Que Encaja Las Mineralizaciones Auríferas Vetiformes En La Region Del Taraira (Vaupés). *Geología Colombiana* 19, 75–83.
- Cordani, U.G., Sato, K., Sproessner, W., Fernandes, F.S., 2016. U-Pb Zircon Ages of Rocks from the Amazonas Territory of Colombia and Their Bearing on the Tectonic History of the NW Sector of the Amazonian Craton. *Braz. J. Geol.* 46 (1), 5–35.
- Cordani, U.G., Tassinari, C.C.G., Teixeira, W., Basei, M.A.S., Kawashita, K., 1979. Evolução Tectónica Da Amazônia Com Base Nos Dados Geocronológicos. *Actas, PP - Ciudad de Arica*.
- Cordani, U. G., and W. Teixeira. 2007. "Proterozoic Accretionary Belts in the Amazonian Craton, in Hatcher, R.D., Jr., Carlson, M.P., McBride, J.H., and Martínez Catalán, J. R., Eds., 4-D." Pp. 297–320 in *Framework of Continental Crust: Geological Society of America Memoir* 200.
- CPRM, 2006. Geología e Recursos Minerais Do Estado Do Amazonas, Escala1: 1.000.000. Manaus.
- Cramer, T., Z. Amaya-Perea, J. A. Franco-Victoria, A. Bonilla-Pérez, and Á. P. Poveda. 2011. "Caracterización de Depósitos Aluviales Con Manifestaciones de Tantalio y Niobio (Coltán) En Las Comunidades Indígenas de Matraca y Caranacoa En El Departamento Del Guainía) - Contrato Interadministrativo No 021 de 2010 Ingeominas-Universidad Nacional de C." <http://Aplicaciones1.Ingeominas.Gov.Co/Sicat/Html/Metadato.Aspx?CID=240476> Last View: 11/6/2011 190. doi: <http://aplicaciones1.ingeominas.gov.co/sicat/html/Metadato.aspx?CID=240476> last view: 11/6/2011.
- Dempster, T.J., Jenkin, G.R.T., Rogers, G., 1994. The Origin of Rapakivi Texture. *J. Petrol.* 35 (4), 963–981. <https://doi.org/10.1093/ptrology/35.4.963>.
- Frost, B.R., Barnes, C.G., Collins, W.J., Arculus, R.J., Ellis, D.J., Frost, C.D., 2001. A geochemical classification for granitic rocks. *J. Petrol.* 42 (11), 2033–2048. <https://doi.org/10.1093/ptrology/42.11.2033>.
- Galvis-Vergara, J., Huguett, A., Ruge, P., 1979. Geología de La Amazonía Colombiana. *Boletín Geológico XXI I* (3), 3–86.
- Galvis-Vergara, J., 1993. Los Sedimentos Precámbricos Del Guainía y El Origen de Las Ocurrencias Auríferas En El Borde Occidental Del Escudo de Guayanas. *Geología Colombiana* 18, 119–136.
- Gansser, A., 1954. The Guiana Shield (S. America) Geological Observations. *Ecol. Geol. Helvet* 47 (1), 77–112.
- Gaudette, H.E., Olszewski, W.J., 1985. Geochronology of the Basement Rocks, Amazonas Territory, Venezuela and Tectonic Evolution of the Western Guiana Shield. *Geol. Mijnbouw* 64 (2), 131–143.
- Gaudette, H.E., Mendoza, V.S., Hurley, P.M., Fairbairn, H.W., 1978. Geology and Age of the Parguaza Rapakivi Granite, Venezuela. *Bull. Geol. Soc. Am.* 89 (9), 1335–1340. [https://doi.org/10.1130/0016-7606\(1978\)89<1335:GAAOTP>2.0.CO;2](https://doi.org/10.1130/0016-7606(1978)89<1335:GAAOTP>2.0.CO;2).

- Goldfarb, R.J., Groves, D.I., Gardoll, S., 2001. Orogenic gold and geologic time: a global synthesis. *Ore Geol. Rev.* 18 (1–2), 1–75. [https://doi.org/10.1016/S0169-1368\(01\)00016-6](https://doi.org/10.1016/S0169-1368(01)00016-6).
- Gómez, J., Schobbenhaus, C., (compilers). Montes, N.E., 2019. Geological Map of South America 2019. Scale 1:5 000 000. Paris.
- Gómez, J., Montes, N., Alcárcel, F., Ceballos, J., 2015. Catálogo de Dataciones Radiométricas de Colombia En ArcGIS y Google Earth." Pp. 63–419 in *Compilando la geología de Colombia: Una visión a 2015*, edited by J. Gómez-Tapias and M. F. Almanza Meléndez. Bogotá: SGC.
- Heinonen, A.P., Fraga, L.M., Rämö, O.T., Dall'Agnol, R., Mänttari, I., Andersen, T., 2012. Petrogenesis of the Igneous Mucajaí AMG Complex, Northern Amazonian Craton — Geochemical, U-Pb Geochronological, and Nd-Hf-O Isotopic Constraints. *Lithos* 151, 17–34. <https://doi.org/10.1016/j.lithos.2011.07.016>.
- Hsu, K.J., 1982. *Mountain Building Processes*. Academic Press, London, p. 263.
- Huggert, R.J., 2007. *Fundamentals of Geomorphology*, 2nd ed. Routledge, London; New York.
- Ibáñez-Mejía, M., 2010. *New U-Pb Geochronological Insights into the Proterozoic Tectonic Evolution of Northwestern South America: The Mesoneoproterozoic Putumayo Orogen of Amazonia and Implications for Rodinia Reconstructions*. The University of Arizona.
- Ibáñez-Mejía, M., Ruiz, J., Valencia, V.A., Cardona, A., Gehrels, G.E., Mora, A.R., 2011. The Putumayo Orogen of Amazonia and Its Implications for Rodinia Reconstructions: New U-Pb Geochronological Insights into the Proterozoic Tectonic Evolution of Northwestern South America. *Precamb. Res.* 191 (1), 58–77. <https://doi.org/10.1016/j.precamres.2011.09.005>.
- INGEOMINAS. 2010. "Geología de La Plancha 297 Puerto Inírida."
- International Organization for Standardization. 2002. Protocol 14869-2:2002(E): Soil Quality - Dissolution for the Determination of Total Element Content - Part 2: Dissolution by Alkaline Fusion.
- Irvine, T.N., Baragar, W.R.A., 1971. A guide to the chemical classification of the common volcanic rocks. *Can. J. Earth Sci.* 8, 523–548.
- Jackson, S.E., Pearson, N.J., Griffin, W.L., Belousova, E.A., 2004. The Application of Laser Ablation-Inductively Coupled Plasma-Mass Spectrometry to In Situ U-Pb Zircon Geochronology. *Chem. Geol.* 211 (1–2), 47–69. <https://doi.org/10.1016/j.chemgeo.2004.06.017>.
- Janoušek, V., Farrow, C.M., Erban, V., 2006. Interpretation of whole-rock geochemical data in igneous geochemistry: introducing geochemical data toolkit (GCDkit). *J. Petrol.* 47 (6), 1255–1259. <https://doi.org/10.1093/ptrology/egl013>.
- Kroonenberg, S., 2019. The Proterozoic Basement of the Western Guiana Shield and the Northern Andes. 115–192.
- Kroonenberg, S., de Roeber, E.W.F., Fraga, L.M., Reis, N.J., Faraco, T., Lafon, J.M., Cordani, U.G., Wong, T.E., 2016. Paleoproterozoic evolution of the Guiana shield in Suriname: a revised model. *Neth. J. Geosci.* 95 (04), 491–522. <https://doi.org/10.1017/njg.2016.10>.
- Laurent, A., Janoušek, V., Magna, T., Schulmann, K., Míková, J., 2014. Petrogenesis and Geochronology of a Post-Orogenic Calc-Alkaline Magmatic Association: The Žulová Pluton, Bohemian Massif. *J. Geosci.* 59 (4), 415–440.
- López, J., Khurama, S., Bernal, L., Cuellar, M., 2007. EL Complejo Mitú: Una Nueva Perspectiva. *Memorias XI Congreso Colombiano de Geología* 34, 1–16.
- Ludwig, K.R., 2012. *User's Manual for Isoplot 3.75 - A Geochronological Toolkit for Microsoft Excel Rev. January 30, 2012*.
- McDonough, W., Sun, S., 1995. The composition of the earth. *Chem. Geol.* 120 (3–4), 223–253. [https://doi.org/10.1016/0009-2541\(94\)00140-4](https://doi.org/10.1016/0009-2541(94)00140-4).
- Mendes, T.A.A., de Mesquita, R.B., Knauer, L.G., Almeida, M.E., Roncato, J., 2020. Spatiotemporal Constraints on the Western Cauburi Belt Tectonics – Northwestern Amazon Craton, Brazil. *Int. Geol. Rev.* 1–24. <https://doi.org/10.1080/00206814.2020.1768441>.
- Mendoza, V.S., 2012. *Geología de Venezuela*. Bogotá{á}.
- Montalvo, R., Fernandes, P., 1975. Grupo Tunuí. *Belm, Proyecto RADAM*.
- Paiva, G., 1928. *Reconhecimentos Geológicos Nas Fronteiras Do Brasil Com Venezuela e Colombia. Estado Do Amazonas. Rio de Janeiro*.
- Paton, C., Woodhead, J.D., Hellstrom, J.C., Hergt, J.M., Greig, A., Maas, R., 2011. Improved Laser Ablation U-Pb Zircon Geochronology through Robust Downhole Fractionation Correction. *Geochem. Geophys. Geosyst.* 11 (3) <https://doi.org/10.1029/2009GC002618>.
- Pearce, J.A., Harris, N.B.W., Tindle, A.G., 1984. Trace element distribution diagrams for the tectonic interpretation of granitic rocks. *J. Petrol.* 25 (4), 956–983. <https://doi.org/10.1093/ptrology/25.4.956>.
- Peccerillo, A., Taylor, S., 1976. Geochemistry of Eocene Calc-Alkaline Volcanic Rocks from Kastmonu Área, Northern Turkey. *Contrib. Miner. Petrol.* 58, 63–81.
- Pinheiro, S.S., Fernandes, P., Pereira, E., Vasconcelos, E., Pinto, A., Montalvo, R., Issler, R., Dall'Agnol, R., Teixeira, W., Fernández, C.A.C., 1976. *Geología - Projeto Radar Na Amazônia*. Folha NA.19-Pico Da Neblina. Pp. 19–137 in *Levantamento de Recursos Naturais- Vol 11*.
- Pinson, W.H., Hurlley, P.M., Mencher, E., Fairbairn, H.W., 1962. K-Ar and Rb-Sr ages of biotites from Colombia, South America. *Geol. Soc. Am. Bull.* 73 (7), 907–910. [https://doi.org/10.1130/0016-7606\(1962\)73\[907:KARA0B\]2.0.CO;2](https://doi.org/10.1130/0016-7606(1962)73[907:KARA0B]2.0.CO;2).
- Pohl, W.L., 2011. *Economic Geology - Principles and Praxis*. First, 201. Blackwell Publishing Ltd.
- Priem, H.N.A., Andriessen, P.A.M., Boelrijk, N.A.I.M., de Boorder, H., Hebeda, E.H., Huguett, A., Verdurmen, E.A.T., Verschure, R.H., 1982. Geochronology of the Precambrian in the Amazonas Region of Southeastern Colombia (Western Guiana Shield). *Geol. Mijnbouw* 61 (3), 229–242.
- Renzone, G., 1989a. Comparación entre las secuencias metasedimentarias de la Serranía de Naquén y de la Serra da Jacobina. *Boletín Geológico* 30 (2), 25–42.
- Renzone, G., 1989b. La Secuencia Aurífera de La Serranía de Naquén. *Boletín Geológico* 30, 103.
- Rodríguez-García, G., Sepúlveda, J., Ramírez, C., Ortiz, F., Ramos, K., Bermúdez, J., Sierra, M., 2011. Cartografía Geológica y Exploración Geoquímica de La Plancha 443 Mitú. 163.
- Rodríguez-García, G., Sepúlveda, J., Ramírez, C., Ortiz, F., Ramos, K., Bermúdez, J., Sierra, M., 2011b. Unidades, Petrografía y Composición Química Del Complejo Migmatítico de Mitú En Los Alrededores de Mitú. *Boletín de Geología* 33 (1), 27–42.
- Rudnick, R.L., Fountain, D.M., 1995. Nature and composition of the continental crust: a lower crustal perspective. *Rev. Geophys.* 33 (3), 267. <https://doi.org/10.1029/95RG01302>.
- Santos, J.O.S., 2003. *Geotectónica Dos Escudos Das Guianas e Brasil Central*. Pp. 169–226 in *Geologia, Tectónica e Recursos Minerais do Brasil: texto, mapas e SIG*. Vol. 4, edited by L. B. Buzzi, C. Schobbenhaus, I. R. Vidott, and J. H. Gonçalves. CPRM – Serviço Geológico do Brasil.
- Santos, J.O.S., Hartmann, L.A., Gaudette, H.E., Groves, D.I., McNaughton, N.J., Fletcher, I.R., 2000. A new understanding of the provinces of the Amazon Craton based on integration of field mapping and U-Pb and Sm-Nd geochronology. *Gondwana Res.* 3 (4), 453–488. [https://doi.org/10.1016/S1342-937X\(05\)70755-3](https://doi.org/10.1016/S1342-937X(05)70755-3).
- Santos, J.O.S., Potter, P.E., Reis, N.J., Hartmann, L.A., Fletcher, I.R., McNaughton, N.J., 2003. Age, source, and regional stratigraphy of the roraima supergroup and Roraima-like Outliers in Northern South America Based on U-Pb Geochronology. *Geol. Soc. Am. Bull.* 115(3), 331–348. doi: 10.1130/0016-7606(2003)115<0331:ASARSO>2.0.CO;2.
- Shand, S.J., 1943. *The Eruptive Rocks*. 2nd ed. edited by J. W. & Sons. New York: John Wiley & Sons.
- Sláma, J., Košler, J., Condon, D., Crowley, J., Gerdes, A., Hanchar, J., Horstwood, M., Morris, G., Nasdala, L., Norberg, N., Schaltegger, U., Schoene, B., Tubrett, M., Whitehouse, M., 2008. Plešovice Zircon - a new natural reference material for U-Pb and Hf isotopic microanalysis. *Chem. Geol.* 249, 1–35. <https://doi.org/10.1016/j.chemgeo.2007.11.005>.
- Tassinari, C.C.G., Macambira, M.J.B., 1999. Geochronological Provinces of the Amazonian Craton. *Episodes* 22 (3), 174–182. <https://doi.org/10.1080/00206819709465329>.
- Tassinari, C.C.G., Cordani, U.G., Nutman, A.P., Schmus, W.R.V., Bettencourt, J.S., Taylor, P.N., 1996. Geochronological Systematics on Basement Rocks from the Rio Negro-Juruena Province (Amazonian Craton) and Tectonic Implications. *Int. Geol. Rev.* 38 (2), 161–175. <https://doi.org/10.1080/00206819709465329>.
- Teixeira, W., Tassinari, C.C.G., Cordani, U.G., Kawashita, K., 1989. A review of the geochronology of the Amazonian Craton: tectonic implications. *Precamb. Res.* 42 (3–4), 213–227. [https://doi.org/10.1016/0301-9268\(89\)90012-0](https://doi.org/10.1016/0301-9268(89)90012-0).
- Toussaint, J., 1993. *Evolución Geológica de Colombia: Precámbrico, Paleozoico*. Medellín {n}: Universidad Nacional de Colombia.
- Veras, R.S., 2012. *Petrologia de Granitóides Dos Arredores Da Missão Tunuí, NW Do Amazonas, Província Rio Negro, Cráton Amazônico*. Dissertação. Manaus: Departamento de Geociências, Universidade Federal do Amazonas.
- Veras, R., Nascimento, R.S., Almeida, M., Paquette, J.L., Carneiro, M., 2018. Paleoproterozoic Basement of Içana Domain, Rio Negro Province, Northwestern Amazonian Craton: Geology, Geochemistry and Geochronology (U-Pb and Sm-Nd). *J. South Am. Earth Sci.* 86, 384–409. <https://doi.org/10.1016/j.jsames.2018.07.003>.
- Whalen, J., Currie, K.L., Chappell, B.W., 1987. A-type granites: geochemical characteristics, discrimination and petrogenesis. *Contrib. Miner. Petrol.* 95, 407–419.
- Wiedenbeck, M., Allé, P., Corfu, F., Griffin, W., Meier, M., Oberli, F., Quadt, A., Roddick, J.C., Spiegel, W., 1995. Three natural zircon standards for U-Th-Pb, Lu-Hf, trace element and REE analyses. *Geostandards Newsletter* 19, 1–23. <https://doi.org/10.1111/j.1751-908X.1995.tb00147.x>.